Stimuli Responsive Polymer Gels for Sensing Applications

Andrew Kavanagh

Thesis submitted for the award of Ph.D.

Supervisor: Professor Dermot Diamond

School of Chemical Sciences

Dublin City University

For my parents,

Sean and Catherine.

Ten two letter words…

"If it is to be it is up to me"

"A mans errors are his portals of discovery"

James Joyce.

"Without continual growth and progress, such words as improvement, achievement and success have no meaning"

Benjamin Franklin.

Declaration

I hereby certify that this material, which I now submit for assessment on the programme of study leading to the award of Doctor of Philosphy is entirely my own work, that I have exercised reasonable care to ensure that the work is original, and does not to the best of my knowledge breach any law of copyright, and has not been taken from the work of others save and to the extent that such work has been cited and acknowledged within the text of my work.

Signed: _____
Andrew Kavanagh

ID No.: 53526224

Date: _____

Peer Reviewed Journal Publications:

1. A two component polymeric optode membrane based on a multifunctional ionic liquid.

Andrew Kavanagh, Robert Byrne, Dermot Diamond and Alekandar Radu, *Analyst,* 2011, 136, 348-353.

2. Photopatternable ionogels for electrochromic applications.

Andrew Kavanagh, Robert Copperwhite, Mohamed Oubaha, Jessica Owens, Colette McDonagh, Dermot Diamond and Robert Byrne, *Journal of Materials Chemistry,* 2011, 21, 8687-8693.

3. Ionic liquid based liquid junction free reference electrode.

Dimitrije Cicmil, Salzitsa Anastasova, **Andrew Kavanagh**, Dermot Diamond, UlriikaMattinen, Johan Bobacka, Andrzej Lewenstam and Aleksandar Radu., *Electroanalysis*, 2011, 23(8), 1881–1890.

4. Wireless radio frequency detection of greatly simplified polymeric membranes based on a multifunctional ionic liquid.

Andrew Kavanagh, Matthias Hilder, Noel Clark, Aleksandar Radu and Dermot Diamond, *Electrochimica Acta,* 2011, 56, 8947-8953.

5. An electrochromic ionic liquid: design, characterisation and performance within a solid-state device.

Andrew Kavanagh, Kevin J. Fraser, Robert Byrne and Dermot Diamond. *Chemistry of Materials, 2011. Submitted.*

6. Photopatternable, photoswitch dictated surface chemistry in hybrid organic/inorganic sol-gels.

Andrew Kavanagh, Mohamed Oubaha, Gabija Bickauskaite, Robert Byrne, Robert Copperwhite, Maria Farsari, Colette McDonagh, and Dermot Diamond. *Langmuir (in preparation).*

7. Graphene-doped photo-patternable ionogels: tuning of conductivity and mechanical stability of 3-D microstructures.

Mohamed Oubaha, **Andrew Kavanagh**, Robert Byrne, Dermot Diamond and Colette McDonagh. *Advanced Materials (in preparation).*

8. Stimuli responsive ionogels for sensing applications - an overview.

Andrew Kavanagh, Robert Byrne, Dermot Diamond and Kevin J. Fraser, *Membranes - Review as part of special edition "Stimuli Responsive Polymers",* 2011. *Submitted*.

Oral Presentations:

1. "Ionic Liquids - Inherent Sensing and Transduction of Metal Ion complexation"

Andrew Kavanagh, Matthias Hilder, Noel Clark, Aleksandar Radu and Dermot Diamond,

@ European Materials Research Society 2010 Spring Meeting, 7th -11th June 2010, Strasbourg, France.

2. "The inherent physical, optical and conductivity properties of Ionic Liquid – polymeric membranes; a self-indicating, simultaneous response upon coordination to transition metal ions"

Andrew Kavanagh, Matthias Hilder, Noel Clark, Aleksandar Radu and Dermot Diamond,

@ Macro 2010: 43rd IUPAC World Polymer Congress, 11th -16th July 2010, Glasgow, Scotland.

Poster Presentations:

1. "Self-Indicating, Simultaneous, Multianalyte recognition using an Ionic Liquid"

Andrew Kavanagh, Robert Byrne, Dermot Diamond and Aleksandar Radu,

@ Pittcon 2009: 60th Pittsburgh Conference on Analytical Chemistry and Applied Spectroscopy, 8th -13th March 2009, Chicago, Illinois,USA.

2. "Multifunctional ionic liquids and their use in the formation of coordinated polymers"

Andrew Kavanagh, Robert Byrne, Dermot Diamond and Aleksandar Radu,

@ COIL- 3: 3rd International Congress on Ionic Liquids, 31st May - 4th June 2009, Cairns, Australia.

3. "The development of an electrochromic device based on photopatternable Ionogels and a viologen dye"

Andrew Kavanagh, Robert Copperwhite, Mohamed Oubaha, Jessica Owens, Colette McDonagh, Dermot Diamond and Robert Byrne,

@ CLARITY Open Day: Dublin City University, 19th November 2010, Dublin, Ireland.

4. "Wireless radio frequency detection of ionic liquid simplified polymeric optodes"

Andrew Kavanagh, Matthias Hilder, Noel Clark, Aleksandar Radu and Dermot Diamond,

@ The 6th Conference on Analytical Sciences in Ireland: Dublin City University, 21st - 22nd February 2011, Dublin, Ireland.

5. "Photopatternable phosphonium/imidazolium ionogels for electrochromic applications"

Andrew Kavanagh, Robert Copperwhite, Mohamed Oubaha, Jessica Owens, Colette McDonagh, Dermot Diamond and Robert Byrne,

@ COIL- 4: 4th International Congress on Ionic Liquids, 15th - 18th June, 2011, Arlington, Virginia, USA.

Chapter 1: General Introduction.

1.1 POLYMER GELS..... 22

1.1.1 SYNTHESIS OF POLYMER GELS 23
1.1.1.1 SOL-GEL CHEMISTRY 23
1.1.1.2 FREE RADICAL INITIATED POLYMERISATION 25

1.2 IONIC LIQUIDS..... 27

1.2.1 SYNTHESIS OF ILS 28
1.2.1.1 QUATERNISATION VIA ALKYLHALIDES 28
1.2.1.2 ION EXCHANGE METATHESIS 30

1.2.2 ELECTROCHEMISTRY OF ILS 33

1.3 IONIC LIQUID-POLYMER GELS (IONOGELS)..... 35

1.3.1 METHODS OF PREPARATION 35
1.3.1.1 IN-SITU POLYMERISATION 36
1.3.1.2 THE PLASTICISER EFFECT 37
1.3.1.3 USE OF ORGANOGELATORS 38

1.3.2 SELF POLYMERISING IONOGELS 39

1.4 STIMULI RESPONSIVE MATERIALS..... 42

1.4.1 POLYMERS AS STIMULI RESPONSIVE MATERIALS 42
1.4.1.1 PANI REDOX CHEMISTRY 43
1.4.1.2 PANI PH CHEMISTRY 45

1.4.2 ILS AS STIMULI RESPONSIVE MATERIALS 47
1.4.2.1 PH, PHOTORESPONSIVE ILS 47
1.4.2.2 ELECTROCHROMIC ILS 51

1.4.3 STIMULI RESPONSIVE IONOGELS 52

1.5 THESIS OVERVIEW…… 55

1.6 REFERENCES…… 57

Chapter 2: Instrumental Techniques

2.1 INSTRUMENTAL TECHNIQUES..... 66

2.1.1 CONTACT ANGLE ANALYSIS 66
2.1.2 DIFFERENTIAL SCANNING CALORIMETRY 66
2.1.3 IR SPECTROSCOPY 67
2.1.4 ELECTROCHEMICAL IMPEDANCE SPECTROSCOPY 67
2.1.5 NMR SPECTROSCOPY 68
2.1.6 PHOTOPATTERNING OF POLYMER GELS 69

2.1.6.1 DIRECT UV LASER WRITING 69
2.1.6.2 2PP MICROSTRUCTURING 69

2.1.7 RAMAN SPECTROSCOPY 70
2.1.8 SPECTROELECTROCHEMISTRY 70
2.1.9 SOLID STATE ELECTROCHROMIC DEVICE 71
2.1.10 SPINCOATING 71
2.1.11 THERMOGRAVIMETRIC ANALYSIS 71
2.1.12 UV/VIS SPECTROSCOPY 72
2.1.13 WRF CONDUCTIVITY ANALYSIS 72
2.1.14 XRF MEASUREMENTS 73

2.2 REFERENCES..... 73

Chapter 3: 2-component optode membranes based on a multifunctional ionic liquid.

3.1 ABSTRACT……75

3.2 INTRODUCTION…… 76

3.3 EXPERIMENTAL…… 78

3.3.1 CHEMICALS AND MATERIALS……78
3.3.2 MEMBRANE PREPARATION ……79

3.4 RESULTS AND DISCUSSION……80

3.4.1 INITIAL IL COMPLEXATION ……80
3.4.2 VIBRATIONAL SPECTROSCOPY ANALYSIS……82
3.4.3 MEMBRANE PREPARATION ……84
3.4.4 RESPONSE TIMES ……86
3.4.5 CALIBRATION OF RESPONSE, LIMIT OF DETECTION ESTIMATION ……87
3.4.6 ESTIMATION OF STOICHIOMETRY AND BINDING CONSTANTS……88
3.4.7 EFFECTS OF INTERFERING IONS……91
3.4.8 DUAL ANALYTE RECOGNITION……92
3.4.9 WRF DETECTION ……93
3.4.10 ELECTROCHEMICAL IMPEDANCE SPECTROSCOPY ……96
3.4.11 XRF MEASUREMENTS……98

3.5 CONCLUSION……100

3.6 REFERENCES……102

Chapter 4: An electrochromic ionic liquid: design, characterisation and performance within a solid-state device.

4.1 ABSTRACT……108

4.2 INTRODUCTION……109

4.3EXPERIMENTAL…… 112

4.3.1 CHEMICALS AND MATERIALS……112
4.3.2 (3-CHLOROPROPYL) TRIOCTYLPHOSPHONIUM BROMIDE SYNTHESIS……112
4.3.3 ELECTROCHROMIC IL SYNTHESIS……115
4.3.4 SOL-GEL SYNTHESIS……115
4.3.5 IONOGEL PREPARATION……116
4.3.6 SOLID-STATE DEVICE FABRICATION……117

4.4 RESULTS AND DISCUSSION……118

4.4.1 SYNTHESIS OF THE ELECTROCHROMIC IL……118
4.4.2 INFRARED SPECTROSCOPY……120
4.4.3 FABRICATION AND SPECTROELECTROCHEMISTRY OF ELECTROCHROMIC DEVICES……122
4.4.4 DEVICE PERFORMANCE……126
4.4.5 DEVICE CALIBRATION AND OPTICAL MEMORY……128
4.4.6 DEVICE SWITCHING……130

4.5 CONCLUSION…… 134

4.6 REFERENCES…… 135

Chapter 5: Photopatternable, photoswitchable surface chemistry in organic/inorganic sol-gels.

5.1 ABSTRACT..... 139

5.2 INTRODUCTION..... 140

5.3 EXPERIMENTAL..... 143

5.3.1 CHEMICALS AND MATERIALS..... 143
5.3.2 SYNTHESIS OF HYBRID SOL-GELS..... 144
5.3.3 SYNTHESIS OF THE SP MONOMER..... 147
5.3.4 PREPARATION OF SP FUNCTIONALISED MATERIALS..... 147

5.4 RESULTS AND DISCUSSION..... 149

5.4.1 VIBRATIONAL ANALYSIS OF SYNTHESISED SOL-GELS..... 149
5.4.2 CONTACT ANGLE DETERMINATION..... 151
5.4.3 PREPARATION OF SP FUNCTIONALISED MATERIALS..... 152

5.4.3.1 SPECTROSCOPIC ANALYSIS..... 152
5.4.3.2 CONTACT ANGLE DETERMINATION..... 158
5.4.3.2.1 Photodynamic Studies..... 158
5.4.3.2.2 Effects of complexation..... 159

5.4.4 PHOTOPATTERNING OF SP FUNCTIONALISED MATERIALS..... 160
5.4.4.1 PHOTODYNAMIC STUDIES..... 161
5.4.4.2 2PP POLYMERISED STRUCTURES..... 162

5.5 CONCLUSIONS..... 164

5.6 REFERENCES..... 165

Chapter 6: Photopatternable, electro-responsive ionogels.

6.1 ABSTRACT..... 171

6.2 INTRODUCTION..... 172

6.3 EXPERIMENTAL..... 174

6.3.1 CHEMICALS AND MATERIALS..... 174
6.3.2 IONOGEL PREPARATION..... 174
6.3.3 GRAPHENE DISPERSED IONOGEL PREPARATION..... 175
6.3.4 ELECTROCHROMIC DEVICE FABRICATION..... 175

6.4 RESULTS AND DISCUSSION..... 176

6.4.1 PHOSPHONIUM AND IMIDAZOLIUM IONOGEL CHARACTERISATION..... 176

6.4.1.1 RAMAN SPECTROSCOPY..... 176
6.4.1.2 EIS SPECTROSCOPY..... 180

6.4.2 GRAPHENE ENCAPSULATED IONOGELS CHARACTERISATION..... 184

6.4.2.1 RAMAN SPECTROSCOPY..... 184
6.4.2.2 EIS SPECTROSCOPY..... 186
6.4.2.3 XRF AND UV/VIS SPECTROSCOPY..... 188

6.4.3 ONE AND TWO PHOTON PATTERNING OF IONOGEL STRUCTURES..... 190
6.4.4 VIOLOGEN SPECTROELECTROCHEMISTRY AND DEVICE FABRICATION..... 192

6.5 CONCLUSIONS..... 195

6.6 REFERENCES..... 196

Chapter 7: Conclusions and future work.

7.1 THESIS CONCLUSIONS..... 199

7.1.1 SENSOR COMPONENT SIMPLIFICATION 199
7.1.2 PHOTOPATTERNING OF STIMULI RESPONSIVE SOL-GELS 203

7.2 FUTURE WORK..... 206

7.2.1 STRATEGIES TO IMPROVE THE LIMIT OF DETECTION OF TWO COMPONENT OPTODES 206

7.2.2 STRATEGIES TO IMPROVE THE LIQUID PROPERTIES OF ELECTROCHROMIC IONIC LIQUIDS 209
7.2.2.1 ION-EXCHANGE METATHESIS 209
7.2.2.2 VARIATION OF THE LINKER 210

7.2.3 STRATEGIES TO QUANTIFY AND OPTIMISE THE CAPACITANCE EFFECTS OF ELECTROCHROMIC DEVICE DESIGN 211

7.3 REFERENCES..... 214

Appendix

APPENDIX EXPERIMENTS..... 215

List of Abbreviations:

2PP	Two photon polymerisation
AC	Alternating current
$[AlCl_4]^-$	Tetrachloroalluminate
AlPO	Aluminium isopropoxide
$[BF_4]^-$	Tetrafluoroborate
$[C_2mIm]^+$	1-ethyl-3-methylimidazolium
$[C_4mIm]^+$	1-butyl-3-methylimidazolium
$[C_6mIm]^+$	1-hexyl-3-methylimidazolium
Co-DCA	Cobalt – Dicyanamide complex
$Co(NO_3)_2$	Cobalt (II) nitrate
Cu-DCA	Copper – Dicyanamide complex
$Cu(NO_3)_2$	Copper (II) nitrate
CV	Cyclic voltammetry
$[DBSA]^-$	Dodecylbenzene sulfonate
$[DCA]^-$	Dicyanamide anion
DC	Direct current
DMPA	2,2’ – dimethoxy-2-phenylacetophenone
DOS	Dioctylsebacate

DSC	Differential scanning calorimetry
EIS	Electrochemical impedance spectroscopy
EV	Ethylviologen dibromide
$[FAP]^-$	tris(pentafluoroethyl)trifluorophosphate.
IL	Ionic liquid
IPA	Isopropyl alcohol
IR	Infra-red
ITO	Indium-tin oxide
KCl	Potassium Chloride
MAAH	Methacrylic acid
MAPTMS	Methacryloxypropyltrimethoxysilane
$[mpyr]^+$	1-methylpyrrolidinium
$[N_{1,8,8,8,}]^+$	Methyltrioctylammonium
NaDBSA	Sodium dodecylbenzenesulfonate
NMR	Nuclear magnetic resonance
$[NTf_2]^-$	*bis(*trifluoromethane)sulfonylamide
$[P_{6,6,6,14}]^+$	trihexyltetradecylphosphonium
$[P_{3Cl,8,8,8}][Br]$	(3-chloropropyl) trioctylphosphonium bromide

$[P_{6,6,6,14}][Cl]$	Trihexyltetradecylphosphonium chloride
$[PF_6]^-$	Hexafluorophosphate
PANI	poly(aniline)
PMMA	poly(methylmethacrylate)
POT	poly(octylthiophene)
PVC	poly(vinylchloride)
R_{CT}	Resistance of charge transfer
TGA	Thermogravimetric analysis
TiPO	Titanium (IV) propoxide
$[TOS]^-$	Toluenesulfonate
UV/Vis	Ultra-violet/visible
WRF	Wireless radio frequency
ZrPO	Zirconium (IV) propoxide
$Z^{'}$	Real component of complex impedance
Z''	Imaginary component of complex impedance
σ	S.I. unit for conductivity

Chapter 1

General introduction

1.1 Polymer Gels

A polymer *gel* is defined as the generation of an interconnected polymer network that takes place within a liquid phase[1, 2]. The network of polymer chains hold the liquid in place within its structure or *matrix*. Well known examples of polymer gels are the hydrogels and in particular poly(n-isopropylacrylamide) (pNIPAAM), whose gels both solvate and expel water above and below a given temperature range[3]. It is a good example of a molecular actuator, as the release or uptake of water associated with temperature causes it to reversibly expand or shrink[4].

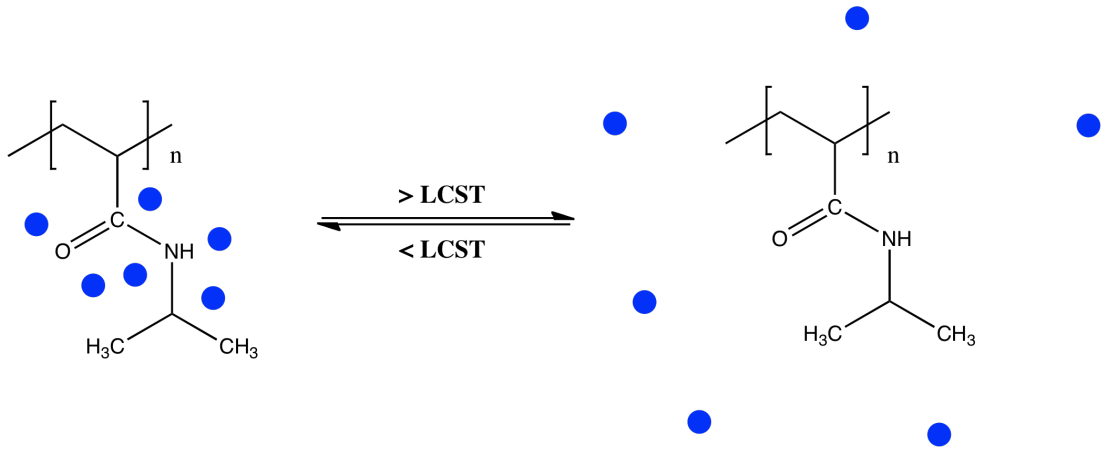

Figure 1.1: Thermal and solvation behaviour of gels based on pNIPAAM. The blue dots represent water molecules.

The temperature at which the reversible actuation/solvation occurs is known as the lower critical solution temperature (Figure 1.1). At this point the polymeric backbone undergoes structural changes in reponse to heat casusing the solvated water molecules to become expelled out of the gels macro structure. As this temperature is close to the temperature of the human body (~32 ^{0}C) for pNIPAAM gels[5], they have found use for the controlled release of drug molecules[6].

1.1.1 Synthesis of polymer gels

Two distinct methods were chosen to fabricate the polymer gels used in this thesis. Chapter 3 takes advantage of the platiciser effect of ILs to produce ILs whilst chapters 4,5 and 6 emply the *in situ* technique. The advantages of each tecnhique will be discussed in future sections of this introduction, to begin the underlying polymerisation mechanisms behind the *in situ* method will be discussed.

1.1.1.1 Sol-Gel chemistry

Sol-gels are prepared via a wet chemistry technique where inorganic precursors (most commonly metal alkoxides) undergo induced condensation to form an interconnected network (or a gel, as previously defined)[7]. Siloxane sol-gels are produced in this manner, where the hydrolysis step is catalysed by the addition of a Bronsted acid [8, 9]. To illustrate this, scheme 1.2 shows the chemistry required to produce a sol-gel from its precursor; *tetraethyl ortho silicate (TEOS)*.

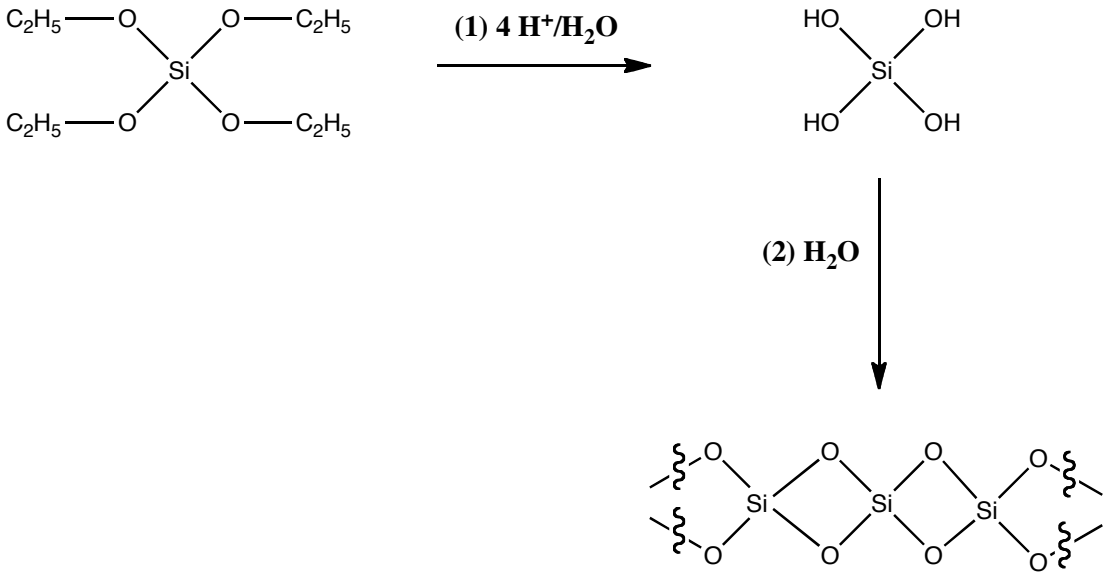

Scheme 1.2: Synthetic route employed to produce siloxane repeating units from TEOS.

The silicon ethoxide starting material is commonly dissolved in a short chain alcohol solvent, to which the acid catalyst is added (scheme 1.2, step 1). As the hydrolysis of the alkoxide moiety to silanols is induced, ethanol is produced as a by-product. Once the concentration of the silanol groups is high enough, condensation occurs between the individual subunits (step 2). The net result is a strong, covalently bound silicon oxide network. As the by products of the reaction are volatile, the gel can be isolated by casting on a suitable substrate and allowing to dry over time[10]. Sol-gels films are porous, glass like materials which exhibit good mechanical and thermal stability[11, 12]. Functional moieties can become embedded within the sol-gel network by their incorporation into the synthetic route (as co-hydrolysis agents)[13]. Popular applications of siloxanes are found in optical communications, where high transmissions of incident light are needed and facilitated by the low refractive index of the material[14].

1.1.1.2 Free radical initiated polymerisation

The first step in free radical mediated polymerisation is the generation of the radical istelf. For this thesis, the free radical mechanisms of polymerisations are generated photochemically. Barner-Kollowik *et al*. have described the photolysis of DMPA under UV-illumination, producing acetal and benzoyl radical fragments (scheme 1.3)[15]. Other methods of free radical polymerisation include those where the initiator molecule degrades thermally[16], or by undergoing redox chemistry with a metal centre[17].

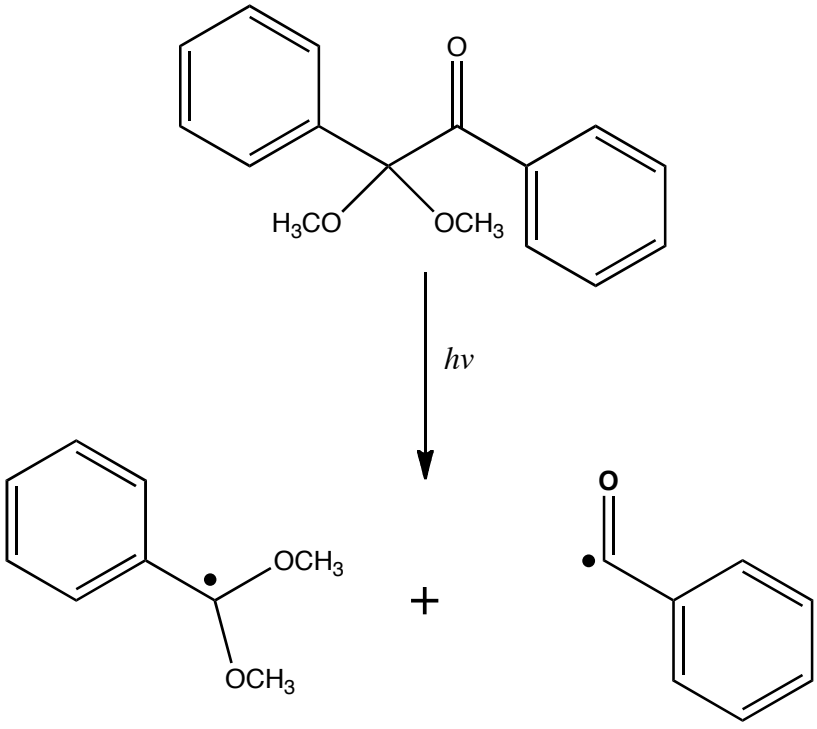

Scheme 1.3: Photolytic fragmentation of the initiator molecule DMPA.

The criteria of any initiator molecule is that they must be the source of radicals and hence must also transfer the radical energy to a monomer efficiently in order for the chain to grow. A particular extension for photo-initiated reactions is that the solvent medium (containing the monomer) must allow resourceful absorption of light by the initiator as defined by the variables in the Beer-Lambert law[18].

For the subsequent free radical mechanisms involving chain growth, the addition mechanism can be summarised under the following equations[19, 20]:

$$I^{\bullet} + M \rightarrow IM^{\bullet} \qquad \textbf{(1.1)}$$

$$IM^{\bullet} + M \rightarrow IMM^{\bullet} \qquad \textbf{(1.2)}$$

$$P^{\bullet} + P^{\bullet} \rightarrow P \qquad \textbf{(1.3)}$$

Once a radical is generated from the initiaor molecule, it then reacts with a monomer, thereby transferring its radical functionality to the monomer (Equation 1.1). Propogation reactions (Equation 1.2) then occur between reactive and passive monomer units causing the repeating unit to gradually grow.
The chain grows to a point where it reaches termination, a point where the two chain ends become inactive (Equation 1.3), or where all of the monomers in the system have become consumed.

A new class of polymer gels are beginning to appear in the literature where the liquid phase of the gel is an Ionic Liquid (IL), and are known as *ionogels*. Before the specific topics regarding ionogels can be discussed, ILs themselves are first introduced.

1.2 Ionic Liquids

According to current convention, a salt melting below the normal boiling point of water is known as an "ionic liquid" (IL), thus forming liquids that are comprised entirely of cations and anions at room temperature. In contrast to conventional organic liquids/solvents, important physical properties of ILs such as viscosity, density, melting point and conductivity can be tuned to some degree to suit a particular need by the appropriate choice of the cation/anion combination[21, 22]. The first publication of an IL is credited to *Paul Walden*, in 1914[23]. The publication described the synthesis of ethylammonium nitrate $[EtNH_3][NO_3]$ by protonation of ethylamine with 3M nitric acid, yielding a liquid with a melting point of 12 ^{0}C after purification. As of November, 2011, inputting the term "Ionic Liquids" as a topic into the Thomson Reuters® online Web of Knowledge® database yields ~34,000 publications, with a diverse research field ranging from studies engaged in biomedical engineering[24] to their performance as fuels for propulsion systems in rocket science[25]. ILs typically contain a large bulky asymmetric cation together with a smaller π-delocalised anion which exhibit mere electrostatic interactions[26]. Variation of important physico-chemical properties can be achieved by the appropriate choice of the cation/anion combination[27].

From a chemistry viewpoint, their use as alternative, inert reaction media for organic synthesis[28, 29], in various analytical instrumental analyses[30, 31], and their physicochemical interactions within[32, 33] and with solvated molecules[34-36] are the subject of many publications.

This literature review will focus on the chemistry of ILs from a materials viewpoint, first dealing with how ILs are prepared synthetically. Properties relevant to the experimental procedures undertaken in future chapters, such as applicatons in electrochemistry and polymer science are then reviewed.

1.2.1 Synthesis of ILs

1.2.1.1 Quaternisation via alkylhalides

The quaternisation of phosphines has been described in the literature by *Bradaric*[37] and Ermolaev[38] *et al*.; whilst the corresponding reaction for amines is described by Busi[39] *et al*. The reaction schemes are somewhat similar in that both electron rich starting materials undergo a S_n2 addition reaction in the presence of a haloalkane at elevated temperatures over time. A general reaction scheme for the quaternisation of a trialkylphosphine with 1-chloropropane to form the phosphonium salt is presented in scheme 1.4 (a); whilst the quaternisation of 1-substituted imidazole with 1-chloropropane to form the imidazolium salt is shown in scheme 1.4 (b).

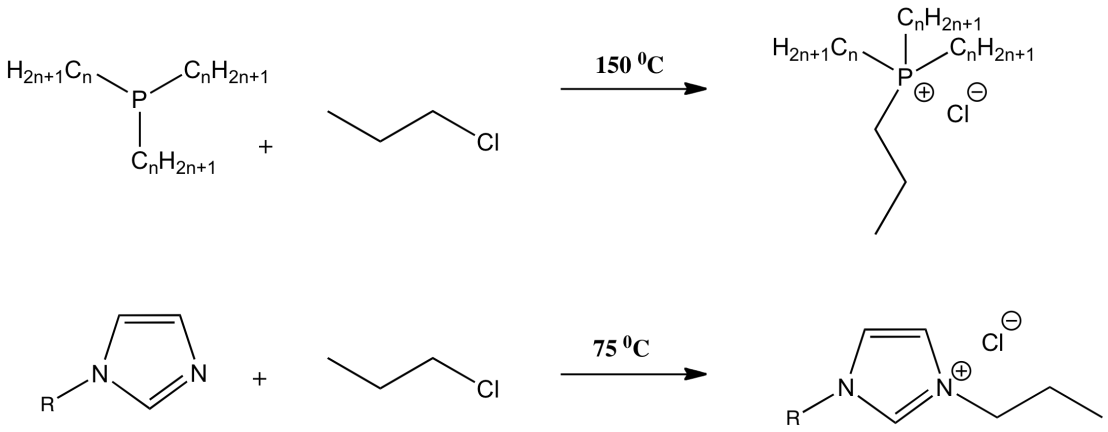

Scheme 1.4: Direct nucleophillic addition of a trialkylphosphine **(top)** and 1-substituted imidazole **(bottom)** with 1-chloropropane to form their corresponding chloride ILs.

Both reactions are performed in ultra dry, nitrogen purged atmospheres in order to control the oxidation of the starting products. The alkylating agent is slowly introduced as the initial reaction is exothermic, so in order to control the heat produced, it is added over 3 – 4 hours . The haloalkane is usually added in 10 mol% excess in order to ensure that the reducing agent is the limiting reactant. The reaction can be performed using chloro, bromo and iodoalkanes in which the temperature of the reaction follows the order Cl > Br > I (higher to lower). As the alkylating agents are usually volatile and the IL formed exhibits negligible vapour pressure, the product of the reaction can be isolated under vacuum for a period of 12 hours or more.

Removal of the impurites is specific for the reaction in question; for the case of phosphonium ILs cleaning is performed by initial washing with hexane, followed by dissolution in dichloromethane and liquid/liquid extractions with water. The IL is then passed through basic alumina and vacuum dried overnight at elevated temperatures[40].

Imidazolium ILs are cleansed by activated charcoal overnight at 40 ^{0}C, followed by filtration of the charcoal and column cleansing using basic alumina and vaccum drying overnight[41].

1.2.1.2 Ion-exchange metathesis

Variants of the halide ILs can be prepared via their ion-exchange with group one organic anions[42]. A reaction scheme for the preparation of $[P_{6,6,6,14}][NTf_2]$, which employs this reaction is shown in figure 1.5.

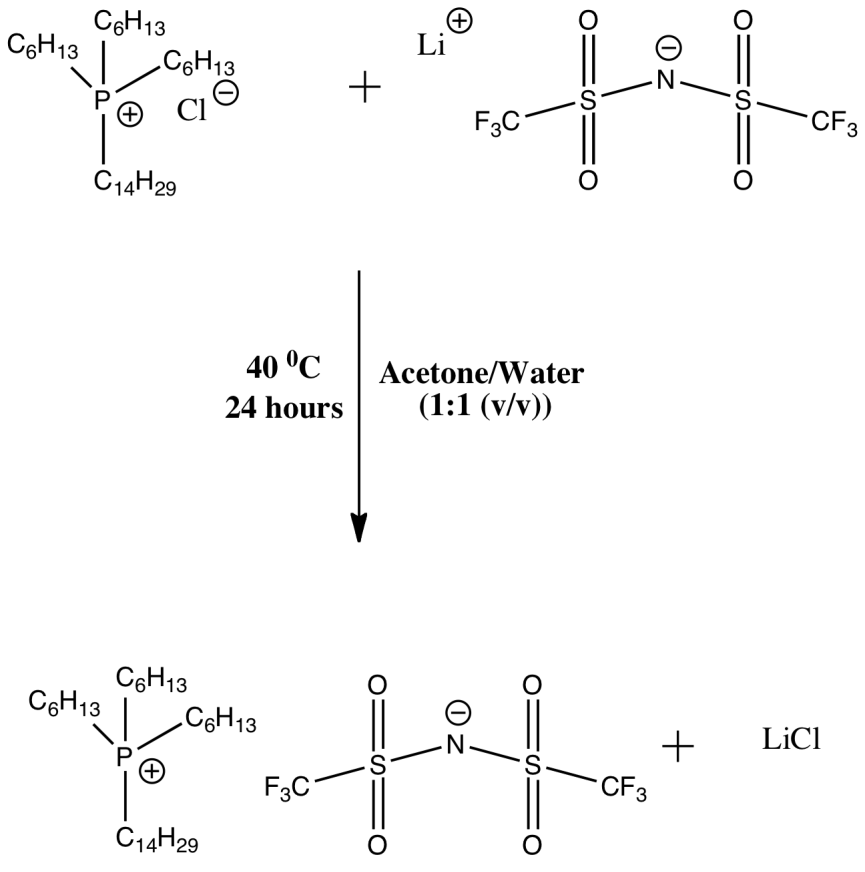

Scheme 1.5: Ion-exchange metathesis reaction of $[P_{6,6,6,14}][Cl]$ with $LiNTf_2$ to produce $[P_{6,6,6,14}][NTf_2]$.

Key to the success of this reaction is the choice of solvent that it is undertaken in. The solvent must serve to solvate the new IL formed and *preferably* promote the precipitation of the by-product.

An alternate strategy is shown in scheme 1.5 ; which describes the synthesis of $[P_{6,6,6,14}][NTf_2]$ in a 1:1 v/v mixture of acetone and water. As the IL begins to form over time, so too do the ionic interactions of Li and Cl respectively, which transfer into the aqueous phase. The new IL is isolated by removing the acetone used by rotary evaopration, folllowed by redissolution and liquid extraction using dichloromethane. After washing with water to remove any residual polar impurites, $[P_{6,6,6,14}][NTf_2]$ is then dried under vacuum.

If the desired IL is soluble in water then care must be taken to ensure that the metal salt by product precipitates out of soution, as described by MacFarlane *et al*[43]. In this publication the authors describe the route to isolate $[C_2mIm][DCA]$ from water by allowing NaDCA to undergo two ion-exchange reactions. In the first step NaDCA undergoes ion exchange with $AgNO_3$ in water to form AgDCA which is easily isolated by filtration. The by-product of the second ion-exchange – AgCl - (as opposed to NaCl); is then removed in the same manner. Finally, vacuum distillation at 100 ^{0}C affords the desired product.

A list of some of the more conventional IL constituents synthesised using quaternisation and ion-exchange reactions can be be viewed in figure 1.2.

Cations

Anions

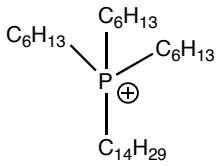

(i) $[P_{6,6,6,14}]^+$

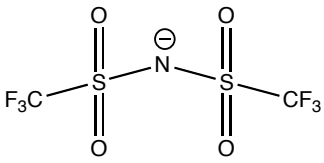

(v) $[NTf_2]^-$

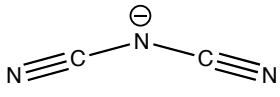

(vi) $[DCA]^-$

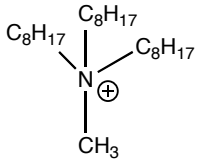

(ii) $[N_{1,8,8,8}]^+$

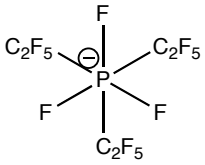

(vii) $[FAP]^-$

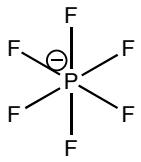

(viii) $[PF_6]^-$

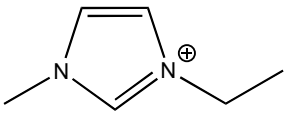

(iii) $[C_2mIm]^+$

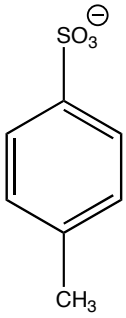

(ix) $[TOS]^-$

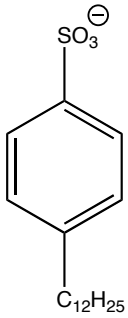

(x) $[DBSA]^-$

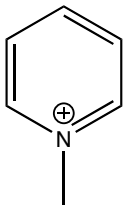

(iv) $[mpyr]^+$

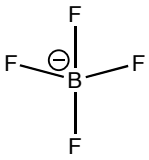

(xi) $[BF_4]^-$

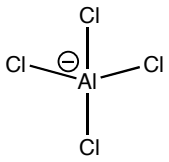

(xii) $[AlCl_4]^-$

Figure 1.2: A list of the more popular ions used throughout the literature for IL syntheses. Cations are listed on the left ((i) – (iv)), and anions are listed on the right ((v) – (xii)).

1.2.2 Electrochemistry of ILs

An electrolyte can be defined simply as an ionic solution that facilitates the rate of charge transfer between two electrodes. Given the inherent nature of ILs they make an excellent candidate for new classes of electrolyte material. IL's display an intrinsic ionic conductivity and do have some major advantages over aqueous based electrolytes; most notably, negligable vapor pressure, higher thermal stability and in some cases, a much wider electrochemical window[44].

The latter property is arguably one of the key advantages of using ILs as electrolytes. It means that processes can be performed within ILs that are simply not possible in aqueous solutions[45]. Some publications have reported electrochemical windows as high as 5 V for ILs[46]. It is accepted within the literature that the limiting cathodic and anodic extremes of the window are due to the reduction of the cation and the oxidation of the anion respectively[47]. The choice of the ion pair and their respective capability to resist redox chemistry at a given electrode, is therefore crucial to understanding the electrochemical window.

For instance, tetralkylated phosphonium and ammonium cations (figure 1.2 (i) and (ii)) have been shown to be more electrochemically stable than their imidazolium counterparts (figure 1.2 (iii)) [48]. The cationic charge is shielded by extensive alkylation in the former cations. Conversely the C-H bond at the 2 position in the imidazolium has been demonstrated to be mildly acidic, one report even detailing carbene formation at the cathode[49].

For anions; extensively fluorinated structures (in particular $[BF_4]^-$ and $[PF_6]^-$, figure 1.2), have been shown to exhibit high stability toward oxidation[50]. However these anions can suffer from hydrolysis, producing undesirable by-products such as hydrofluoric acid. Fortunately, anions such as $[NTf_2]^-$ and $[FAP]^-$ ((v) and (vii)) have been shown to avoid this unwanted feature[48].

Combining both redox resistive ions as part of an IL can yield high electrochemical windows; by using a tetra-alkylated phosphonium and $[NTf_2]$ in tandem, Tsunashima *et al*. reported an electrochemical window of 6.2 V[51].

One particular application taking advantage of the wide electrochemical window of IL is the direct electroplating of Aluminium. This process has proved difficult in aqueous solvents as the deposition potential of Aluminium occurs at potentials that induce hydrolysis in aqueous electrolyte solutions. Caporali *et al*. published the direct electoplating of carbon steel with Aluminium coatings using chloroalluminate based ILs[52].

More specific examples on the electrochemistry of ILs (such as their performance in electrochemical devices), are discussed in further detail in **sections 1.4.2.2** and **1.4.3.**

1.3 Ionic Liquid - polymer gels (Ionogels)

Ionic Liquid – polymer gel composites are now termed within the literature as ionogels[53] or ion gels[54], for the purpose of this review any polymer gels containing ionic charges (as part of the polymer structure[55], or in addition of solid, ionic species[56]) do not fall under this category.

Ionogels are hybrid materials in which the chemistry of an IL encapsulated within a polymer support matrix is facilitated in the solid state. By endowing a polymer gel with an IL important characteristics such as thermal stability and ionic conductivity can be improved upon. Ionogels have been subdivided and classified as chemical and physical gels respectively[53]. The route to a chemical or a physical gel is dependent on the principal preparation technique.

1.3.1 Methods of preparation

This next section will deal with the popular routes undertaken within the literature for the prearation of ionogels. It should be noted that these techniques can and have been applied for the preparation of polymer gels. The underlying polymerisation mechanism that occur within are similar to those already discussed.

1.3.1.1 In-situ polymerisation

Chemical ionogels are those in which the polymerisation process results in a strong, mechanically stable, covalently bound polymer network. When an IL is used as the polymerisation solvent, it becomes encapsulated within the chained network as it develops. Such a technique is called *in-situ* polymerisation, of which there are two distinct, popular approaches.

The first technique is to perform sol-gel hydrolysis-condensation chemistries in the presence of an IL, as first described by Neouze *et al*[57]. The key to achieving this particular gel was the choice of the IL, as it needed to be miscible with the sol-gel precursor and the acid catalyst (in this case formic acid). The authors used the IL $[C_4mIm][NTf_2]$ for this purpose. Formic acid was chosen as its relatively high pKa enusred a mild environment for the IL during the sol-gel process. As this was one of the first major publications on ionogels, the authors studied the effect of the molar composition of the IL within the sol-gel matrix. Thermal investigations revealed the gel was stable up to 370 ^{0}C, whilst the ionogel exhibited conductivities similar to the IL at elevated temperatures. Other noteworthy examples of ionogels prepared by the sol-gel technique are discussed in **section 1.4.3**.

The second *in-situ* technique is similar to the sol-gel method in that it involves the pre-preparation of an IL-monomer solution. However in this case the polymerisation is initiated via an external stimulus. The net result is the same in this case, as the IL becomes encapsulated within the polymer network as it develops.

In-situ developed, all organic polymer based ionogels have been mainly characterised again as alternative solid state electrolytes throughout the literature[58, 59].

1.3.1.2 The plasticiser effect

A particular trait of amorphous materials is that rather than undergoing a phase change (e.g. liquid/solid) over a given temperature range, they exhibit a change from a glassy brittle state to a more elastic rubbery state. The temperature change at which this occurs is known as the glass transition (T_g). Popular polymers such as PVC and PMMA exhibit high T_g's, whilst plasticisers exhibit T_g at much lower temperatures. By mixing the two, a composite material is produced exhibiting one T_g at a temperature in between (depending on the mole fraction of the plasticiser)[60].

Organic plasticisers such as *dioctylsebacate (DOS)* and *2-nitrophenyloctyl ether (NPOE)* work particularly well for PVC and PMMA, producing flexible elastic films at 66 wt% plasticiser. Both phosphonium and imidazolium ILs are amorphous in nature and exhibits low glass transitions around -70 ^{0}C[61]. They are therefore suitable for use as platicisers, producing ionogels similar in mechanical properties to their conventional plasticiser alternatives[62]. These ionogels are prepared by co-dissolution of the polymer/IL (at a given w/w ratio) in a suitable volatile solvent. Once the solution becomes homogenous it is cast on a substrate, and the film is formed as the solvent evaporates[63].

A particular advantage of using ILs as plasticisers for PVC/PMMA gels is that its ionic conductivity can be exploited for applications already optimised for these particular repeating units. One of the essential components of ion-selective electrodes is the ion-exchaging salt which facilitates movement of the analyte between the aqueous and polymeric phase. Chernyshov *et al*. have reported the selective detection of dopamine and adrenaline as low as 1 x 10^{-7} M, using an IL as plasticiser without the need for an ion-exchanging salt[64].

1.3.1.3 Use of organogelators

Physical ionogels differ from their chemical couterparts in that the internal network is built upon a foundation of (sometimes reversible) weak chemical interactions, such as hydrogen bonding. Physical gels are formed by en-masse aggregation, thereby creating the network, the rate of which is solvent dependent[65]. *Organogelators* are the chemical entities that are added to liquids to induce gelling. They are commonly added to liquid mixtures at elevated temperatures and - upon cooling - they have the effect of coagulating the whole mixture[66].

One report details the use of the gelator *cyclohexane- carboxylic acid-[4-(3-tetradecylureido)phenyl]amide* (which works particularly well for polar solvents) in the fabrication of ionogels for studies involving dye sensitised solar cells[67]. Just 2 wt.% of the gelator was needed to produce the quasi-solid state after cooling. Most importantly, the chemical ingredients critical for device functionality were maintained within the gel network, and so the ionogel could be scrutinised under the topic of device performance.

1.3.2 Self-polymerising ionogels

Another interesting technique for the fabrication of ionogels is where the polymerisable moiety is integrated into the IL state. In fact there are two separate reports in which the gelation is achieved by the simple addition of water. In both cases the IL is based on a tetraalkylammonium cation containing an extensively saturated alkyl-ether chain[68, 69] (Figure 1.3).

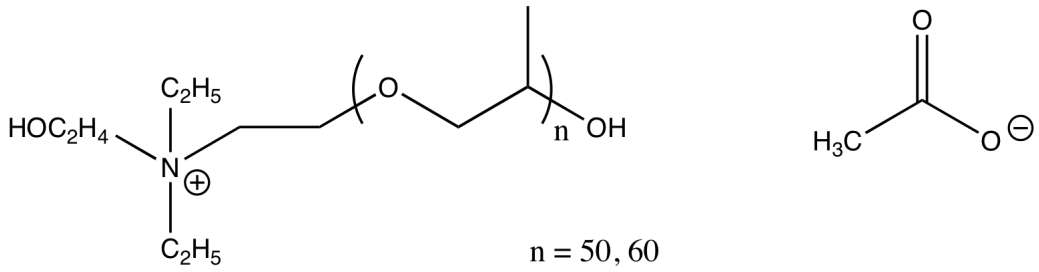

Figure 1.3: Self gelating IL based on a tetralkylated ammonium cation and acetate anion.

In both cases the addition of water produces a physical gel, where the water acts as a gelator through creation of a hydrogen bonded 3-D network. The authors reported ionic conductivities as high as 3 mS/cm for the IL gel shown in figure 1.3. As the gelation agent (H_2O) was needed in concentrations as high as 60 wt.%, the authors attributed the high conductivity value to the high dissociation of ions with the aqueous gel environment.

Washiro *et al*. have published their investigations into the effects of chain spacer length (between the acryl and IL subunits) and the effect of crosslinking agents on self-polymerising imidazolium ionogels[70]. A detailed representation on the synthetic route used to achieve self-polymerising ionogels is shown in scheme 1.6.

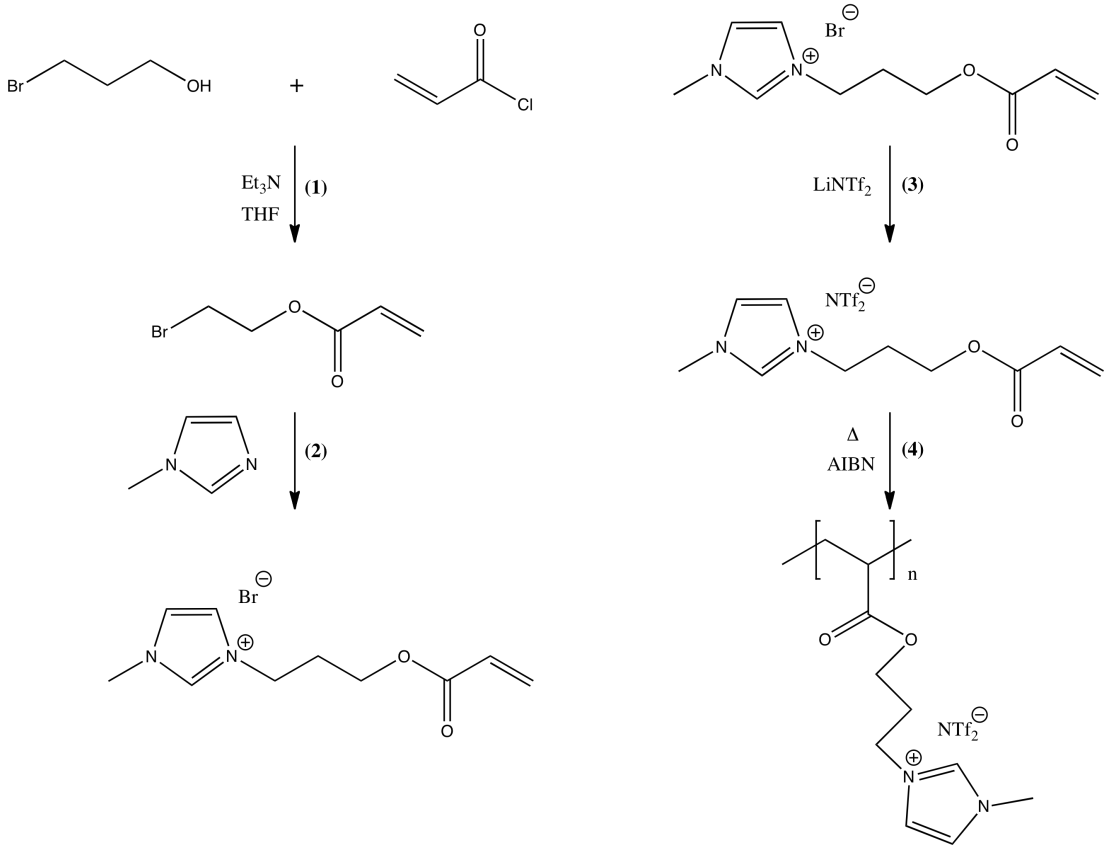

Scheme 1.6: The synthetic route adapted by Washiro *et al*. to achieve self-polymerising ionogels.

Acryl chloride was first allowed to react with a 1-bromoalcohol, producing a bromo-acryl monomer stabilised by an ether linkage (Step 1, Scheme 1.6). This allowed the monomer to undergo quarterisation with 1-methylimidazole (Step 2) and ion-exchange with $LiNTf_2$ (Step 3), producing a monomeric IL subunit. The polymerisation was then thermally initiated using *2,2' Azobisisobutyronitrile (AIBN)* to produce the ionogel (Step 4).

The variants in the synthesis were the chain length of the bromoalcohol used in the first step. This allowed its effects to be manifested in the ionic conductivity of the final polymerised ionogels, which was analysed using EIS. The gel that maintained most of its conductivity after polymerisation was found to be that based on a hexamethylene spacer between the monomer and the Imidazolium ring (figure 1.4)

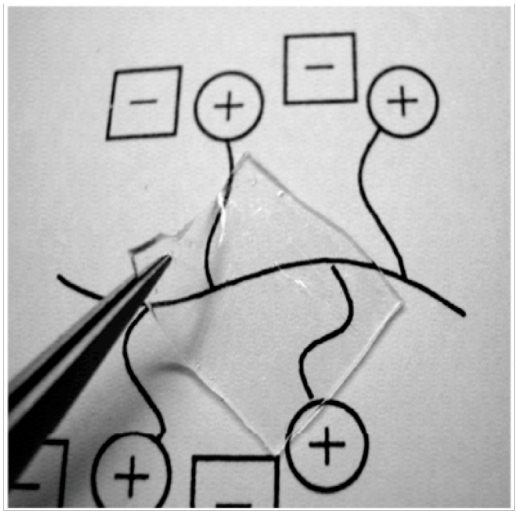

Figure 1.4: Ionogel prouced from self-polymerising ILs. Hexamethylene spacer and 1 mol. % cross linker used[70].

1.4 Stimuli responsive materials

Stimuli responsive materials are those that can undergo (in some cases a reversible) change in their molecular configuration in response to an external applied stimulus. They can of course be subdivided in relation to the particular stimulus applied, for example: in response to light[71], to an applied voltage[72] or a change in the pH[73] of the local environment. The change in molecular configuration is usually accompanied by a observable signal, for example a change in colour, conductivity or surface energy. The main applications that take advantage of these properties are in chemical sensing[74] and sensor devices[75], and in molecular actuators[76, 77]. This section of the literature review will focus on examples of both polymeric subunits and ILs acting as stimuli responsive materials.

1.4.1 Polymers as stimuli responsive materials

In some applications, be it in ion selective electrodes[78, 79] (a particular brand of electrochemical sensing) or for optical platforms[80, 81]; it is desirable for the polymer to be chemically inert so it can facilitate the particular chemistries within its matrix. The role of the polymer is therefore more of a support structure in these circumstances. However, there are some examples where the structure of the repeating unit is such that it can act as a stimuli responsive material. PANI is a good example of this, as it exhibits reversible pH[82] and redox[83] chemistry.

1.4.1.1 PANI redox chemistry

PANI is prepared by the oxidation of aniline, an amino mono-substituted phenyl ring. Oxidative polymerisation has been achieved using two distinct techniques: (a) using wet chemistry[84], or (b) with the use of an electrochemical cell. MacDiarmuid *et al*. have described the wet chemistry technique, using ammonium persulphate as the oxidising agent in an acidic environment[85]. The resultant polymer after synthesis was filtered and obtained as powder.

The electrochemical alternative provides a platform for thin films of PANI to be deposited directly onto an electrode. Using this technique oxidation is promoted at the electrode surface, to which the polymer adheres as it grows[86].

PANI exists as four distinct chemical forms. The leucoemeraldine base (LEB) can undergo partial oxidation forming the emeraldine salt (ES) (where an anion acts to preserve electroneutrality), which can itsef undergo further oxidation to its pernigraniline base (PB)[87]. These three distinct redox equilibria of PANI are shown below in figure 1.5.

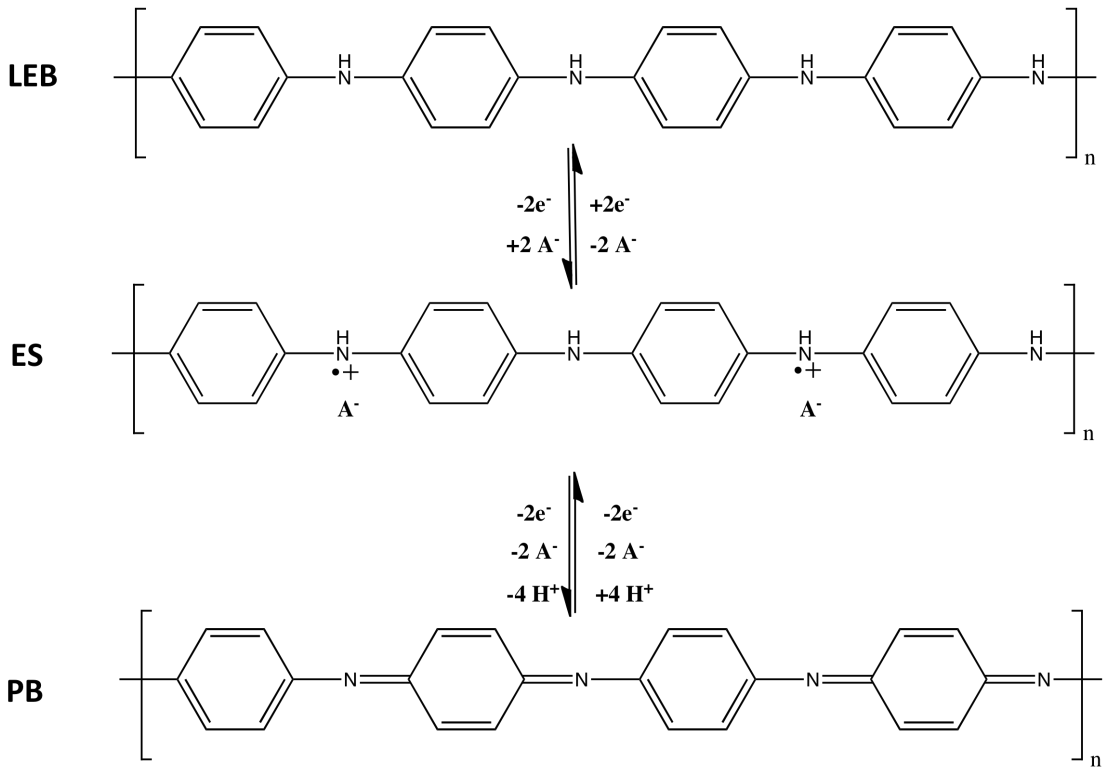

Figure 1.5: Redox chemistry of PANI: LEB undergoes partial oxidation to ES, which can undergo further oxidation to PB.

As the redox processes involve the direct injection and ejection of electrons into and out of the polymer backbone, each redox state has its own unique optical properties. EB (yellow) can be converted to ES (green) and PB (violet) respectively by addition of another redox couple in solution[88].

1.4.1.2 PANI pH chemistry

The ES form of PANI is rich in secondary amines, which act as classical Lewis/Bronsted bases resulting in a new equilibrium between ES and the deprotonated emeraldine base (EB). Deprotonation of the polymer backbone leads to a decrease in charge carriers, leading to a change in the conjugation along the backbone and a change in its optical properties (Figure 1.6 (Top)).

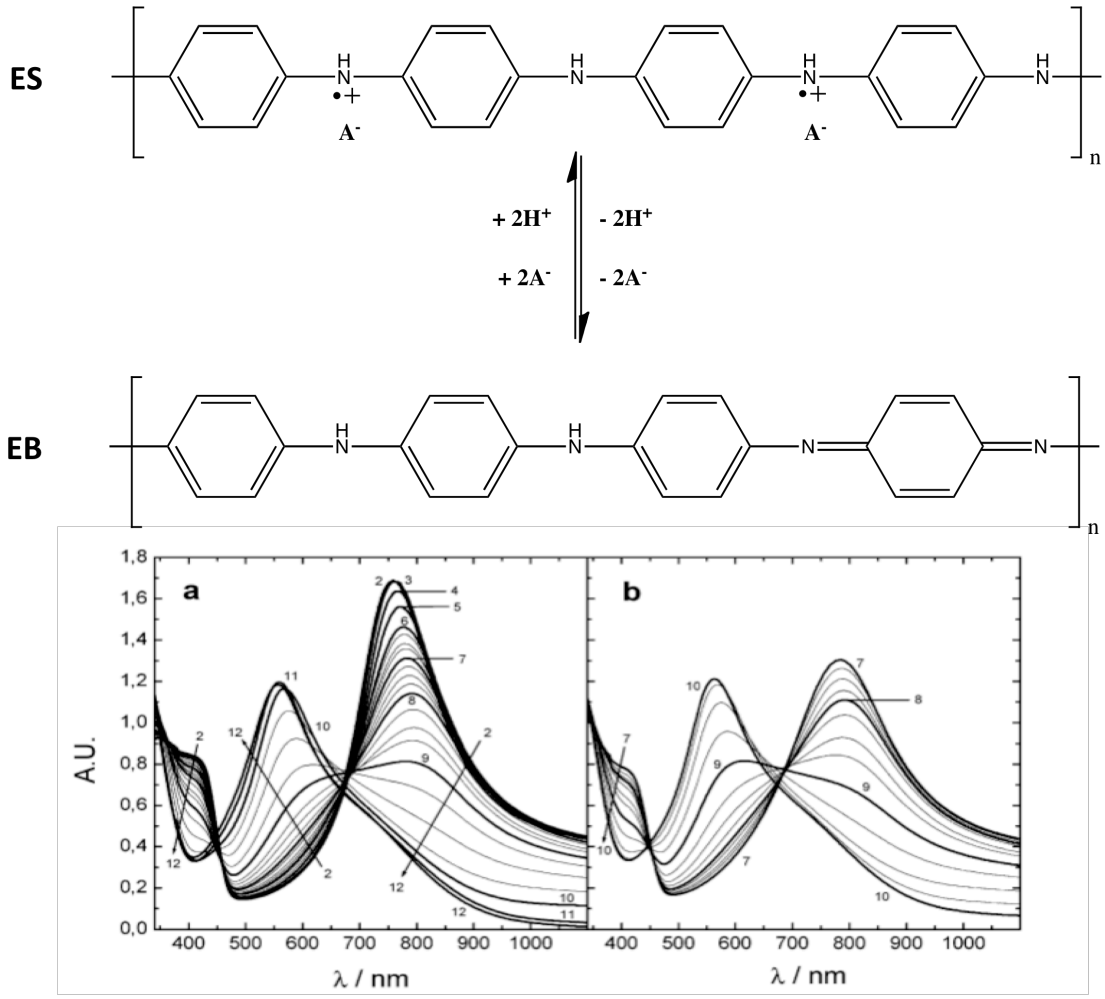

Figure 1.6: Acid-Base chemistry of ES and EB: **(Top)** Structural equilibria of ES and EB and **(Bottom)** the absorbance spectra obtained for PANI between pH 2-12 **(a)** and 7-10 **(b)**[88].

Lindfors *et al*. examined the pH chemistry of PANI nanoparticles in aqueous solutions stabilised by a surfactant and buffered accordingly[88]. By changing the pH of the dispersions using the appropriate agent, the changes in the visible spectrum could be recorded (Figure 1.6 (bottom(a) and (b)). The sensitivity of the reported results were attributed to long equilibriation times at each individual pH value.

The initial measurements took place at pH 2 which stabilised the ES form, therefore the absorption maxima at 415 and 757 nm could easily be attributed to this state. Increasing the pH of the solution caused the latter signals to linearly decrease, with a new absorbance centered at 568 nm. Based on the experimental parameters, the authors conclude the new spectral feature as a result of high pH's to arise from the EB form.

By combining the redox and pH responsive chemistries of PANI as discussed, these polymer based systems have found use within the literature as electrochromic displays[89] , in electrochemical sensing[90] and as optical pH sensors[91].

1.4.2 ILs as stimuli responsive materials

1.4.2.1 pH, photo-responsive ILs

As the explosion of interest in ILs as diverse, functional agents for multidisciplinary research continues, so too has the advent of ILs as stimuli responsive materials. This subsection for both research fields combines the respective chemistries of both, with a view to producing sensing liquids with negligible viscosity, intrinsic conductivity etc. Recently, three individual communications described ILs based on the photo and pH responsive chemistries of azobenzene. A general overview of the photo- and pH chemistry of the azobenzenes is described in figure 1.7.

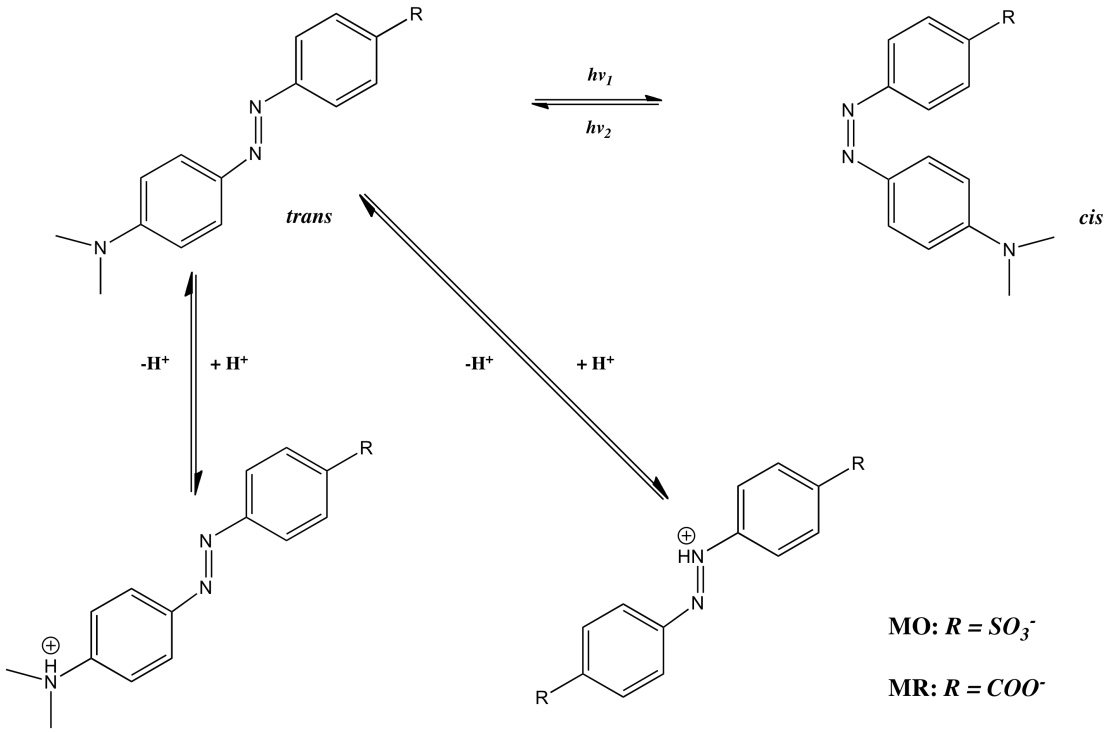

Figure 1.7: The photo and pH responsive chemistry of the azobenzenes dyes MO and MR adapted from Sanchez *et al.*[92] (for clarity the protonated *cis* isomers are omitted).

Azobenzenes are two phenyl subunits bridged by a central azo bond[93]. Photoisomerism can be achieved by light of the appropriate frequency, which causes the two phenyl subunits to switch between *cis* and *trans* conformations relative to the azo bond[94]. The two isomers also produce distinct absorption maxima[95]. Arguably the most common azobenzene derivatives in use are the pH responsive dyes methyl orange (MO) and red (MR)[96]. Both derivatives contain a dimethylamine substituted phenyl constituent but differ in structure at R, where they contain a carboxylate (MR) and a sulfonate (MO) group respectively (figure 1.7).

Pina *et al*. first described the synthesis of ILs based on MO[97]. ILs were prepared by allowing the sodium salt of MO to undergo ion-exchange metathesis with halide ILs of $[C_4mIm]^+$, $[P_{6,6,6,14}]^+$ and derivatives of sulfonium and guanidinium respectively, yielding intrinsically photochromic ionic liquids. The author's detail how the behaviour of photochromic ILs can be tuned by choice of the cation, as measured by the individual thermal relaxation rates from the *cis* back to *trans* structure of four different ILs dissolved in water and ethanol.

Zhang *et al*. developed on the concept of azobenzene functionalised ILs in two separate publications. In the first case, ILs based on imidazolium and pyrrolidinium cations and methyl red (MR) were prepared for use as acido-responsive sensors in aqueous and non-aqueous solutions[98]. MR differs slightly to MO in that a carboxylate group replaces the sulfonate in position R_1. The authors detail the advantages in preparing ILs with MR as shown in figure 1.8.

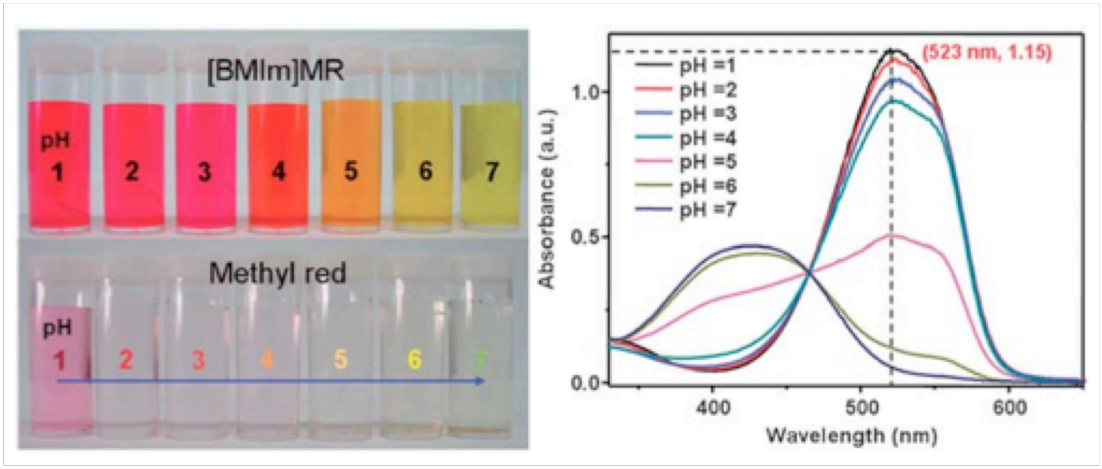

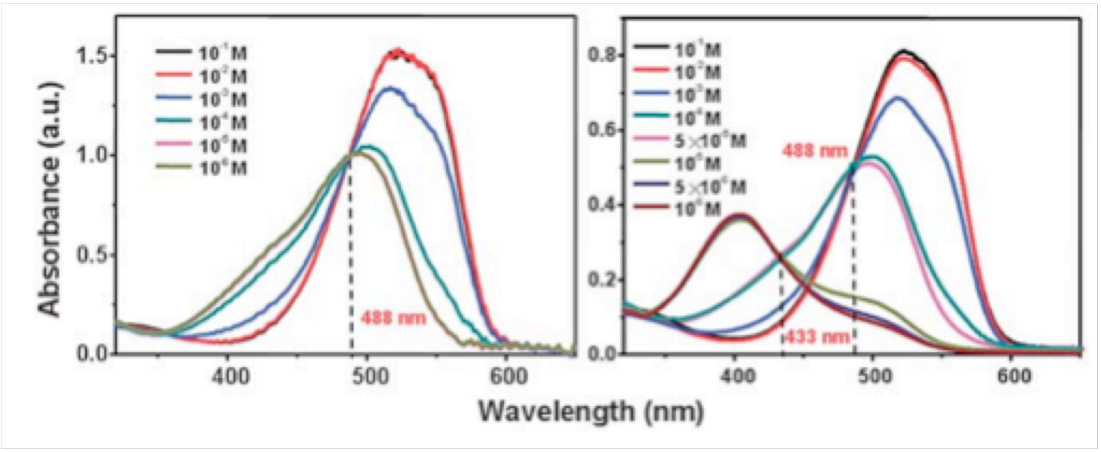

Figure 1.8: (Top) Increased selectivity of $[C_4mIm][MR]$ over the conventional Na^+ salt of MR from pH 1 to 7, and **(bottom)** the increased selectivity of the $[C_4mIm][MR]$ (*right*) to HOTf over the conventional sodium salt in ethanol (*left*)[98].

The sodium salt of MR was shown to be sparingly soluble in water, meaning its pH responsive chemistry is void in this solvent. By exchanging sodium for $[C_4mIm]^+$, the resultant IL was completely miscible with water and the pH responsiveness of the chromophore allowed a selective response to be observed in pH's ranging from 1 – 7 (figure 1.8 (top)).

Furthermore, an increased selectivity for the same IL over MR for *trifluoromethanesulfonic acid (HOTf)* was observed in solutions of ethanol (figure 1.8, (bottom)). The authors postulate a differing response mechanism for the ILs response over MR and attribute it to the increased response to HOTf at low concentrations.

This particular publication highlights the novelty and advantages of preparing ILs with stimuli responsive chromophores. The unique ionic nature of these liquids allows well-known chemistries to be performed in previously inhospitable solvent environments.

Zhang and co-workers published further work on ILs functionalised with azobenzenes, where they investigated the difference in ionic conductivity of the ILs in solution as a function of the *cis* and *trans* isomers[99]. Instead of performing an ion-exchange reaction, the authors prepared liquids where the chromophore was chemically tethered to an imidazolium cation via an ether linker. Physicochemical studies were peformed where chemical variants of the linker and the *ortho*-substituted phenyl ring subtituents were related to the photoresponsive ionic conductivity measurement obtained.

The authors demonstrated reversible changes in conductivity of the ILs in solution as high as 7 % in one instance. By inducing the *cis* isomer of a derivative with a methyl disubstitued phenyl ring, sterical disorder was induced throughout the whole system. It is this physical hindrance that predominates the reversible change in conductivity, the authors conclude.

1.4.2.2 Electrochromic ILs

A recent communication by Pina *et al*. described the syntheses of intrinsically electrochromic ILs based on the transition metal complexes of ethylenediaminetetraacetic acid (EDTA)[100]. Again the ILs were prepared via ion-exchange of its Na^+ salt with the relevant halide salt of cations based on $[P_{6,6,6,14}]^+$, $[C_2mIm]^+$ and a tetralkylammonium derivative.

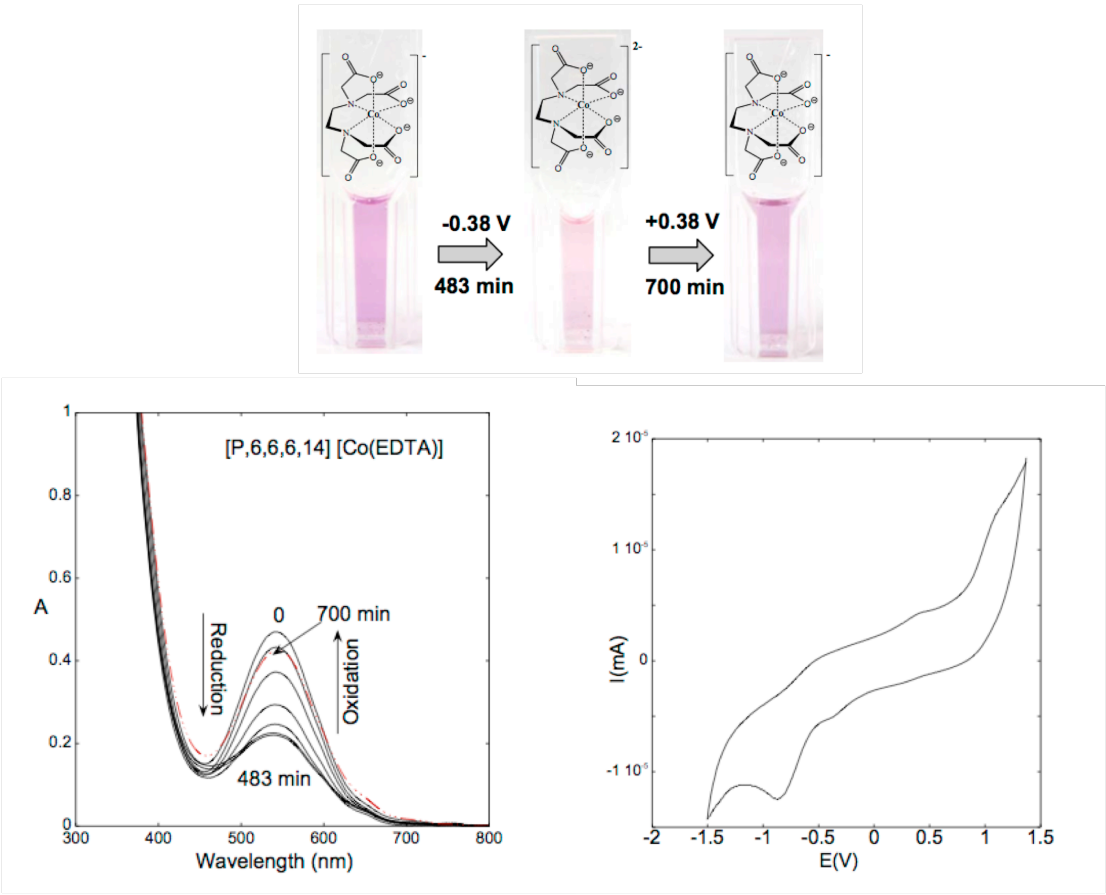

Figure 1.9: (Top) The reversible optical redox chemistry of $[P_{6,6,6,14}][Co(EDTA)]$.

(Bottom, Left) Change in absorbance as a function of the applied voltage and (**Bottom, Right)** the CV obtained for of $[P_{6,6,6,14}][Co(EDTA)]$[100].

Electrochromic materials change their optical properties in response to an applied voltage and are discussed in more detail in **sections 4.1 and 6.4.4.** In this case the electrochromic functionality of the IL is a result of the co-ordinated central atom switching between two distinct redox states ($Co^{2+/3+}$). A secondary electrolyte was not needed as the intrinsic conductivity of the IL facilitated the current between two electrodes. However the response times were poor , as high as 700 minutes for the oxidation of the cobalt complexed IL of $[P_{6,6,6,14}]$, and as low as 300 minutes for both reduction and oxidation of the $[C_2mIm]$ IL of the same complex.

1.4.3 Stimuli responsive ionogels

The advent of ionogels is proving to be a niche area of study within materials science. However, there are a few reports, which take advantage of **(a)** the chemistry of the IL and **(b)** the support matrix of the polymer to facilitate the chemistry required to gain an observed response from a stimuli responsive material.

The first report by Ahmad *et al*. describes the development of a complementary electrochromic device based on Tungsten oxide and Prussian blue[101]. The authors prepared on ionogel using sol-gel hydrolysis chemistry of TEOS in the presence of $[C_2mIm][NTf_2]$, which formed a solid state device upon solidification between two electrodes. In this case the responsive chemistry of the ionogel facilitated the current flow toward the electrodes (to which the chromophores were deposited), followed by a change in the optical properties of the device. The authors reported an ionic conductivity of 1.2×10^{-2} S/cm for the ionogel, which allowed the colouration efficiency of the device to be calculated at 64 cm^2/C.

Lunstroot *et al*. have developed the concept of ionogels exhibiting luminescence in two separate publications[102, 103]. Here the choice of the constituents of the IL and the supporting structure are critical in order to achieve this goal, and can be seen in figure 1.10.

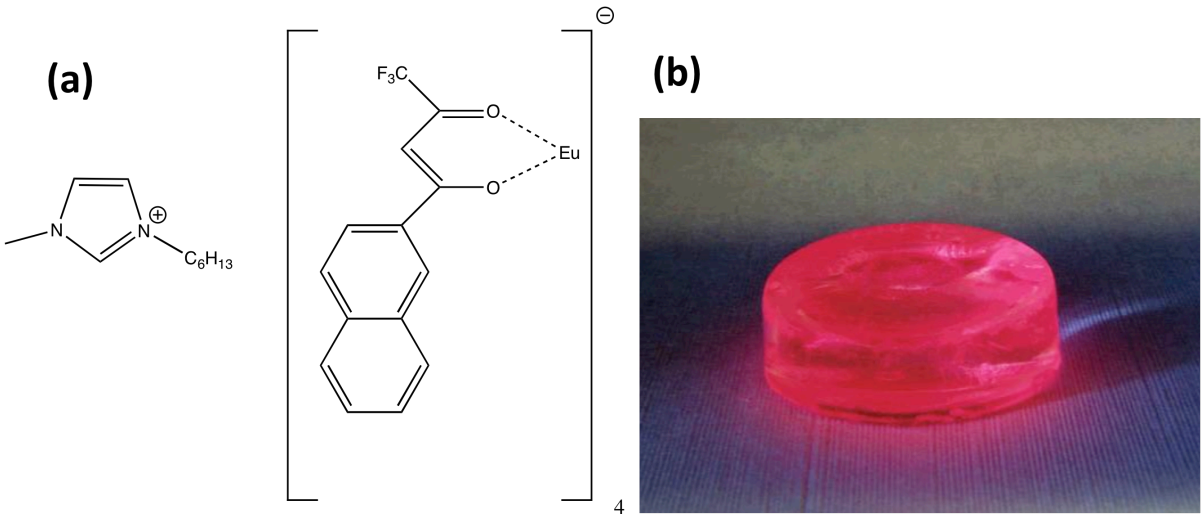

Figure 1.10: (a) The IL and Eu complex used by *Lunstroot et al*., which was immobilised within a sol-gel forming a solid state luminescent platform **(b)**[102]**.**

The authors describe the preparation of the luminescent ionogel platform in four individual steps. The first is similar to Ahmad *et al*[101]., in that the hydrolysis sol-gel chemistry is performed in the presence of an acid catalyst and an IL (in this case $[C_6mIm][NTf_2]$).

An ion-exchange reaction between [C_6mIm][Br] and the de-protonated anionic luminescent ligand was performed, to which $EuCl_3$ was added. Over time the imidazolium salt of the Eu complex precipitated out of this solution (Figure 1.10 (a)).

The incorporation of the luminescent complex was achieved through two steps: first the IL of the un-doped ionogel was removed via soxhlet extraction, and then the sol-gel was exposed to a liquid solution of the imidazolium/europium salt in [C_6mIm][NTf_2] over 48 hours. The sol-gel absorbed the Eu containing IL solution back into its porous framework.

In order for this detailed preparative route to be achieved the sol-gel structure must have exhibited a high porosity to facilitate the movement of liquids in and out. It must have also been mechanically stable without the presence of any liquid structure within. The ionogel exhibited red emission luminescence in response to UV light, leading the authors to conclude that a new platform had been achieved for luminescent optical device applications.

1.5 Thesis Overview

This thesis is based on the integration of three distinct areas of materials chemistry for the ongoing development of novel, chemical sensing platforms. These three distinct areas include: polymeric gels (*both organic and hybrid co-polymers*), stimuli responsive materials (*photo, electro, metalo and pH responsive)* and ionic liquids (*phospohonium and imidazolium based)*.

Polymer gel structures represent an ideal platform for the development of solid-state chemical sensors, as they can provide a support structure for specific interactions that lie within them. In fact if these interactions are those of the stimuli responsive material, the polymer gel presents a stable platform for the measurement of the chemical activity as a sensor signal response.

Chapter 3 is a summary of the initial studies of ionogels acting as *optodes*, a type of chemical sensor where the chemical event produces an optical signal. It was found that a phosphonium ionic liquid dramatically simplified the composition of the optode, producing a two-component system capable of discriminatory detection of Cu^{2+} and Co^{2+} ions. Furthermore, the ionogels behaved as mixed opto/electrical materials as characterised by their radio frequency signal when passed through an electrode channel.

Chapter 4 builds on the principles behind its previous chapter, however in this case the synthetic option was chosen to employ an IL within an optical device. A phosphonium IL based on a viologen moiety was synthesised, which acted as the supporting electrolyte and the electrochrome when photopolymerised between two

electrodes. Therefore, the device displayed a change in its optical properties when a voltage was applied to it.

The premise behind chapter 5 is to optimise the synthetic conditions used to produce class II hybrid sol-gels, so that they can accommodate the photo-responsive chemistry of an organic chromophore, *Spiropyran (SP)*. A particularly attractive feature of class II sol-gels is that they have been found to be of the optimum mechanical stability for sub-micron patterning, using a high focal point technology known as two-photon polymerisation. SP was found to chelate to sol-gels containing d-orbital metals, however Al based gels facilitated its chemistry and were subsequentially photopatterned into spiral structures exhibiting sub-micron resolution.

Chapter 6 explores photopatterning of novel sol-gel systems further. However in this case electro-responsive (*ILs, viologens and graphene)* were encapsulated within the polymer structures. Impedance spectroscopy was used to optimise the conductivity of the ionogels as a function of the concentrations of all three variants (gel, IL, graphene). In order to exhibit that these ionogels did indeed facilitate a current, a patterned electrochromic device of the ionogel that exhibited the highest conductivity was performed.

Finally chapter 7 includes some experiments designed to improve on some of the issues that arose within chapters 3 – 6. In particular: some experiments are suggested which could lower the detection limit of metal ion responsive ionogels; whilst other experiments are designed to optimise the various mechanisms towards the development of electrochromic ionogels.

1.6 References

1. S.-K. Ahn, R. M. Kasi, S.-C. Kim, N. Sharma and Y. Zhou, *Soft Matter*, 2008, **4**, 1151-1157.
2. Y. Osada and J. P. Gong, *Advanced Materials*, 1998, **10**, 827-837.
3. H. G. Schild and D. A. Tirrell, *Langmuir*, 1991, **7**, 665-671.
4. C. S. Brazel and N. A. Peppas, *Macromolecules*, 1995, **28**, 8016-8020.
5. S. Fujishige, K. Kubota and I. Ando, *Journal of Physical Chemistry*, 1989, **93**, 3311-3313.
6. D. Schmaljohann, *Advanced Drug Delivery Reviews*, 2006, **58**, 1655-1670.
7. L. L. Hench and J. K. West, *Chemical Reviews*, 1990, **90**, 33-72.
8. S. K. Lee and I. Okura, *Anal. Chim. Acta*, 1997, **342**, 181-188.
9. M. Stevens, *Polymer Chemistry: An Introduction*, Oxford University Press, New York, 1999.
10. U. Narang, P. N. Prasad, F. V. Bright, K. Ramanathan, N. D. Kumar, B. D. Malhotra, M. N. Kamalasanan and S. Chandra, *Analytical Chemistry*, 1994, **66**, 3139-3144.
11. M. Oubaha, M. Smaihi, P. Etienne, P. Coudray and Y. Moreau, *Journal of Non-Crystalline Solids*, 2003, **318**, 305-313.
12. G. Schottner, *Chemistry of Materials*, 2001, **13**, 3422-3435.
13. F. R. Zaggout, N. M. El-Ashgar, S. M. Zourab, I. M. El-Nahhal and H. Motaweh, *Materials Letters*, 2005, **59**, 2928-2931.
14. M. Oubaha, R. K. Kribich, R. Copperwhite, P. Etienne, K. O'Dwyer, B. D. MacCraith and Y. Moreau, *Optics Communications*, 2005, **253**, 346-351.

15. C. Barner-Kowollik, P. Vana and T. P. Davis, *Journal of Polymer Science Part a-Polymer Chemistry*, 2002, **40**, 675-681.

16. O. Krejza, J. Velicka, M. Sedlarikova and J. Vondrak, *Journal of Power Sources*, 2008, **178**, 774-778.

17. H. J. Naghash, A. Massah and A. Erfan, *European Polymer Journal*, 2002, **38**, 147-150.

18. P. Hiemenez and T. Lodge, *Polymer Chemistry (Second Edition)* Taylor & Francis Group, Boca Raton, FL., 2007.

19. J. M. Cowie, *Polymers: Chemistry & Physics of Modern Materials*, Stanley Thornes Ltd., Cheltenham, UK., 1991.

20. Z. Szablan, T. M. Lovestead, T. P. Davis, M. H. Stenzel and C. Barner-Kowollik, *Macromolecules*, 2007, **40**, 26-39.

21. K. J. Fraser and D. R. MacFarlane, *Australian Journal of Chemistry*, 2009, **62**, 309-321.

22. P. Wasserscheid and T. Welton, *Ionic Liquids in Synthesis*, WILEY-VCH, Weinheim, 2003.

23. P. Walden, *Bull. Acad. Imp. Sci. St. Petersbourg*, 1914, 1800.

24. S. Murugesan, S. Mousa, A. Vijayaraghavan, P. M. Ajayan and R. J. Linhardt, *Journal of Biomedical Materials Research Part B-Applied Biomaterials*, 2006, **79B**, 298-304.

25. B. R. Donius and J. L. Rovey, *J. Spacecr. Rockets*, 2011, **48**, 110-123.

26. T. Welton, *Chemical Reviews*, 1999, **99**, 2071-2083.

27. C. Zhao, G. Burrell, A. A. J. Torriero, F. Separovic, N. F. Dunlop, D. R. MacFarlane and A. M. Bond, *Journal of Physical Chemistry B*, 2008, **112**, 6923-6936.

28. D. E. Kaufmann, M. Nouroozian and H. Henze, *Synlett*, 1996, 1091-&.

29. P. Ludley and N. Karodia, *Tetrahedron Letters*, 2001, **42**, 2011-2014.

30. M. C. Tseng and Y. H. Chu, *Chemical Communications*, 2010, **46**, 2983-2985.

31. J. F. Liu, J. A. Jonsson and G. B. Jiang, *Trac-Trends Anal. Chem.*, 2005, **24**, 20-27.

32. C. Hardacre, J. D. Holbrey, M. Nieuwenhuyzen and T. G. A. Youngs, *Accounts of Chemical Research*, 2007, **40**, 1146-1155.

33. Z. Hu and C. J. Margulis, *Accounts of Chemical Research*, 2007, **40**, 1097-1105.

34. C. Reichardt, *Green Chem.*, 2005, **7**, 339-351.

35. R. Byrne, S. Coleman, K. J. Fraser, A. Raduta, D. R. MacFarlane and D. Diamond, *Physical Chemistry Chemical Physics*, 2009, **11**, 7286-7291.

36. R. Byrne, S. Coleman, S. Gallagher and D. Diamond, *Physical Chemistry Chemical Physics*, 2010, **12**, 1895-1904.

37. C. J. Bradaric, A. Downard, C. Kennedy, A. J. Robertson and Y. H. Zhou, *Green Chem.*, 2003, **5**, 143-152.

38. V. Ermolaev, V. Miluykov, I. Rizvanov, D. Krivolapov, E. Zvereva, S. Katsyuba, O. Sinyashin and R. Schmutzler, *Dalton Transactions*, 2010, **39**, 5564-5571.

39. S. Busi, M. Lahtinen, H. Mansikkamaki, J. Valkonen and K. Rissanen, *Journal of Solid State Chemistry*, 2005, **178**, 1722-1737.

40. T. Ramnial, S. A. Taylor, M. L. Bender, B. Gorodetsky, P. T. K. Lee, D. A. Dickie, B. M. McCollum, C. C. Pye, C. J. Walsby and J. A. C. Clyburne, *Journal of Organic Chemistry*, 2008, **73**, 801-812.

41. A. K. Burrell, R. E. Del Sesto, S. N. Baker, T. M. McCleskey and G. A. Baker, *Green Chem.*, 2007, **9**, 449-454.

42. D. R. MacFarlane, J. M. Pringle, K. M. Johansson, S. A. Forsyth and M. Forsyth, *Chemical Communications*, 2006, 1905-1917.

43. D. R. MacFarlane, J. Golding, S. Forsyth, M. Forsyth and G. B. Deacon, *Chemical Communications*, 2001, 1430-1431.

44. S. A. Forsyth, K. J. Fraser, P. C. Howlett, D. R. MacFarlane and M. Forsyth, *Green Chem.*, 2006, **8**, 256-261.

45. M. Armand, F. Endres, D. R. MacFarlane, H. Ohno and B. Scrosati, *Nature Materials*, 2009, **8**, 621-629.

46. J. Sun, M. Forsyth and D. R. MacFarlane, *Journal of Physical Chemistry B*, 1998, **102**, 8858-8864.

47. P. Hapiot and C. Lagrost, *Chemical Reviews*, 2008, **108**, 2238-2264.

48. M. C. Buzzeo, C. Hardacre and R. G. Compton, *Chemphyschem*, 2006, **7**, 176-180.

49. P. A. Z. Suarez, V. M. Selbach, J. E. L. Dullius, S. Einloft, C. M. S. Piatnicki, D. S. Azambuja, R. F. deSouza and J. Dupont, *Electrochimica Acta*, 1997, **42**, 2533-2535.

50. L. Xiao and K. E. Johnson, *Journal of the Electrochemical Society*, 2003, **150**, E307-E311.

51. K. Tsunashima and M. Sugiya, *Electrochemistry Communications*, 2007, **9**, 2353-2358.

52. S. Caporali, A. Fossati, A. Lavacchi, I. Perissi, A. Tolstogouzov and U. Bardi, *Corrosion Science*, 2008, **50**, 534-539.

53. J. Le Bideau, L. Viau and A. Vioux, *Chemical Society Reviews*, 2011, **40**, 907-925.

54. T. Ueki and M. Watanabe, *Macromolecules*, 2008, **41**, 3739-3749.

55. M. Shahinpoor and K. J. Kim, *Smart Materials & Structures*, 2001, **10**, 819-833.

56. C. F. J. Faul and M. Antonietti, *Advanced Materials*, 2003, **15**, 673-683.

57. M. A. Neouze, J. Le Bideau, P. Gaveau, S. Bellayer and A. Vioux, *Chemistry of Materials*, 2006, **18**, 3931-3936.

58. J. Jiang, D. Gao, Z. Li and G. Su, *Reactive & Functional Polymers*, 2006, **66**, 1141-1148.

59. Z. Li, J. Jiang, G. Lei and D. Gao, *Polymers for Advanced Technologies*, 2006, **17**, 604-607.

60. M. A. Susan, T. Kaneko, A. Noda and M. Watanabe, *Journal of the American Chemical Society*, 2005, **127**, 4976-4983.

61. R. E. Del Sesto, C. Corley, A. Robertson and J. S. Wilkes, *Journal of Organometallic Chemistry*, 2005, **690**, 2536-2542.

62. B. Peng, J. W. Zhu, X. J. Liu and Y. Qin, *Sensors and Actuators B-Chemical*, 2008, **133**, 308-314.

63. N. V. Shvedene, D. V. Chernyshov, M. G. Khrenova, A. A. Formanovsky, V. E. Baulin and I. V. Pletnev, *Electroanalysis*, 2006, **18**, 1416-1421.

64. D. V. Chernyshov, N. V. Shuedene, E. R. Antipova and I. V. Pletnev, *Anal. Chim. Acta*, 2008, **621**, 178-184.

65. K. Hanabusa, K. Hiratsuka, M. Kimura and H. Shirai, *Chemistry of Materials*, 1999, **11**, 649-655.

66. P. Terech and R. G. Weiss, *Chemical Reviews*, 1997, **97**, 3133-3159.

67. N. Mohmeyer, D. Kuang, P. Wang, H.-W. Schmidt, S. M. Zakeeruddin and M. Graetzel, *Journal of Materials Chemistry*, 2006, **16**, 2978-2983.

68. J. C. Ribot, C. Guerrero-Sanchez, R. Hoogenboom and U. S. Schubert, *Journal of Materials Chemistry*, 2010, **20**, 8279-8284.

69. J. C. Ribot, C. Guerrero-Sanchez, R. Hoogenboom and U. S. Schubert, *Chemical Communications*, 2010, **46**, 6971-6973.

70. S. Washiro, M. Yoshizawa, H. Nakajima and H. Ohno, *Polymer*, 2004, **45**, 1577-1582.

71. F. Ercole, T. P. Davis and R. A. Evans, *Polymer Chemistry*, 2010, **1**, 37-54.

72. R. J. Mortimer, in *Annual Review of Materials Research, Vol 41*, ed. D. R. F. P. Clarke, 2011, pp. 241-268.

73. D. Roy, J. N. Cambre and B. S. Sumerlin, *Progress in Polymer Science*, 2010, **35**, 278-301.

74. R. Byrne, F. Benito-Lopez and D. Diamond, *Materials Today*, 2010, **13**, 9-16.

75. R. Yerushalmi, A. Scherz, M. E. van der Boom and H. B. Kraatz, *Journal of Materials Chemistry*, 2005, **15**, 4480-4487.

76. Y. Z. Long, M. M. Li, C. Z. Gu, M. X. Wan, J. L. Duvail, Z. W. Liu and Z. Y. Fan, *Progress in Polymer Science*, 2011, **36**, 1415-1442.

77. F. Benito-Lopez, R. Byrne, A. M. Raduta, N. E. Vrana, G. McGuinness and D. Diamond, *Lab on a Chip*, 2010, **10**, 195-201.

78. S. Anastasova-Ivanova, U. Mattinen, A. Radu, J. Bobacka, A. Lewenstam, J. Migdalski, M. Danielewskic and D. Diamond, *Sensors and Actuators B-Chemical*, 2010, **146**, 199-205.

79. E. Bakker, P. Buehlmann and E. Pretsch, *Chemical Reviews*, 1997, **97**, 3083-3132.

80. I. Oehme and O. S. Wolfbeis, *Mikrochimica Acta*, 1997, **126**, 177-192.

81. O. S. Wolfbeis, *Journal of Materials Chemistry*, 2005, **15**, 2657-2669.

82. U. Lange, N. V. Roznyatouskaya and V. M. Mirsky, *Anal. Chim. Acta*, 2008, **614**, 1-26.

83. M. Deepa, A. Awadhia and S. Bhandari, *Physical Chemistry Chemical Physics*, 2009, **11**, 5674-5685.

84. P. C. Wang, E. C. Venancio, D. M. Sarno and A. G. MacDiarmid, *Reactive & Functional Polymers*, 2009, **69**, 217-223.

85. D. Chaudhuri and D. D. Sarma, *Pramana-Journal of Physics*, 2006, **67**, 135-139.

86. H. Goto, H. Yoneyama, F. Togashi, R. Ohta, A. Tsujimoto, E. Kita and K.-i. Ohshima, *Journal of Chemical Education*, 2008, **85**, 1067-1070.

87. I. Sapurina and J. Stejskal, *Polymer International*, 2008, **57**, 1295-1325.

88. T. Lindfors, L. Harju and A. Ivaska, *Analytical Chemistry*, 2006, **78**, 3019-3026.

89. D. R. Rosseinsky and R. J. Mortimer, *Advanced Materials*, 2001, **13**, 783-+.

90. P. C. Pandey and V. Singh, *Analyst*, 2011, **136**, 1472-1480.

91. D. J. Schmidt, E. M. Pridgen, P. T. Hammond and J. C. Love, *Journal of Chemical Education*, 2010, **87**, 208-211.

92. A. M. Sanchez, M. Barra and R. H. de Rossi, *Journal of Organic Chemistry*, 1999, **64**, 1604-1609.

93. K. Ichimura, S. K. Oh and M. Nakagawa, *Science*, 2000, **288**, 1624-1626.

94. C. L. Forber, E. C. Kelusky, N. J. Bunce and M. C. Zerner, *Journal of the American Chemical Society*, 1985, **107**, 5884-5890.

95. S. K. Oh, M. Nakagawa and K. Ichimura, *Journal of Materials Chemistry*, 2002, **12**, 2262-2269.

96. M. S. Masoud and H. H. Hammud, *Spectrochimica Acta Part a-Molecular and Biomolecular Spectroscopy*, 2001, **57**, 977-984.

97. L. C. Branco and F. Pina, *Chemical Communications*, 2009, 6204-6206.

98. Q. Zhang, S. Zhang, S. Liu, X. Ma, L. Lu and Y. Deng, *Analyst*, 2011, **136**, 1302-1304.

99. S. Zhang, S. Liu, Q. Zhang and Y. Deng, *Chemical Communications*, 2011, **47**, 6641-6643.

100. A. Branco, L. C. Branco and F. Pina, *Chemical Communications*, 2011, **47**, 2300-2302.

101. S. Ahmad and M. Deepa, *Electrochemistry Communications*, 2007, **9**, 1635-1638.

102. K. Lunstroot, K. Driesen, P. Nockemann, C. Gorller-Walrand, K. Binnemans, S. Bellayer, J. Le Bideau and A. Vioux, *Chemistry of Materials*, 2006, **18**, 5711-5715.

103. K. Lunstroot, K. Driesen, P. Nockemann, K. Van Hecke, L. Van Meervelt, C. Goerller-Walrand, K. Binnemans, S. Bellayer, L. Viau, J. Le Bideau and A. Vioux, *Dalton Transactions*, 2009, 298-306.

Chapter 2

Instrumental Techniques

2.1 Instrumental Techniques

2.1.1 Contact Angle Analysis

Contact Angle measurements were performed using a FTA 200® dynamic contact angle analyser, using deionized water as the probing liquid. All measurements were undertaken under ambient humidity and temperature conditions. The values quoted are the averages of 5 individual measurements.

2.1.2 Differential Scanning Calorimetry

DSC analysis was performed using a Q200 series calorimeter under the convention that endothermic is up and exothermic is down. All scans were performed using a 5 ^{0}C heating rate in the range from -80 to 100 ^{0}C (in triplicate). Thermal scans above room temperature were calibrated with the indium, tin and zinc with melting points at 156.6, 231.93 and 419.53 °C respectively. Transition temperatures were taken from the peak maximum of the thermal transition.

2.1.3 IR Spectroscopy

IR spectroscopy was performed using a Perkin Elmer Spectrum GX FT-IR System®. 40 scans were performed in the spectral range of 600 to 4,000 cm^{-1}, with a resolution of 2.00 cm^{-1}.

2.1.4 Electrochemical Impedance Spectroscopy

EIS characterization was performed using a CHI® Instruments 660A potentiostat. Screen-printed carbon paste silver electrodes with an active electrode area of $9mm^2$ were prepared in-house using a previously reported technique[1].

The electrodes were initially dropcast with a layer of POT (10^{-2}M in chloroform) to act as a transducer in order to aid the conversion of ionic to electronic conductivity[2].

For the results obtained in chapter 3: 100 μL of the optode membrane mixture composition to be analysed was dropcast onto the working electrode using a 1mL microsyringe. The optode membranes were then left to dry for one-hour, and finally placed in their metal salt solutions overnight before analysis.

In order to obtain the impedance of the non-complexed membrane, the electrode in question was placed in 6ml of a 0.1M KCl solution. K^+ is a soft, non-coordinating cation, and with no reported complexation behaviour with $[DCA]^-$.

For the results obtained in chapters 4 and 5: 50 μL of the ionogel mixture to be analysed was dropcast onto the working electrodes using a 1,000 μL autopipette.

The ionogels were then photopolymerised using the UV light source for a total period of 10 minutes. All EIS measurements for these chapters were performed using 0.1M KCl as the supporting electrolyte.

The impedance measurements were performed in the frequency range of 1 MHz to 0.01 Hz with a perturbation signal of 100mV. The reference electrode used was an aqueous Ag/AgCl (CHI® Instruments 111, surface area: 3.14 mm^2).

A platinum wire electrode (CHI® Instruments 115, surface area: 3.14 mm^2) was used as the counter. A nF capacitance shunt was used to reduce high frequency noise. All measurements were performed in triplicate.

2.1.5 NMR Spectroscopy

^1H and ^{31}P NMR spectroscopy was performed using a Bruker Avance® spectrometer (400 MHz.). $CDCl_3$ was used as the solvent in all cases and was used as purchased from Sigma-Aldrich® Ireland Ltd. Approximately 10 mg of sample per 0.7ml of deuterated solvent was used. Spectra were run at 30 ^oC and were calibrated with residual protonated solvent peak (i.e. $CHCl_3$ in $CDCl_3$).

2.1.6 Photo-Patterning of Polymer Gels

2.1.6.1 Direct UV Laser Writing

Fabrication of the photopatterned structures was carried out by UV exposure using the direct laser writing process. The laser writing system comprises a He–Cd laser (Kimmon Electric Co. Ltd, λ = 325 nm) and a computer controlled two-axis linear motor system. The co-ordinated movement of both axes of the linear motors moves the polymer gel thin film beneath the stationary laser beam polymerizing the film as it moves. This permits the direct imprinting of any desired pattern in the sol-gel. The speed of movement of the sol-gel coating beneath the laser beam was maintained at a constant 0.6 mm/s throughout all experiments. In order to evaluate the photoreactivity of the polymer gels, simple photopatterned lines were written over a range of UV energy densities (from 100–2200 $mJ.cm^{-2}$). The laser beam energy was controlled by a computer controlled acousto-optical modulator, which is synchronized with the linear motors through a custom-written Visual Basic user interface. After UV laser writing, the samples were rinsed in 1-butanol for 20 seconds in order to etch unexposed regions of the coatings, thus revealing the photopatterned sol-gel microstructures.

2.1.6.2 2PP Microstructuring

For the experiments conducted in chapters 5 and 6, a Ti:sapphire laser (Chameleon, Coherent) delivering pulses of 140 fs duration at a repetition rate of 80 MHz and a central emission wavelength of 780 nm was used. A 100X microscope objective lens (Zeiss, Plan Apochromat, N.A. = 1.4) was used to focus the laser beam into the volume of the photosensitive material.

2.1.7 Raman Spectroscopy

Raman spectroscopy was performed using a Perkin Elmer Raman Station 400F®. 40 scans were performed in the spectral range of 600 to 4,000 cm^{-1}, with a resolution of 2.00 cm^{-1}. Each spectrum was obtained with a total laser exposure time of 10 seconds, with a total of 20 exposures in each case.

2.1.8 Spectroelectrochemistry

Spectroelectrochemistry was performed using a Cary 50 Probe® UV/Vis spectrophotometer and a CHI® Instruments 660A potentiostat in tandem.

For chapter 4: The experiments were performed on all solid state devices based on ITO. The specifics of the device fabrications are discussed accordingly in **sections 4.3.6** and **4.4.3.**

For chapter 6: The experiments were performed using KCl (0.1M) as the supporting electrolyte. The reference electrode used was an aqueous Ag/AgCl (CHI® Instruments 111, surface area: 3.14 mm^2). A platinum wire electrode (CHI® Instruments 115, surface area: 3.14 mm^2) was used as the counter. ITO (to which the ionogel was photopolymerised) was used as the working electrode.

2.1.9 Solid-State Electrochromic Device Experiments

Solid-state electrochromic device experiments for experiments performed in **sections 4.4.5** and **6.4.5** were performed using a Isotech IPS1603D D.C. power supply, using an incident perturbation voltage in the range from 1 to 3 V.

2.1.10 Spincoating

Spin-coating was performed using a Laurell WS-650S® spin-coater, at a speed of 1000 rpm under an alcohol saturated environment. The purpose of spin-coating in an alcohol saturated environment is to control the kinetic of evaporation of the solvents during the deposition process, thus obtaining high optical quality and homogeneous thin films. For this purpose, the spin-coater was adapted to receive alcohol saturated N_2 which was produced by flowing nitrogen through sealed flasks containing IPA. Also, the introduction of N_2 into the spin-coater significantly reduces the levels of atmospheric humidity present during spin-coating (relative humidity was typically reduced to <10%).

2.1.11 Thermogravimetric Analysis

TGA analysis was conducted using a TA Q50® in a flowing dry N_2 atmosphere (50 mL / min.) between 25 and 800 °C with a heating rate of 10 °C / min. Sample sizes ranged between 10-20 mg. The instrument was calibrated using the curie points of four reference materials, Alumel, perkalloy, iron and nickel. Platinum pans were used in all experiments.

2.1.12 UV/Vis Spectroscopy

Unless specified, all UV/Vis absorption spectra were obtained using a Perkin Elmer Lambda 900 UV/Vis/NIR® spectrometer [*].

All spectra were obtained in the wavelength region spanning from 300 to 900 nm at 200 nm/minute, using a 1 nm data interval.

[*]The spectra obtained in figure 3.2 were obtained using a μQuant® plate well reader, under the same experimental parameters.

2.1.13 WRF Conductivity Analysis

WRF conductivity analysis measurements were performed using an A PCIS-3000 10-95 6536® radio frequency detector (Detection Systems, Melbourne, Australia). All measurements were performed at 83.18 kHz, the speed of the carousel was kept at 8.9 metres per minute.

The individual membranes to be analysed were initially cut to a 10 x 20 mm strip. The film strip was then placed onto a non-conducting glass slide and placed inside a polystyrene container. In order to improve the accuracy of the reading, the strip was aligned vertically with the signal vector from the instrument.
To further improve the accuracy of the measurement all samples were allowed to pass through the electrode channel 5 times.

2.1.14 XRF Measurements

XRF measurements were performed using the Thermo NITON® portable XRF analyser, using the standard thin film mode. In order to improve the accuracy of the measurement batch readings of 3 x 180 seconds were performed.

2.2 References

1. A. Morrin, A. J. Killard and M. R. Smyth, *Analytical Letters*, 2003, **36**, 2021-2039.

2. J. Bobacka, A. Ivaska and A. Lewenstam, *Electroanalysis*, 2003, **15**, 366-374.

Chapter 3

2-component optode membranes based on a multifunctional ionic liquid

3.1 Abstract

This chapter is based on simplifying the design template of an optical sensor through the multifunctionality imparted on it by an IL. The IL simplified polymer gel is termed an optode within this chapter as (a) it is prepared the same manner as optodes, (b) the IL performs many of the same functions as previous materials used in optode design and (c) the analyte or ion movement between the aqueous and organic phases follows the same convention for optodes.

The 2-component optode membrane is capable of generating three distinct colours in the presence of Cu^{2+} and Co^{2+} ions. It has been found that the IL $[P_{6,6,6,14}][DCA]$ can act as plasticizer, ligand and transducer dye when used in PVC membranes, which significantly simplifies the optode membrane cocktail.

Upon exposure to an aqueous Cu^{2+} solution, a yellow colour is generated within the membrane, while exposure to aqueous Co^{2+} solution generates a blue colour. Exposure to a solution containing both ions produces a green colour. Vibrational spectroscopy has been used to investigate the molecular basis of the IL-metal ion binding mechanism. Analytical characteristics of the membranes including the effect of interfering ions, binding constants and the limit of detection for both ions have been estimated. A case of simultaneous dual-analyte recognition is presented based on two distinct absorption maxima.

The inherent conducting properties of the IL membranes are then investigated as a possible detection channel using WRF. WRF is a novel detection technique, which monitors the conductivity of a given sample *wirelessly,* allowing non-contact detection and measurement of IL-PVC membranes. The various co-ordinated membranes produce a discriminatory drop in the resulting signal, which is a direct

function of the specific metal ion (Cu^{2+}, Co^{2+} or a mixture) co-ordinated to the IL. The results of the novel WRF technique have been validated principally by EIS; whilst XRF is used to elucidate both WRF and EIS trends.

3.2 Introduction

The vast majority of chemical sensors are based on a ligand that selectively binds an ion of interest. The ligand is typically incorporated within a polymer matrix,[1] or directly immobilised on the surface of a transducer[2]. In addition to a suitable ligand, polymer membrane-based chemical sensors normally require an ion-exchanging salt, and if detection is performed using optical spectroscopy, a chromo-responsive dye.

There has been great interest in simplifying these chemical sensor cocktails, for example, through the development of plasticizer-free matrices,[3, 4] covalent attachment of active sensing components to polymer backbone[3-5], and improving the lipophilicity of sensing components[6-8].

Whilst the development of smart materials designed for more sophisticated chemical sensing templates is still ongoing [9, 10], the engineering of new sensing instrumentation and on how the information is retrieved is actively pursued in parallel[11, 12]. The development of new sensing materials seems to be based on the use of single molecular probes capable of simultaneous determination of multianalytes [13, 14], and also on simultaneous detection via multiple detection channels inherent to the material studied [15-17].

At the same time, the instrument used for detection should be non-invasive on the sample, and be capable of performing multiple analyses in a short space of time. Combining these efforts represents an obvious incentive to improve many aspects of chemical sensing, such as in the remote, autonomous monitoring of analytes [18, 19].

Interestingly, utilization of more universal components that employ several roles thereby reducing the actual *number* of active components whilst retaining the membrane functionality has not been explored much, perhaps because of the lack of suitable materials.

$[P_{6,6,6,14}]$[DCA] was identified as an IL capable of fulfilling multiple roles in polymeric optodes thereby dramatically simplifying their composition. First used to impart low viscosity in a new generation of ILs [20, 21], $[DCA]^-$ had previously been termed a pseudohalide that behaves as a ligand capable of binding to a variety of d-block elements (most notably Cu^{2+}, but also Co^{2+}, Mn^{2+} and Fe^{2+})[22-24].

This co-ordination chemistry has been utilised in order to demonstrate simultaneous, dual analyte recognition using a very simple, two component (polymer and IL) optical sensing membrane in "proof of concept" experiments.

This concept is then expanded to incorporate the use of IL's in polymeric membrane based sensors capable of generating optical and electrochemical signal responses. The WRF detection instrument used in this study works particularly well for solid state, conductive samples. A signal is produced that is a direct function of the ability of the solid material to facilitate an electrical conductivity through ion movement. It has the required sensitivity, is non-invasive on the sample to be analysed and is capable of batch analyses in short spaces of time[25].

The WRF instrument produces a signal in arbitrary units; its response has been validated principally by EIS. The level of ion coordination within the respective membrane has been characterised XRF; which allows the reader to elucidate both observable trends in the WRF and EIS results.

3.3 Experimental

3.3.1 Chemicals and materials:

PVC, POT, $Cu(NO_3)_2$, $Co(NO_3)_2$, Potassium Chloride, Europium (III) Chloride, Manganese (II) Chloride, Nickel (II) Nitrate hexahydrate and Aluminum oxide (activated, basic, Brockmann 1) and were used as purchased from Sigma-Aldrich® Ireland Ltd.

$[P_{6,6,6,14}]$[DCA] was generously donated by Cytec® industries. Further purification was achieved by washing with both water and hexane, and by column cleansing with basic alumina[26].

3.3.2 Membrane preparation:

Both PVC and $[P_{6,6,6,14}][DCA]$ (1:2 (w/w)) were added to 2 ml THF and stirred until dissolved. The membrane solution was then poured into a glass ring on a glass slide held together by rubber bands. The resulting films were covered until THF fully evaporated (approx. 24 hours).

For multiple analyses, 100µL aliquots of the cocktail solution can also be streaked over a square, unsilanized microscope cover slide (2.2 cm wide) and again left to dry.

In order to generate the optical response, the membranes obtained were then exposed to 500µL of the respective metal ion salt solution of desired concentration for 30 mins. The salt solution was then removed using a pipette and dried overnight at 40^0C, leaving the desired colour free for analysis.

3.4 Results and Discussion

3.4.1 Initial IL complexation

In order to examine the co-ordinating abilities of $[P_{6,6,6,14}]$ [DCA], it was initially exposed to salts of $Cu(NO_3)_2$ and $Co(NO_3)_2$ independently. This resulted in a strong yellow coloration of the IL in the presence of $Cu(NO_3)_2$, and a deep blue coloration in the case of $Co(NO_3)_2$. Furthermore when $[P_{6,6,6,14}]$[DCA] was exposed to an equal mixture of both ions a green colouration was observed due to the co-existence of the two coloured complexes, indicating simultaneous binding of both Co^{2+} and Cu^{2+} ions. The individual colours are depicted in figure 3.1 below.

Figure 3.1: *From left to right*: IL, IL + $Cu(NO_3)_2$ (yellow), IL+ equimolar mixture (green) and IL + $Co(NO_3)_2$ (blue).

In order to document to change in optical properties, UV/Vis absorption spectra were obtained using a µQuant® plate well reader. In both cases the spectra were obtained by adding 500µL of a 0.1M respective metal salt solution to 500µL of $[P_{6,6,6,14}][DCA]$. The aqueous layer was removed by leaving the plate well in an oven overnight at 60 ^{0}C (Figure 3.2).

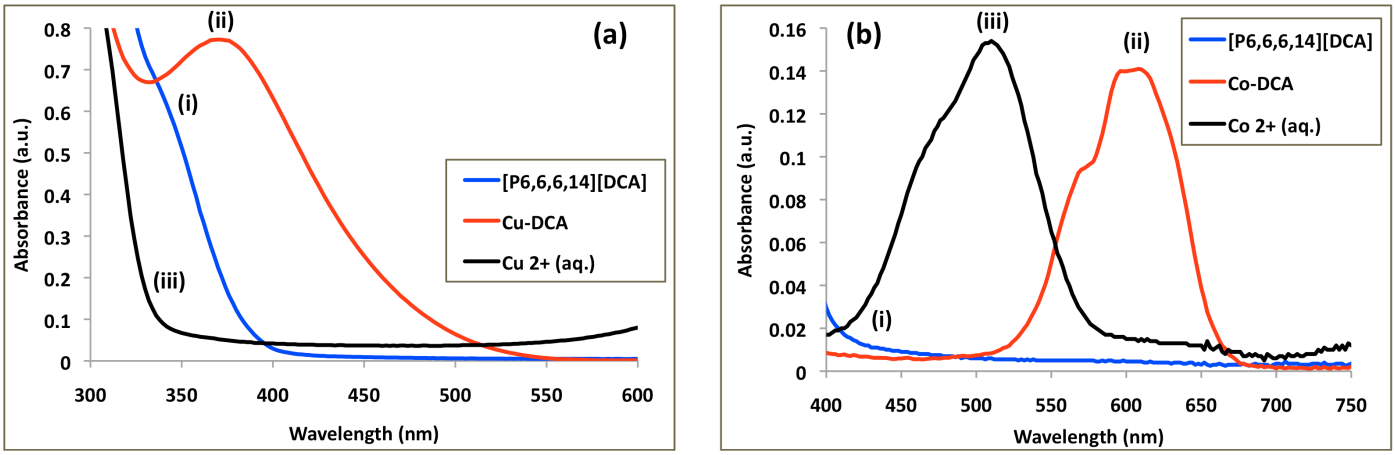

Figure 3.2: The UV/Vis absorption spectra obtained for (i) $[P_{6,6,6,14}][DCA]$, (ii) the co-ordinated sample and (iii) the original aqueous metal salt solution. **(a)** represents the spectra involving Cu^{2+} and **(b)** represents those occurring with Co^{2+}.

$[P_{6,6,6,14}][DCA]$ was found to observe an absorption maximum at 346 nm, upon complexation to Cu^{2+} this maximum undergoes a red shift to 370 nm characteristic of the yellow colour. A red shift was also observed upon complexation with Co^{2+}, in this case the new maxima was observed at 600 nm.

3.4.2 Vibrational Spectroscopy Analysis

The next step was to explore the role of the IL in the complexation process. For this, both IR and Raman Spectroscopy were employed.

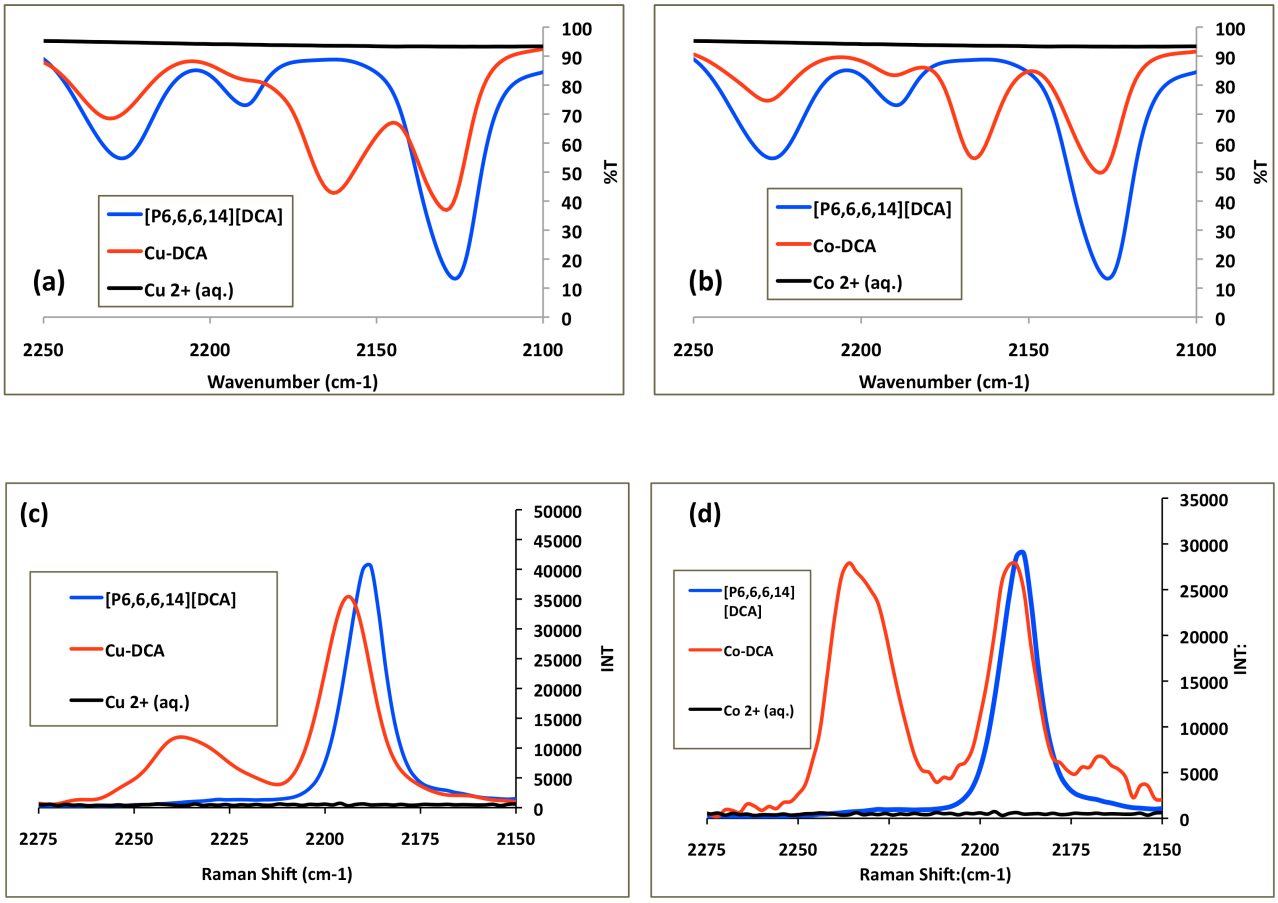

Figure 3.3: (a) and **(b)** The IR spectra obtained for (i) $[P_{6,6,6,14}][DCA]$, (ii) $[P_{6,6,6,14}][DCA]$ exposed to metal salt and (iii) the aqueous salt solution, **(c)** and **(d)** The corresponding raman spectra obtained for three distinct species.

Figure 3.3 (above) shows the region in the vibrational spectrum where the contribution of the asymmetric nitrile stretch of the anion occurs[29, 30].

In all four cases the spectra depict the following: (a) the initial stretch of the IL before complexation (ν_{max}/cm^{-1} ~2125), (b) the effect of co-ordination of the metal ion to the IL and (c) the spectra of the metal ion aqueous solution.

The IR and Raman co-ordination spectra of nitrile based complexes have been the subject of previous reviews by Nakamoto[31] and Griffith[32], and further specialised work by Friedrich[33]. A feature of the spectrum that is agreed upon by all is that the initial nitrile stretch is substantially reduced upon co-ordination, along with the formation of a new stretch at higher frequencies.

The degree of this new stretch is a direct function of the electronegativity of the complexing metal, with increasing metal electronegativity resulting in new stretches at higher frequencies[31]. Figure 3.3 clearly shows that upon co-ordination a new band appears at ν_{max}/cm^{-1} 2162 (for Cu-DCA) and ν_{max}/cm^{-1} 2166 (for Co-DCA), which can be attributed to the impact of ion-binding on the nitrile stretch.

It is important to note that similar effects were not observed upon addition of other ions such as H^+, K^+, Eu^{3+}, and Mn^{2+}, suggesting that $[DCA]^-$ does not complex these ions.

3.4.3 Membrane preparation

In view of these encouraging results, the possibility of preparing a polymer membrane-based optode using polyvinylchloride (PVC) as a polymer and the IL as a plasticizer was explored. The membrane composition was 33% wt PVC and 66% wt $[P_{6,6,6,14}][DCA]$, a composition typical of PVC-plasticizer-based optodes[34].

However, it was expected that the IL would fulfil multiple roles – membrane plasticizer, ion-complexing ligand and indicator/transducer dye – thereby simplifying the platform by significant reduction of active components. The resulting membranes were transparent, homogeneous and approximately ~10 μm thick.

Exposure of the membranes to the respective metal ion solutions yielded the same colours as obtained with the IL (Figure 3.4).

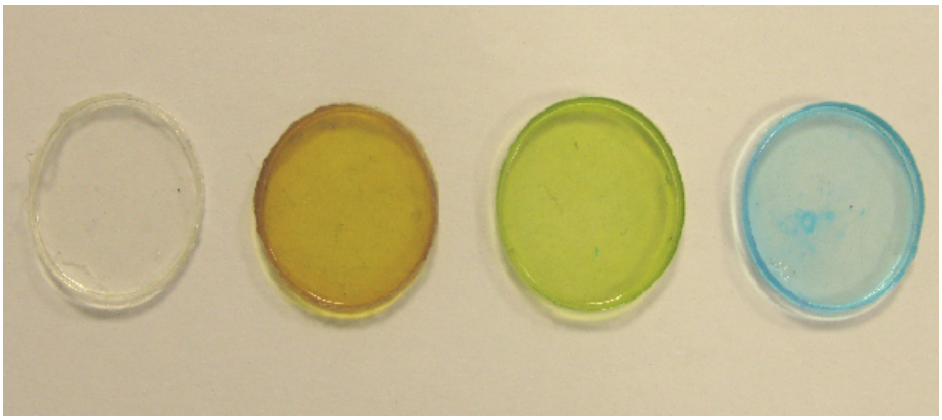

Figure 3.4: Two-component IL-PVC polymeric optode membranes capable of generating 3 distinct optical responses.

As the migration of ions into polymeric optode membranes can occur via one of two distinct mechanisms, co-extraction or ion-exchange[34-36], it is important to determine which is occurring in the case.

Ion-exchange mechanisms typically involve the deliberate addition of an ion-exchanging salt, which facilitates ion transfer between both phases. These so called "ionic sites" are typically composed of an organic, lipophillic ion and a mobile counter ion. The charge of the mobile ion is dependent on the charge of the target analyte. For the cation exchange process the target analyte initially enters the organic phase whilst at the same time the moblie counter ion of the ionic sites migrates out in order to preserve the membrane charge balance.

In contrast, the co-extraction mechanism involves simultaneous extraction of the target ion and its counter ion from the aqueous phase into the membrane to preserve charge balance. If the anion from the IL serves as a charged ionophore and binds to a sample ion, the ion-exchange mechanism would only be possible if the cation from the IL migrates into the solution.

This mechanism clearly cannot be the case in our system, since the high lipophilicity of the high molecular weight tetraalkylphosphonium cation would not allow it to partition easily into the aqueous phase. Therefore, in this work co-extraction is assumed as the prevailing mechanism of ion transfer.

3.4.4 Response times

The response time for these membranes is given by the time necessary to achieve a uniform concentration of optically relevant components. Diffusion of ions into the membrane phase is usually the limiting process. The time needed to achieve 95% of the signal is given as:

$$t_{95\%} = 1.13\frac{d^2}{D} \qquad (3.1)$$

Where d is the membrane thickness and D is the diffusion coefficient of the ion-ligand complex in a typical PVC-plasticizer based membrane species. With a membrane thickness of 10mm and a typical $D \approx 10^{-8} cm^2/s$ the $t_{95\%}$ response time should be approximately 100 seconds[34].

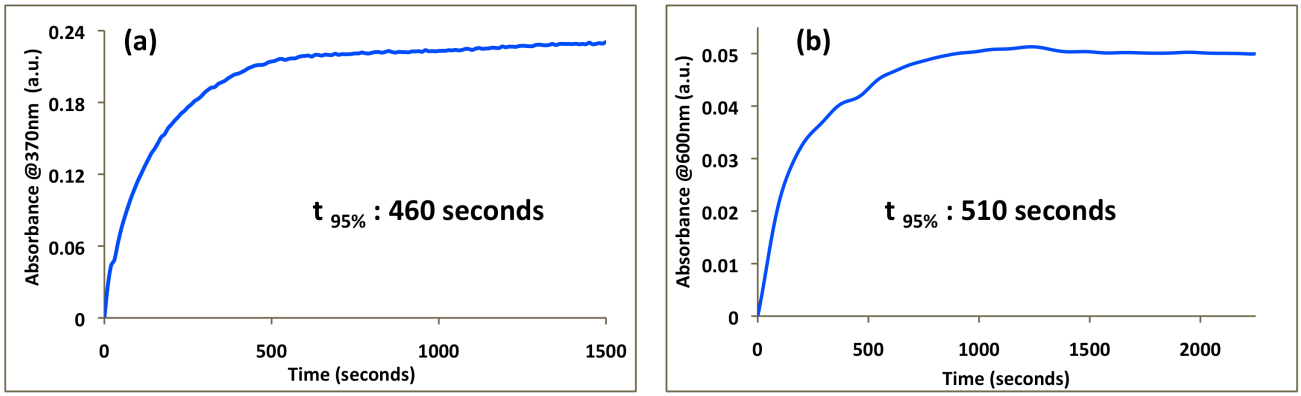

Figure 3.5: Response times obtained for Copper (left) and Cobalt (right) complexation.

Figure 3.5 shows the response of PVC-[$P_{6,6,6,14}$][DCA] based membranes that have been exposed to 2 ml of 0.1M $Cu(NO_3)_2$ (left) and $Co(NO_3)_2$ (right) solutions respectively.

The results of the device thickness analysis can be found in figure A1, yielding an average thickness of 120 μm ± 6.6 μm. The response values obtained for $t_{95\%}$ are 460 ± 14 seconds for Cu^{2+} and 510 ± 13 seconds for Co^{2+}. As the membrane is approximately an order of magnitude higher in this case, the response times obtained are within acceptable levels.

3.4.5 Calibration of response, limit of detection estimation

In order to determine the limit of detection for both analytes, individual membranes were exposed to a series of Cu^{2+} and Co^{2+} solutions and measured the UV/Vis absorbance at the maximum absorbance wavelength (370nm for Cu^{2+} and 600 nm for Co^{2+} ions).

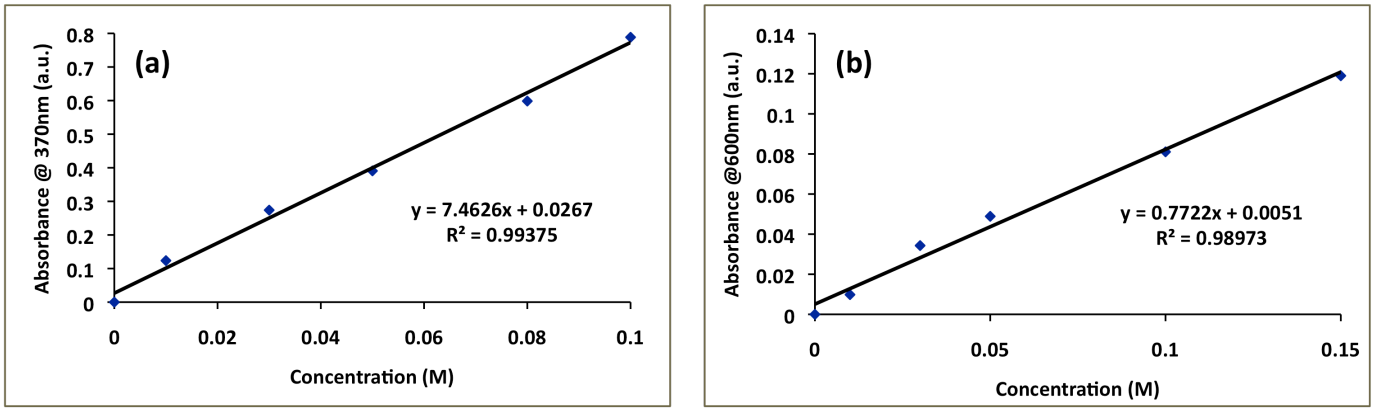

Figure 3.6: Calibrated response curves obtained for Cu^{2+} **(a)** and Co^{2+} **(b)** complexation.

The limit of detection was calculated by first obtaining the standard deviation of three blank membrane measurements, and then by adding three times this value to the absorbtion of the blank membrane at the individual complexation absorbtion maxima. By fitting this value to the equation of the line of the calibrated response, the limit of detection for Cu-DCA was estimated to be 7.62 x 10^{-4} M and 2.91 x 10^{-4} M for Co-DCA.

3.4.6 Estimation of stoichiometry and binding constants

The binding constants for both ions were calculated using a series of equations based on a previously reported theory[37, 38].

In these equations; α represents the ratio between both the free and initial ligand concentrations (equation 3.2).

$$\alpha = \frac{[L]}{[L_{tot}]} = \frac{(A_{complexed} - A)}{(A_{complexed} - A_{uncomplexed})} \qquad (3.2)$$

$A_{complexed}$ values were obtained from a series of membranes exposed to metal ion salt solutions (concentrations were the same as for calibration curves). $A_{uncomplexed}$ was obtained by measuring the absorbance of a blank membrane prior to exposure to metal salt solution, and A was obtained by measuring the absorbance of the original metal ion .

By plotting α against the logarithmic concentration of metal ion present, both the binding constant and stoichiometric ratio can be estimated.

$$[M^{n+}]^m = \frac{1-\alpha}{nK[L_{tot}]^{n-1}\alpha^n} \qquad (3.3)$$

Equation 3.3 was used to determine the results one would obtain from model stoichiometries; i.e. M1:L1, M1:L2 and M2:L1 ((M= metal, L = Ligand)) and these have been plotted against the experimentally obtained values (black dots). In this case $[M^{n+}]^m$ represents a metal ion of charge n, and K can be defined as the equilibrium constant of metal-ligand complexation.

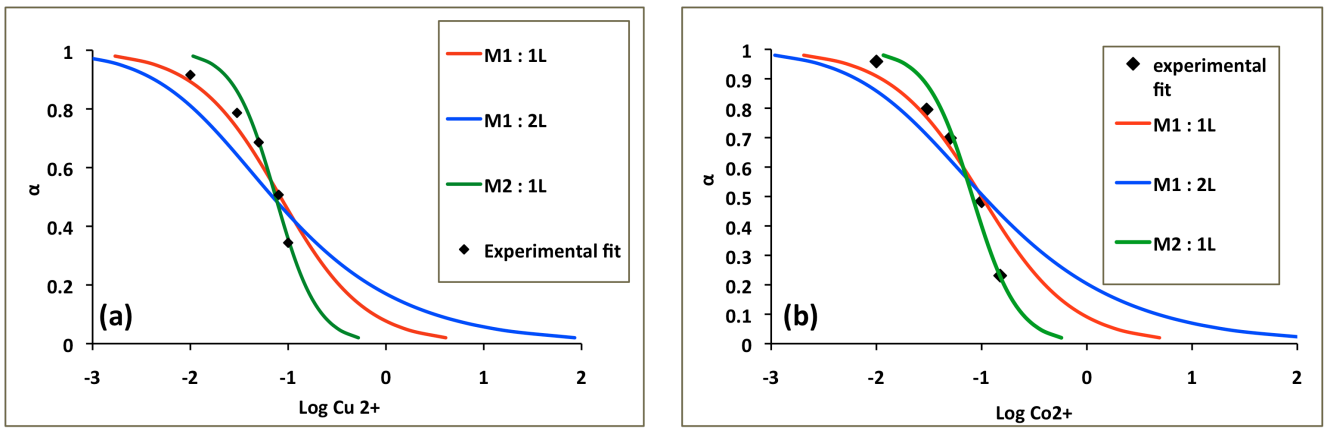

Figure 3.7: Response parameter α as a function of logarithm of Cu^{2+} (a) and (b) Co^{2+} concentration.

Counter-intuitively, the best fit is obtained in the case when M=2 and L=1 i.e. two metal ions for every $[DCA]^-$ binding site which represents an obvious charge imbalance.

One possible explanation is that this reflects the complex binding nature of the ligand. High delocalization of charge across $[DCA]^-$ results in many possible binding modes, with Batten *et al.* stating that up to 8 mono, bi and multidentate co-ordination modes have been reported[39]. This rich binding diversity has led to $[DCA]^-$ being used as a bridging ligand in chain structures, in various 1,2 and 3-D co-ordinated networks[40, 41] and in topologies exhibiting magnetic properties[42], with some unusual and unexpected binding modes also reported in the latter case[43]. Therefore, the unusual binding stoichiometry obtained here is not as surprising as would initially seem to be the case.

The binding constants obtained by fitting the aforementioned curves with experimental data were log K = 2.25 and log K = 2.17 for the Cu^{2+} and Co^{2+} complexes, respectively.

3.4.7 Effects of interfering ions

To explore the relative affinity of $[DCA]^-$ for Cu^{2+} and Co^{2+}, and its selectivity against other cations, a series of membranes were exposed to solutions containing either Cu^{2+} or Co^{2+}, and the competing ion in a 1:1 (vol. /vol.) mixture. The concentration of both ions in the mixture were kept at 0.1M.

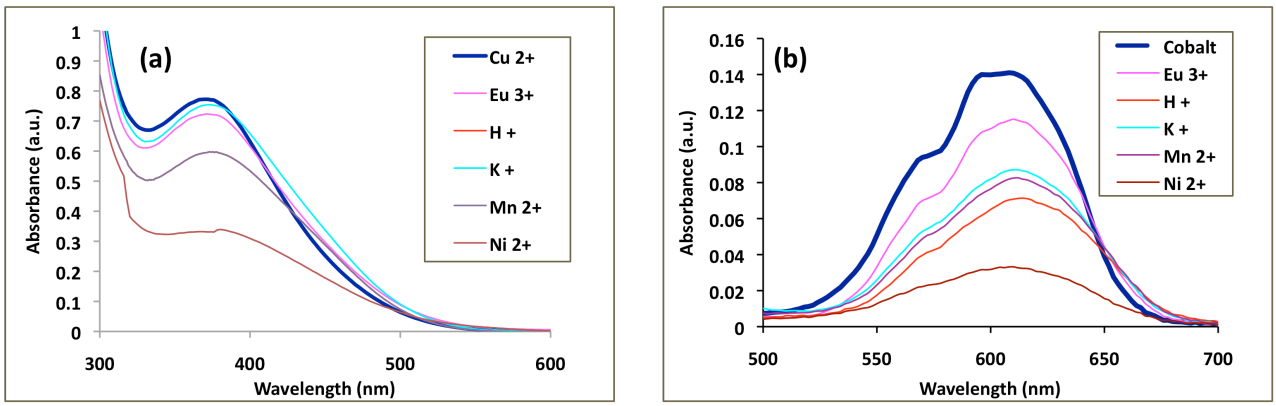

Figure 3.8: Interference spectra obtained for Copper (left) and Cobalt (right) complexation.

The potential interference effects measured were the effects of pH, monovalent cations, other d-block elements such as Ni^{2+} and Mn^{2+} with which $[DCA]^-$ has been reported to bind, and a trivalent lanthanide cation.

From Figure 3.8 (above) it can be seen that, of the interferents screened, a reduction in the absorbance occurs in each case, and the order of influence is similar (Ni^{2+} >>H^+>>Mn^{2+}>K^+≈Eu^{3+}). The effect of potential interfering ions was much smaller in the presence of Cu^{2+} ions, than for Co^{2+} ions.

Although the binding constants obtained are similar, the calculated exctinction coefficient for Cu^{2+} complexes is much higher, which explains the less dramatic interference effects.

One result to note is the substantial interference arising from Ni^{2+} in both cases. As stated previously, Ni^{2+} has been reported as forming complexes with $[DCA]^{-}$[24]. The addition of a Ni^{2+} to the IL- based membrane however, produces no notable colour which opens the door for an alternate detection technique; and will be discussed accordingly later in this text.

3.4.8 Dual analyte recognition

Interestingly, even though the interferents screened above do, to a greater or lesser extent, reduce the spectral absorbance, they do not generate *new* absorbance peaks. Given the fact that the complexes formed absorb at two distinct regions in the visible spectrum, the possibility of generating a dual analyte sytem capable of measuring a series of mixtures of both ions was explored.

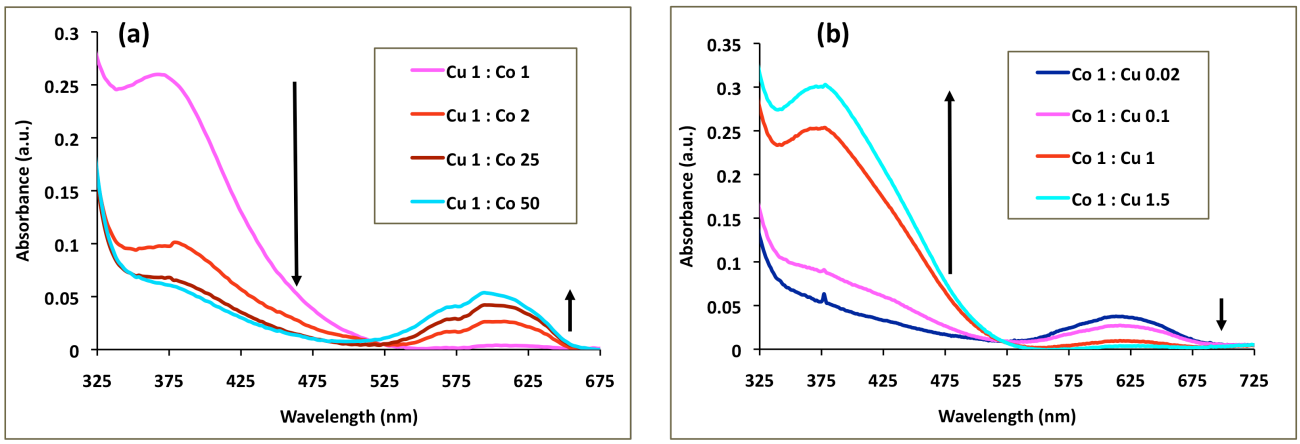

Figure 3.9: Dual-Analyte recognition based on two absorption maxima.

The results of these experiments are shown above in Figure 3.9. In both cases the concentration of one ion in the original mixture is kept constant, while the other in incrementally increased. This allowed for an inverse relationship to occur at both absorption maxima, in both cases.

The change in absorbance at the characteristic wavelength for each of the involved ions originates from competition for the same ligand and displacement of bound cations by the competing cation. The great importance of this finding is that this two component system is effectively self-indicating. It clearly shows whether ions of interest are present as individual or as a mixture without the need to add a dye.

3.4.9 WRF detection

The WRF detector system used in this study utilises radio frequency technology in order to obtain the conductivity of a sample as it passes through a defined point.

This point is the transmitting electrode, which passes a low voltage, low-frequency AC signal toward a receiving electrode wirelessly. The sample to be analysed is housed in an insulating polystyrene based container, which is then placed on a miniature conveyor (Figure 3.10 (a)).

The insulating container with the sample placed inside is then allowed to pass through the electrode channel where it is processed and analysed via a PC. It has been used to great effect previously for the wireless detection of acetic acid and ammonia vapour using ink-jet printed polyaniline dispersions [25].

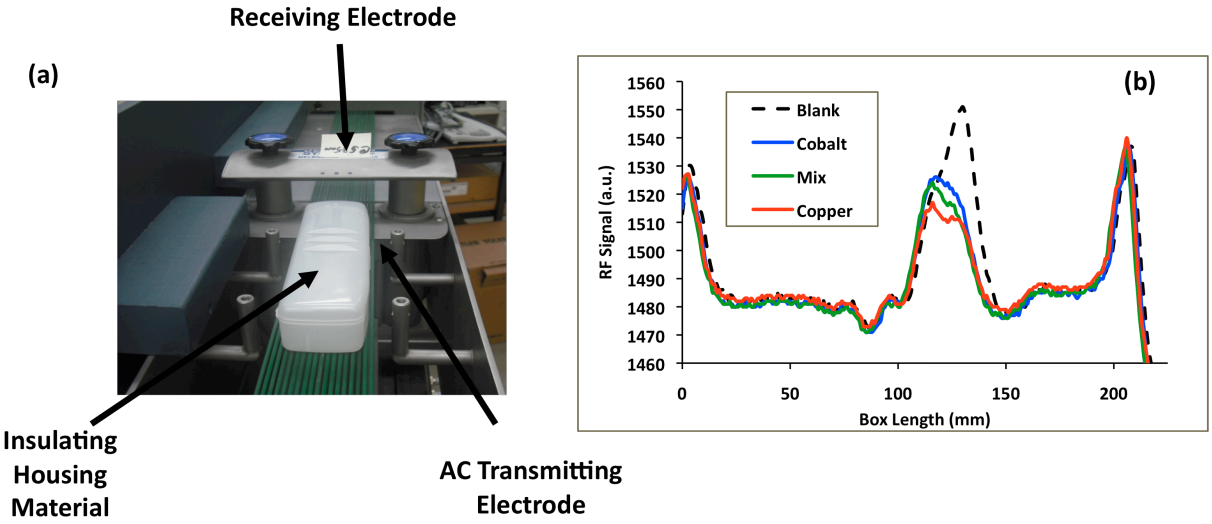

Figure 3.10: (a) The WRF instrument used in this work. The sample to be analysed is placed in the insulating material (centre) and passed along the green carousel through the detection channel containing the transmitting and receiving electrodes, **(b)** signals obtained for membranes containing PVC:IL (1:2).

Figure 3.10 (b) shows the results obtained for a set of membranes containing a component ratio of 2:1, IL: PVC. Firstly a "blank" membrane (i.e. no metal ion exposure) was allowed to pass through the electrode channel. Next, three membranes individually exposed to (a) Cu^{2+}, (b) Co^{2+} and finally (c) a solution containing a mixture of both ions were then allowed to pass through the electrode channel.

One can see from this result that the response obtained for the blank membrane (bold, dashed line). It demonstrates that this membrane is indeed electroactive (due to the presence of the IL) as the WRF instrument proved capable of detecting it as it passed through the electrode channel.

What is also interesting to observe is the signal reduction seen for the respective co-ordinated membranes, which ultimately means that they have become less conductive. This downward trend is most likely due to ion transfer and co-ordination of the metal ions to $[DCA]^-$; as previously discussed. The coordination results in neutralisation of the ligand and a drop in conductivity. The observed signal trend is Cobalt > Mix > Copper which is directly related to the level of ion transfer and co-ordination within the membrane; which will be discussed later in this text.

Some features inherent to this technique are so called “edge effects” which occur as the sample container first enters and leaves the electrode channel. These signals occur as the dielectric constant of the insulating housing material changes upon initial and final contact with the voltage vector.

This, coupled with the signal produced from the conductive strip, means that the graph obtained is an effective picture of the dimensions of the container as it passes through the channel, with the conductive sample housed safely inside.

3.4.10 Electrochemical impedance spectroscopy

WRF detection is a novel technique producing peak heights of arbitrary units, and therefore its results must be validated appropriately. For this purpose EIS was employed, as this provides an independent estimation of the sample conductivity in S/cm.

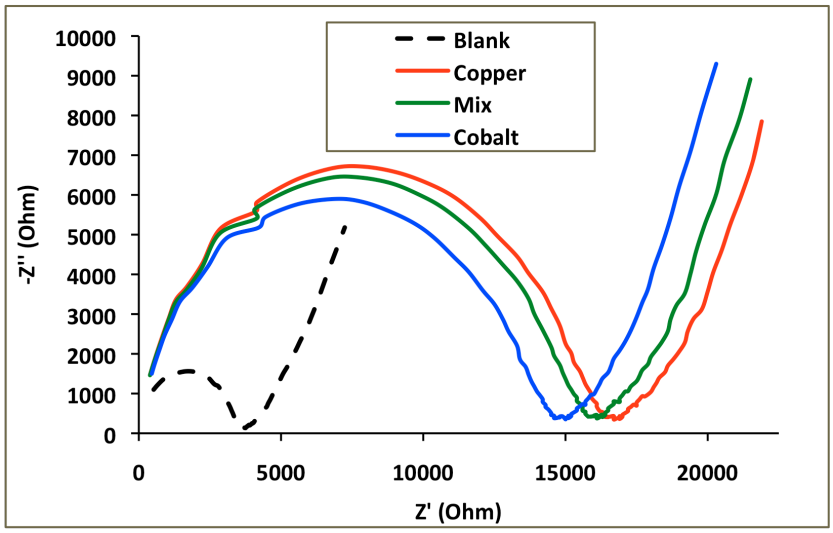

Figure 3.11: The Nyquist plots obtained for membranes containing PVC :IL (1:2).

Figure 3.11 shows the results obtained from *Nyquist* analyses of the membranes on a working electrode. When expressed as a complex number, the Nyquist plot is used to depict the relationship between Z' and -Z'' components of impedance.

The resulting x-axis intercept is used to determine the R_{CT} of the membrane, which is then easily converted to the corresponding conductivity via the equations:

$$G = 1/R \qquad (3.4)$$

$$\sigma = GL/A \qquad (3.5)$$

where G is the conductance, R is the resistance, σ is the conductivity, A is the cross sectional area of the working electrode and L is the estimated thickness of the polymer membrane on the electrode [44, 45].

The screen printed, in-house electrodes used have a cross sectional area of 9mm^2 [27]. In order to estimate the average thickness of the membrane; the Mitutoyo® micrometer calibrated to a resolution of 1μm was used and yielded an average thickness of 0.111mm across 7 electrodes. Table 2.1 provides a summary of the results obtained.

Membrane:	***R_{CT}: (Ω)***	***σ: (S/cm)***
Blank	3738 (131)	3.3×10^{-5}
Cobalt	14550 (664)	8.49×10^{-6}
Mix	15840 (212)	7.8×10^{-6}
Copper	16615 (247)	7.44×10^{-6}

Table 3.1: Resistance of charge transfer and conductivity values obtained via EIS analysis for membranes with component ratio 2:1, IL: PVC.

One can see from both Figure 3.11 and table 2.1 that the impedance of the metal ion co-ordinated membranes has increased. Here the trend is inverted from the previous result obtained. EIS is therefore an effective validation of the novel WRF instrumental result; whilst also providing an independent estimation of the increase in response seen.

3.4.11 XRF measurements

It is proposed that the inverse trends seen must be related to the level of co-ordination within the membrane. In order to confirm this; XRF was then finally used. Previous optical characterisation shows (figures 3.8 and 3.9) that whilst [$P_{6,\ 6,\ 6,\ 14}$] [DCA] is capable of binding to both Co^{2+} and Cu^{2+}, its preferentiality is toward Cu^{2+}. Again for this analysis, membranes containing the same component ratio were analysed and the metal salt solutions concentration were also kept constant.

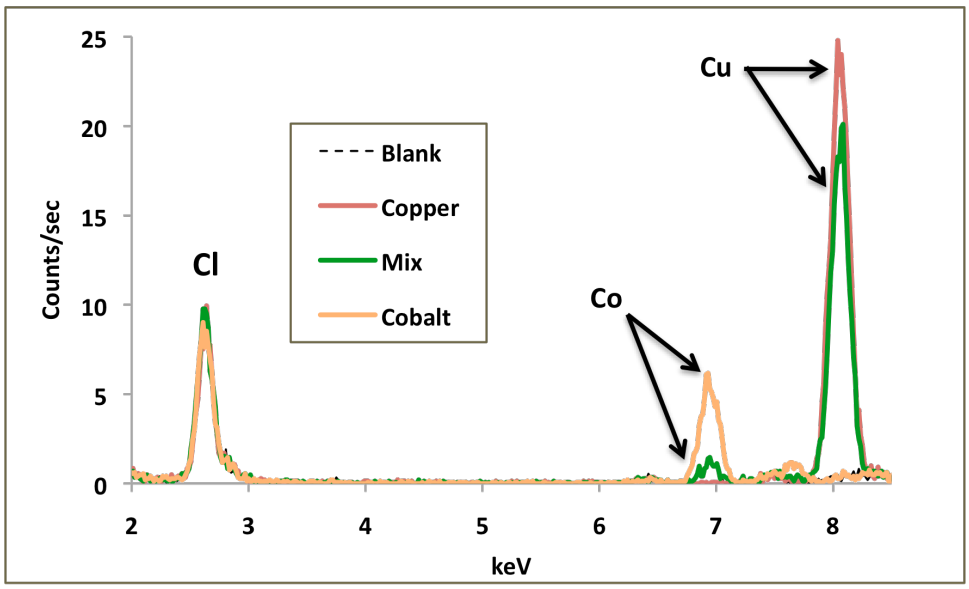

Figure 3.12: XRF spectra obtained for membranes with component ratio 2:1, IL: PVC.

Figure 3.12 (above) depicts the spectra obtained; the first feature to note is that the peak height obtained for chlorine is approximately the same for all 4 membranes. This illustrates that the ratio of PVC is indeed kept constant for all measurements, and so acts as an internal standard. The peaks for both Cobalt and Copper are also labelled, it can be seen that the peak height is considerably higher for Copper over Cobalt, which is indicative of the binding preferentiality of the IL.

The peak heights obtained for the mixture are also labelled; they are, of course lower than those obtained for the pure ion solutions. The reduction in peak height is more dramatic for Cobalt over Copper, and given that the initial metal salt solution contained a volume ratio of 1:1, Co^{2+}:Cu^{2+}, further strengthens our binding preferentiality argument.

By examining the case of Cu^{2+} co-ordination; the trends observed from the three imstrumental techniques can be summarised as follows: Cu^{2+} exhibits the highest binding preferentiality to the IL (XRF), thereby producing the lowest WRF signal and the highest EIS response. The opposite then applies for Co^{2+} co-ordination with the mixture inevitably in between.

3.5 Conclusion

This chapter effectively demonstrates how the multifunctional properties of an IL form the basis of a simple, 2-component ion-sensing membrane. $[P_{6,6,6,14}][DCA]$ fulfils roles as a diverse ligand, transducer dye and plasticiser; whilst the binding mechanism eliminates the need for an ion-exchanger.

Exposure of the membranes to a Cu^{2+} salt produces a yellow colour with an absorption maxima at 370 nm, whilst exposure to a Co^{2+} salt produces a blue colour with an absorption maxima at 600 nm. The diverse nature of the ligand, plus the distinct absorption maxima of the two individual complexes allowed a series membranes to sense various mixture of the two salts combined.

The IL based membranes also act as electroactive materials which - when co-ordinated to heavy metals - provide a measured sensor response. The use of WRF technology effectively demonstrates this concept, whilst the validation experiments successfully explain how 3 differing techniques definitively summarise the inherent co-ordinating chemistry of these membranes.

In this case the IL based polymeric optodes are again capable of discriminatory co-ordination of the heavy metals Cu^{2+}, Co^{2+} and both ions in a mixture, which produces an equal discriminatory conductivity decrease in the WRF signal. By documenting the inverse trend of impedance, this novel conductivity result has been validated. Both the WRF and EIS trends were then easily explained by studying the level of ion transfer and the co-ordinating preferences of the IL ligand $[DCA]^-$. This was achieved by quantifying the amount of metal present in the membrane using XRF.

The somewhat modest limit of detection, and the interferent effect of other ions does highlight the need for improvement if ILs are to be used to sense these ions in real scenarios. In view of the relative ease of synthesis of ILs, the relative ease of incorporating specific functionality into ILs[46, 47], and the availability of charged ionophores[48-50] for a wide range of analytes; there is now considerable potential to generate very effective sensing membranes tuned for specific analyte.

3.6 References:

1. A. Bakker, S. Gejji, J. Lindgren, K. Hermansson and M. M. Probst, *Polymer*, 1995, 36, 4371-4378.
2. P. K. Jal, S. Patel and B. Mishra, *Talanta*, 2004, 62, 1005-1028.
3. W. Gu, H. D. Bian, J. Y. Xu, Z. Q. Liu, P. Cheng, S. P. Yan, D. Z. Liao and Z. H. Jiang, *Inorg. Chem. Commun.*, 2003, 6, 966-970.
4. B. Peng, J. W. Zhu, X. J. Liu and Y. Qin, *Sens. Actuator B-Chem.*, 2008, 133, 308-314.
5. K. Kimura, T. Sunagawa, S. Yajima, S. Miyake and M. Yokoyama, *Analytical Chemistry*, 1998, 70, 4309-4313.
6. C.-Z. Lai, S. S. Koseoglu, E. C. Lugert, P. G. Boswell, J. Rabai, T. P. Lodge and P. Buhlmann, *J. Am. Chem. Soc. FIELD Full Journal Title:Journal of the American Chemical Society*, 2009, 131, 1598-1606.
7. P. G. Boswell, C. Szijjarto, M. Jurisch, J. A. Gladysz, J. Rabai and P. Buehlmann, *Anal. Chem. (Washington, DC, U. S.) FIELD Full Journal Title:Analytical Chemistry (Washington, DC, United States)*, 2008, 80, 2084-2090.
8. P. G. Boswell and P. Buehlmann, *J. Am. Chem. Soc. FIELD Full Journal Title:Journal of the American Chemical Society*, 2005, 127, 8958-8959.
9. A. Aghaei, M. R. M. Hosseini and M. Najafi, *Electrochim. Acta*, 2010, 55, 1503-1508.
10. N. Zine, J. Bausells, F. Vocanson, R. Lamartine, Z. Asfari, F. Teixidor, E. Crespo, I. A. M. de Oliveira, J. Samitier and A. Errachid, *Electrochim. Acta*, 2006, 51, 5075-5079.

11. L. Yang, R. W. Zhang, D. Staiculescu, C. P. Wong and M. M. Tentzeris, *Ieee Antennas and Wireless Propagation Letters*, 2009, 8, 653-656.

12. Y. Kim, R. G. Evans and W. M. Iversen, *Ieee Transactions on Instrumentation and Measurement*, 2008, 57, 1379-1387.

13. N. Kaur and S. Kumar, *Chemical Communications*, 2007, 3069-3070.

14. N. Kaur and S. Kumar, *Tetrahedron Letters*, 2008, 49, 5067-5069.

15. D. Jimenez, R. Martinez-Manez, F. Sancenon, J. V. Ros-Lis, J. Soto, A. Benito and E. Garcia-Breijo, *European Journal of Inorganic Chemistry*, 2005, 2393-2403.

16. D. Jimenez, R. Martinez-Manez, F. Sancenon and J. Soto, *Tetrahedron Letters*, 2004, 45, 1257-1259.

17. S. E. Andria, C. J. Seliskar and W. R. Heineman, *Analytical Chemistry*, 2010, 82, 1720-1726.

18. J. Cleary, C. Slater, C. McGraw and D. Diamond, *Ieee Sensors Journal*, 2008, 8, 508-515.

19. C. M. McGraw, S. E. Stitzel, J. Cleary, C. Slater and D. Diamond, *Talanta*, 2007, 71, 1180-1185.

20. D. R. MacFarlane, S. A. Forsyth, J. Golding and G. B. Deacon, *Green Chem.*, 2002, 4, 444-448.

21. D. R. MacFarlane, J. Golding, S. Forsyth, M. Forsyth and G. B. Deacon, *Chem. Commun.*, 2001, 1430-1431.

22. B. Vangdal, J. Carranza, F. Lloret, M. Julve and J. Sletten, *J. Chem. Soc.-Dalton Trans.*, 2002, 566-574.

23. M. Hvastijova, J. Kohout, M. Okruhlica, J. Mrozinski and L. Jager, *Transit. Met. Chem.*, 1993, 18, 579-582.

24. J. Kohout, L. Jager, M. Hvastijova and J. Kozisek, *J. Coord. Chem.*, 2000, 51, 169-218.

25. N. B. Clark and L. J. Maher, *Reactive & Functional Polymers*, 2009, 69, 594-600.

26. T. Ramnial, S. A. Taylor, M. L. Bender, B. Gorodetsky, P. T. K. Lee, D. A. Dickie, B. M. McCollum, C. C. Pye, C. J. Walsby and J. A. C. Clyburne, *Journal of Organic Chemistry*, 2008, 73, 801-812.

27. A. Morrin, A. J. Killard and M. R. Smyth, *Analytical Letters*, 2003, 36, 2021-2039.

28. J. Bobacka, A. Ivaska and A. Lewenstam, *Electroanalysis*, 2003, 15, 366-374.

29. A. Nag and W. Schnick, *Z. Anorg. Allg. Chem.*, 2006, 632, 609-614.

30. B. Jurgens, H. A. Hoppe and W. Schnick, *Solid State Sciences*, 2002, 4, 821-825.

31. K. Nakamoto, *Infrared and Raman Spectra of Inorganic and Coordination Compounds, Wiley,New York,5th edn.,105-113*, Wiley, New York, 1997.

32. W. P. Griffith, *Coordination Chemistry Reviews*, 1975, 17, 177-247.

33. K. A. Friedrich, W. Daum, C. Klunker, D. Knabben, U. Stimming and H. Ibach, *Surface Science*, 1995, 335, 315-325.

34. E. Bakker, P. Buehlmann and E. Pretsch, *Chemical Reviews*, 1997, 97, 3083-3132.

35. U. E. Spichiger, D. Freiner, E. Bakker, T. Rosatzin and W. Simon, *Sens. Actuator B-Chem.*, 1993, 11, 263-271.

36. I. Oehme and O. S. Wolfbeis, *Mikrochimica Acta*, 1997, 126, 177-192.

37. R. H. Yang, K. A. Li, K. M. Wang, F. L. Zhao, N. Li and F. Liu, *Analytical Chemistry*, 2003, 75, 612-621.

38. A. Radu, R. Byrne, N. Alhashimy, M. Fusaro, S. Scarmagnani and D. Diamond, *Journal of Photochemistry and Photobiology a-Chemistry*, 2009, 206, 109-115.

39. S. R. Batten and K. S. Murray, *Coordination Chemistry Reviews*, 2003, 246, 103-130.

40. L. F. Jones, L. O'Dea, D. A. Offermann, P. Jensen, B. Moubaraki and K. S. Murray, *Polyhedron*, 2006, 25, 360-372.

41. W. Dong, M. Liang, Y. Q. Sun and Z. Q. Liu, *Z. Anorg. Allg. Chem.*, 2003, 629, 2443-2445.

42. M. Kurmoo and C. J. Kepert, *New J. Chem.*, 1998, 22, 1515-1524.

43. Y. J. Shi, L. H. Li, Y. Z. Li, X. T. Chen, Z. L. Xue and X. Z. You, *Polyhedron*, 2003, 22, 917-923.

44. P. E. Stallworth, J. J. Fontanella, M. C. Wintersgill, C. D. Scheidler, J. J. Immel, S. G. Greenbaum and A. S. Gozdz, *Journal of Power Sources*, 1999, 81, 739-747.

45. L. A. Neves, J. Benavente, I. M. Coelhoso and J. G. Crespo, *Journal of Membrane Science*, 2010, 347, 42-52.

46. P. Wasserscheid, B. Driessen-Holscher, R. van Hal, H. C. Steffens and J. Zimmermann, *Chem. Commun.*, 2003, 2038-2039.

47. E. D. Bates, R. D. Mayton, I. Ntai and J. H. Davis, *J. Am. Chem. Soc.*, 2002, 124, 926-927.

48. S. Amemiya, P. Buhlmann, E. Pretsch, B. Rusterholz and Y. Umezawa, *Analytical Chemistry*, 2000, 72, 1618-1631.

49. P. Buhlmann, E. Pretsch and E. Bakker, *Chem. Rev.*, 1998, 98, 1593-1687.

50. P. Buhlmann, S. Amemiya, S. Yajima and Y. Umezawa, *Analytical Chemistry*, 1998, 70, 4291-4303.

Chapter 4

An electrochromic ionic liquid: design, characterisation and performance within a solid-state device

4.1 Abstract

The focus of this chapter is built upon the ideology explored in chapter 3, which is to use an IL as an agent that performs multiple roles within a device. However in this case a synthetic route is employed that yields an IL as a key component in an electrochromic device. A device based on two individual components is achieved through the synthesis of an electrochromic IL that also acts as the supporting electrolyte between two electrodes.

This work therefore describes the synthesis and characteristics of a novel electrochromic IL based on a phosphonium core tethered to a viologen moiety. When integrated into a solid-state electrochromic device, the viologen modified IL behaved as both the electrolyte and the electrochromic material. Device fabrication was achieved through *in situ* photo-polymerisation and encapsulation of this novel IL within a hybrid sol-gel. Important parameters of the device performance, including its coloration efficiency, switching kinetics and optical properties were characterised using UV/Vis spectroscopy. Despite the rather viscous nature of the material, the device exhibited approximately two orders of magnitude faster switching kinetics (221 seconds to reach 95 % absorbance) when compared to previously reported electrochromic ILs (18,000 seconds).

4.2 Introduction:

Electrochromic materials have the ability to switch between two distinct optical states as a function of the voltage applied[1, 2]. In order for this phenomenon to occur, the molecule in question must exist in at least two redox states, where the change in redox states results in a change in the optical properties of the molecule. In order for a material to be considered electrochromic, it must adhere to equation 4.1:

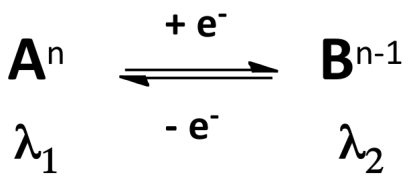

(4.1)

Where A and B are two distinct chemical species with redox states of *n* and *n-1* respectively. The electron mediated equilibrium yields the absorption maxima λ_1 and λ_2 respectively.

The usual mode of fabrication involves immobilisation of a suitable polymeric substrate between two electrodes[3]. Typically, the polymer requires a plasticiser to produce a flexible film, and a suitable electrolyte in the form of a lipophilic salt in order to facilitate charge transport[4].

The electroactive chromophore is usually doped within the material in order to form a fully functional solid-state device that will change its colour in response to a voltage[5]. In fact some systems can contain complementary anodically and cathodically colouring electrochromes in which the redox chemistry occurs at both electrodes respectively[6, 7]. In their most complex form therefore, these devices can contain up to six individual molecular components.

Efforts at simplifying these systems have seen some electrochromes covalently attached to the polymer backbone[8] or to the electrode itself[9]. Other approaches have focused on π-conjugated conducting polymers, which can conduct current and exhibit electrochromic traits[10]. However, examples of these polymers with negligible residual absorbance in the visible region are rare[11].

Arguably the most popular choice of organic electrochromic materials are the *viologens*[12]. These bipyridinium ions undergo a reversible one-electron reduction to switch from a dicationic to a monocationic radical state[13]. This process promotes a high transmittance change in the visible region whilst the kinetics of electron transfer between the two states has been shown to be in the order of seconds[14]. Further reduction to a quinoid-based state can be achieved but is undesirable as this state is colourless and has shown to be irreversible in some cases[12]. The optical properties of the monocationic form[15] and the particular potential at which the redox chemistry occurs[16] can be altered by quaternising the pyridine centre with differing electrophiles. A general overview of the three-redox states observed for viologen compounds is presented in scheme 4.1

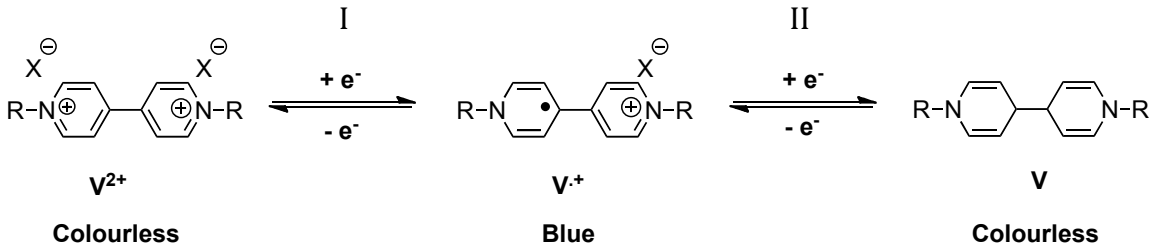

Scheme 4.1: The two step (I, II) redox equilibria of the viologen species. "R" is used to represent the quaternizing agent and X^- denotes the counter ion.

The ability to tailor the properties of an IL to suit a particular need by addition of a specific functional group offers fascinating possibilities for materials science. Liquids can be designed that exhibit all of the favourable properties of ILs as discussed *and* possess the previous chemistries of the functional group. To this end recent publications describing the syntheses of photo[17, 18], magneto and electrochromic[19] ILs have been described.

For the latter case involving electrochromic ILs, coloration switching kinetics were reported to be as high as 300 minutes. If ILs are to be used as efficient coloration materials for electrochromic devices then this response time clearly must be improved upon. Indeed the onset of ionogels as popular materials of choice has stimulated investigations of their use in electrochromic systems. In these studies the electrochromic material is doped within the ionogel which is then used to facilitate the current needed for the colour switching redox process within the polymeric device[20, 21].

The goal of this work is to simplify the composition of an electrochromic device through combining the properties of the viologen molecule with a phosphonium based IL. The dual functionality of the synthesised IL sees it employed both as the electrolyte *and* the electrochrome when encapsulated within a hybrid ionogel sandwiched between two indium tin oxide (ITO) electrodes. The optoelectrical performance of this device has been characterised and compared to a similar device employing an ionogel based on a conventional phosphonium IL as the supporting electrolyte in which the viologen is a dopant rather than covalently integrated.

4.3 Experimental

4.3.1 Chemicals and Materials:

Trioctylphosphine and ($[P_{6,6,614}][Cl]$) were generously donated by Cytec® industries. The latter was purified in accordance with the techniques outlined in the previous chapter **(Section 3.3.1)**.

1-bromo-3-chloropropane, DMPA, ITO coated polyethylene, MAPTMS, MAAH, AlO, POT and 1-heptyl-4-(4-pyridyl)pyridinium bromide (*herein referred to as "mono-alkylated viologen" (MAV))* were used as purchased from Sigma-Aldrich® Ireland Ltd.

4.3.2 (3-chloropropyl) trioctylphosphonium bromide synthesis:

A conventional three necked round bottom flask and a pressure funnel was initially acid washed, allowed to dry overnight at 100 ^{0}C, and then subsequently purged with nitrogen for a further 20 minutes in order to create an inert atmosphere. The nitrogen flow was facilitated using the right neck of the round bottom flask; the middle neck was closed using a conventional rubber seal.

The synthesis was performed according to scheme 4.2. 8.25 g (2.22×10^{-2} mol) of trioctylphosphine was added to the reaction chamber using a glass syringe, and allowed to equilibriate to 100 ^{0}C for 20 minutes.

3.85 g (2.44 x 10^{-2} mol) of 1-bromo-3-chloropropane was added slowly over 4 hours to the reaction flask using the pressure funnel. The reaction was then allowed to complete for a further 8 hours. Once complete the excess dihaloalkane was removed using a high vacuum line. (3-chloropropyl) trioctylphosphonium bromide ([$P_{3Cl,8,8,8}$][Br]; where 3Cl represents the 3-chloropropyl group and 8 the octyl chains) was obtained as a colourless oily liquid (8.15 g, 67.35 wt.% yield).

^{1}H NMR: δ_H (400 MHz, $CDCl_3$) 0.88ppm (9H), 1.2ppm (24H), 1.51ppm (12H), 2.17ppm (2H), 2.43ppm (6H), 2.8ppm (2H), 3.7ppm (2H).

^{31}P NMR: (400MHz, $CDCl_3$) 33.2ppm.

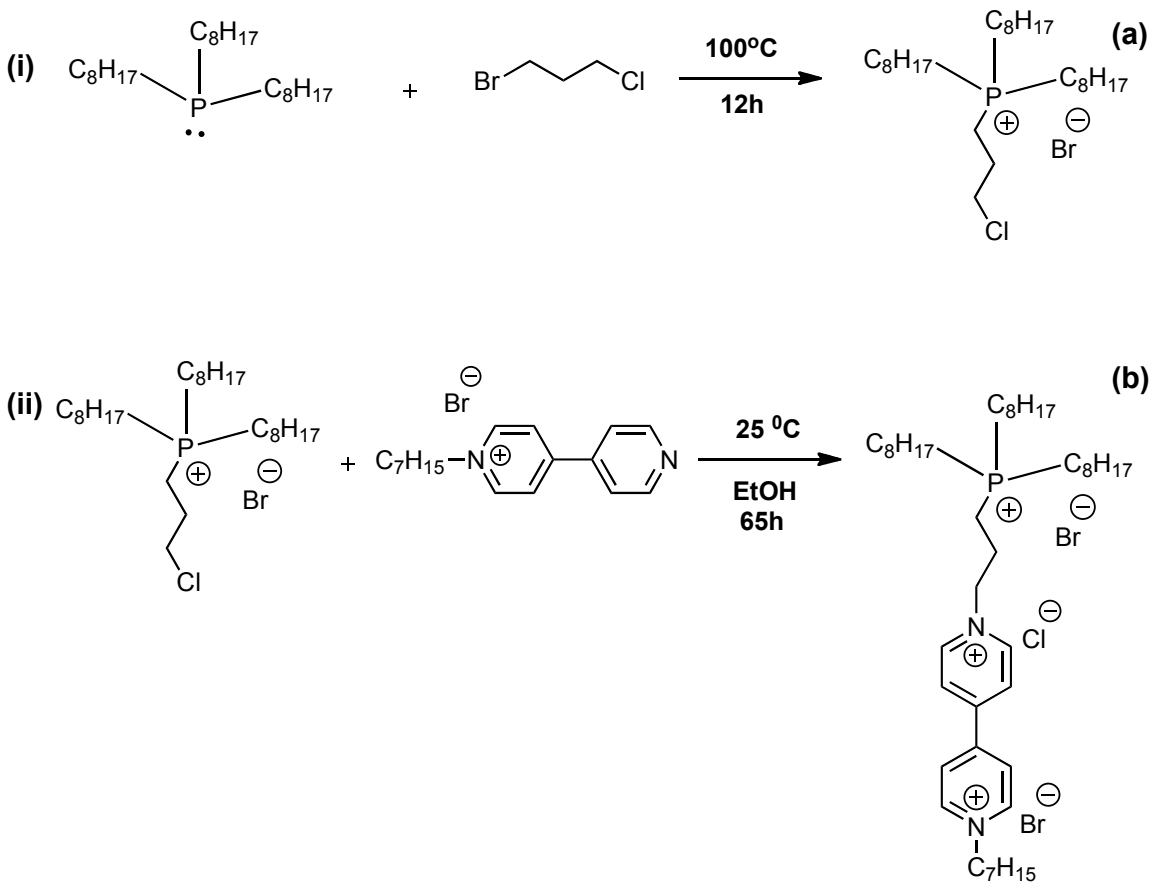

Scheme 4.2: (i) Synthesis of **(a)** $[P_{3Cl,8,8,8}][Br]$ via quaternisation of trioctylphosphine with a dihaloalkane, **(ii)** its subsequent secondary quaternisation with MAV to form $[P_{V,8,8,8}][3X]$ **(b)**.

4.3.3 Electrochromic IL synthesis:

The second step of the synthetic route is outlined in scheme 4.2 (b). $[P_{3Cl,8,8,8}][Br]$ (2 g, 3.8 x 10^{-3} mol) was dissolved in 15 ml of ethanol to which 1.4 g (4.1 x 10^{-3} mol) of MAV was added and the reaction was left for 65 hours at 25 ^{0}C. The ethanol was then removed by rotary evaporation. As $[P_{3Cl,8,8,8}][Br]$ was used as the limiting reagent, re-dissolving in dichloromethane precipitated out the excess MAV.

The electrochromic IL ($[P_{V,8,8,8}][3X]$; where 8 again represents the octyl chains, V represents the tethered viologen moiety, and X represents the halide counter ions) was filtered, dried by rotary evaporation and left under vacuum overnight. The final product obtained was a yellow, highly viscous liquid (2.5 g, 73.5 wt.% yield).

^{1}H NMR: δ_H (400MHz, $CDCl_3$) 0.82ppm (12H), 1.23ppm (44H), 2.02ppm (5H), 2.3ppm (5H), 2.37ppm (2H), 7.69ppm (2H), 8.36ppm (2H), 8.8ppm (2H), 9.61ppm (2H).

^{31}P NMR: (400MHz, $CDCl_3$) 32.28ppm.

4.3.4 Sol-Gel Synthesis:

For experiments involving the solid-state the direct photopolymerisation of a hybrid sol-gel was employed as it is miscible with the ILs used and produces a flexible, transparent film. The in-depth syntheses of these materials are the focus of chapters 5 and 6. For an in-depth discussion on the sol-gel preparation, please refer to **section 5.4.2.**

For the purposes of this chapter it is used solely as an inert matrix that is easily photo-polymerised between two electrodes, this forming the electrical seal for ion diffusion. The gel prepared for the analysis undertaken in this chapter was of the stoichiometry: 10/0.5/0.5 (MAPTMS,AlO,MAAH).

4.3.5 Ionogel preparation:

All ionogels were prepared according to scheme 2. In order to prepare the 2-component ionogel for analysis; 40 mg of $[P_{V,8,8,8}][3X]$ was added to 60 mg of the sol-gel solution. 3 mg (3 wt%) of DMPA was then added and the final ionogel sonicated for 10 minutes to ensure a complete homogenous liquid mix.

The control ionogel was prepared as follows: 0.5 g (40 wt.%) of $[P_{6,6,6,14}][Cl]$ was added to 0.75 g (60wt%) of the sol-gel; followed by 38 mg (3 wt%) of DMPA and 22 mg of MAV(5×10^{-2} M). The control ionogel mixture was again sonicated for 10 minutes.

A brief schematic overview of the ionogel preparation with a graphic depicting the polymerised gel can be seen in scheme 4.3.

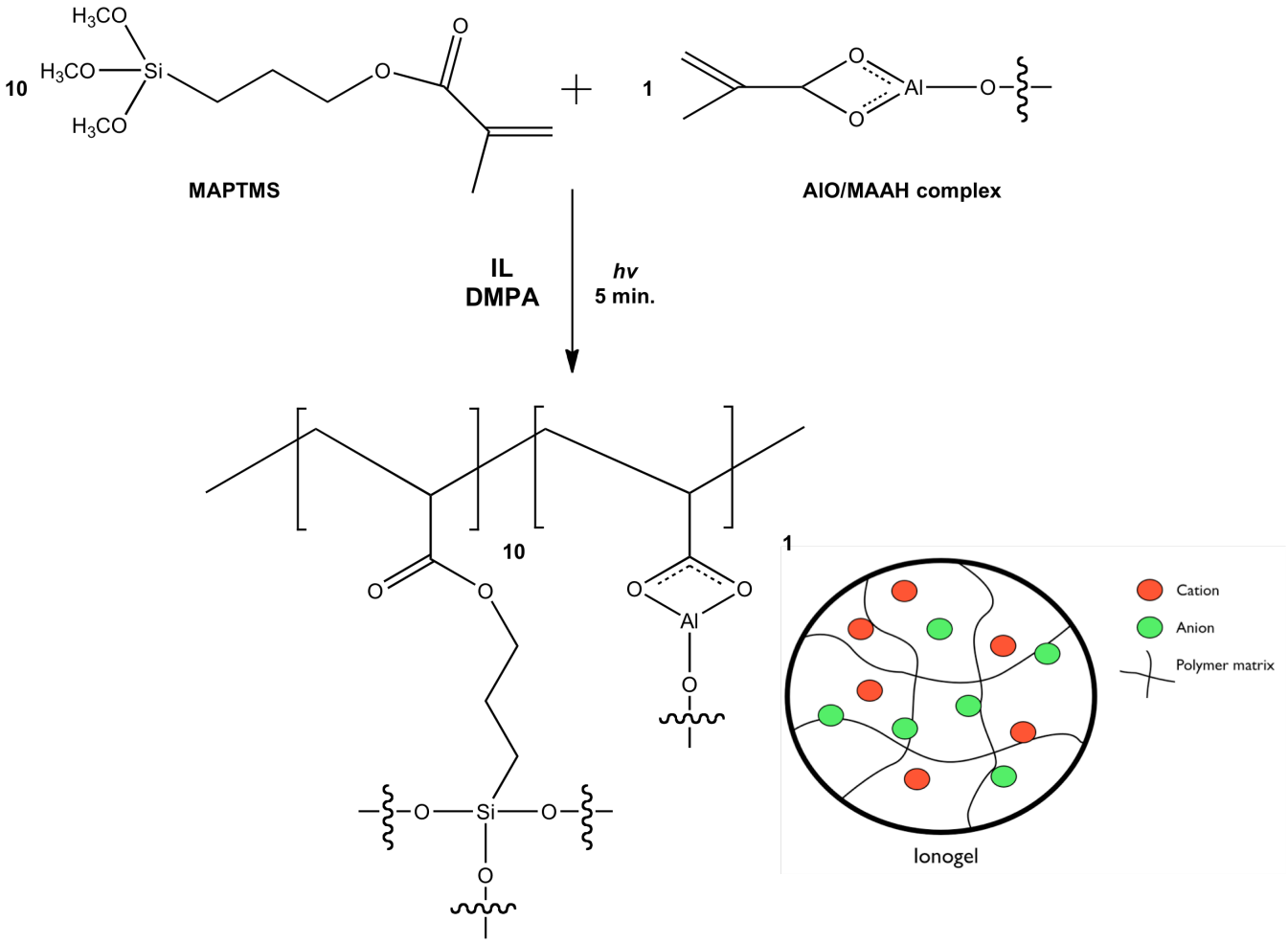

Scheme 4.3: Synthesis and photo-polymerisation of the ionogels used in this work. The inset is a graphical illustration of the resulting ionogel i.e. a polymer network with an encapsulated IL (represented by coloured circles). In device I the viologen is covalently attached to the phosphonium cation (Scheme 4.3) whereas in Device II the viologen is a dopant.

4.3.6 Solid-state device fabrication:

The solid-state electrochromic device was prepared by dropcasting 50 μL of the ionogel onto ITO. In order to generate an electrical seal a second ITO layer was then placed on top of the ionogel layer. UV light exposure for 5 minutes allowed polymerisation and the seal to be formed.

4.4 Results and Discussion

4.4.1 Synthesis of the electrochromic ionic liquid

The first step in the synthesis of the electrochromic ionic liquid was achieved by allowing trioctylphosphine to undergo direct nucleophillic addition with a dihaloalkane. As bromine is the better leaving group in this case the controlled temperature of the reaction resulted in it becoming the counter ion of the new IL formed. This left the terminal chloro group free to undergo a further reaction if required.

NMR analysis identified the near 60 ppm shift from -30.78 ppm (phosphine) to 33.2 ppm (phosphonium) in the ^{31}P spectra indicating the quaternisation reaction had occurred (Figure A3 (v)). A complete summary of the NMR analyses can be viewed in figures A3 (i) – (viii).

$[P_{3Cl,8,8,8}][Br]$ is a colourless liquid at room temperature. Its thermal phase transitions were investigated by performing a DSC ramp (figure 4.1 (a)) from -80 to 100 ^{0}C. $[P_{3Cl,8,8,8}][Br]$ showed a glass transition only at -61 ^{o}C. This behavior is typical of amorphous materials and is characteristic of tetralkylated phosphonium ILs[22, 23]. The high thermal decomposition temperature of the IL is also in line with phosphonium based ILs, the salt having a degradation range between 220 - 420 ^{o}C[37] (figure 4.1 (b)).

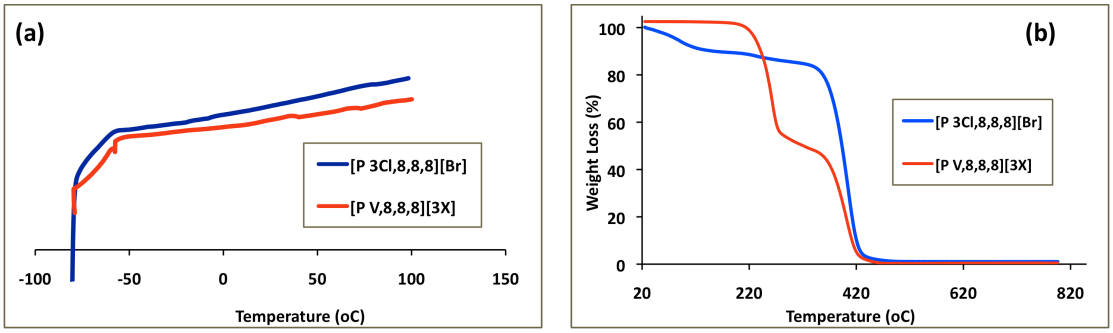

Figure 4.1: Thermal properties of novel synthesized ILs: **(a)** DSC traces -80 ^{o}C to 100 ^{o}C, **(b)** Decomposition profile of ILs in the region of 25 – 800 ^{o}C.

The second step of the synthesis ([$P_{V,8,8,8}$][3X]) involved a secondary quaternisation of [$P_{3Cl,8,8,8}$][Br] with MAV. As the chloro group was left unreacted from the first step it was used as the quaternizing agent thereby linking the phosphonium core to the MAV. Subsequent ^{1}H NMR analysis yielded the aromatic upfield signals characteristic of the dipryidinium ions and the extensive alkylation of the phosphonium core (Figure A3 (vii)). ^{31}P NMR analysis showed no shift in the previous signal, confirming the phosphonium centre remained unreacted(Figure A3 (viii).

DSC ramp analysis (figure 4.1 (a)) revealed that [$P_{V,8,8,8}$][3X] exhibits the same thermal features of parent IL compound. A glass transition was observed at -57 ^{0}C, and TGA analysis showed that [$P_{V,8,8,8}$][3X] degraded in 2 steps, at 218 ^{0}C and 418 ^{o}C (figure 4.1 (b)). This may be due to the cleavage and degradation of the viologen component followed by degradation of the phosphonium component at higher temperatures. This behaviour has also been seen in previously published papers[24]. A complete summary of the thermal data obtained is seen below in table 4.1.

IL	T_g (^0C)	T_{dec} (^0C)
(a)	-61	420
(b)	-57	218, 418

Table 4.1: Thermal data obtained for $[P_{3Cl,8,8,8}][Br]$ **(a)** and $[P_{V,8,8,8}][3X]$ **(b)**. T_g refers to the glass transition temperature and T_{dec} is the decomposition temperature (calculated using onset).

4.4.2 Infrared Spectroscopy:

Infrared spectroscopy was first used to identify any structural changes on a molecular level. In order to construct a valid comparison the IR spectra of (i) $[P_{3Cl,8,8,8}][Br]$, (ii) MAV and (iii) $[P_{V,8,8,8}][3X]$ were obtained and are shown below in figure 4.2.

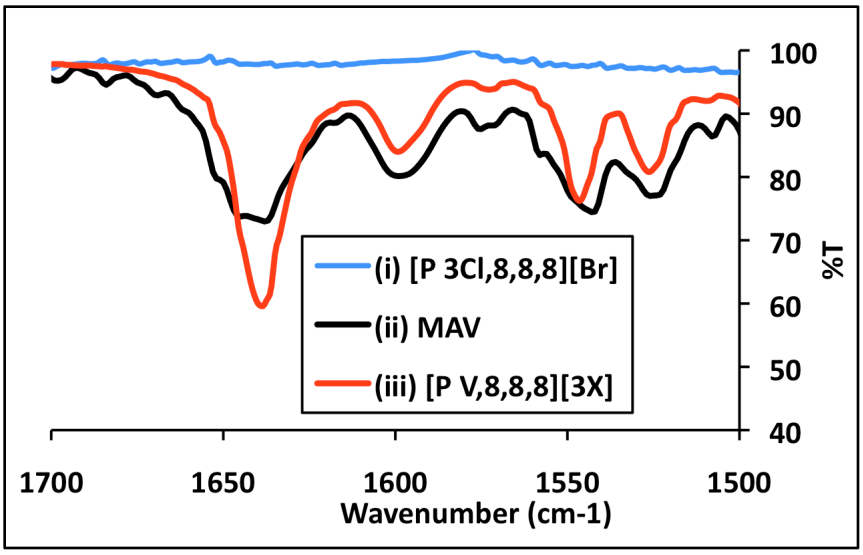

Figure 4.2: Comparative IR spectra obtained for (i) $[P_{3Cl,8,8,8}][Br]$; (ii) MAV and (iii) $[P_{V,8,8,8}][3X]$.

The spectra were baseline corrected in the region between 1700 and 1900 cm^{-1}, as there is no activity for all spectra in this region until the alkyl chain contributions at ~2900 cm^{-1}.

The presence of the viologen moiety within $[P_{V,8,8,8}][3X]$ is attributed to multiple stretches between 1500 and 1700 cm^{-1} which are assigned to various C-C and C-N modes within the pyridinium ring[25, 26]. These assignments are justified as the spectra for MAV (which contains the same heterocycles) exhibits the same stretching characteristics at the same frequencies.

This serves to validate the presence of this moiety within the $[P_{V,8,8,8}][3X]$ as no activity is observed in this region of the $[P_{3Cl,8,8,8}][Br]$ spectrum.

4.4.3 Fabrication and spectroelectrochemistry of electrochromic devices:

Spectroelectrochemistry was performed by connecting the fabricated devices to a 2-electrode cell (which was controlled by a potentiostat) in the light path of the UV spectrometer. Results obtained with the new electrochromic ionogel (Device I) can be seen below in figure 4.3.

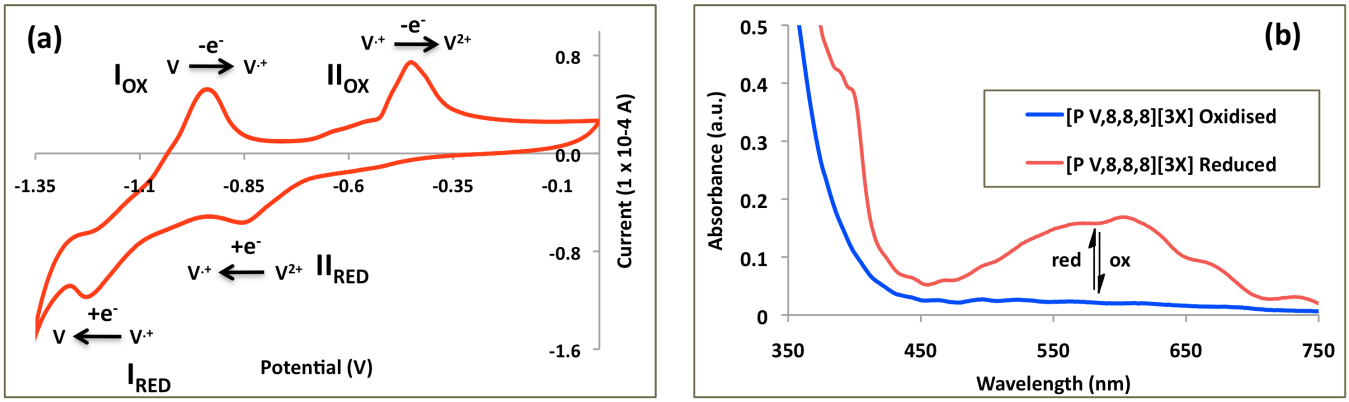

Figure 4.3: (a) Cyclic voltammogram (Scan rate: 100 mV/Sec) obtained for $[P_{V,8,8,8}][3X]$ as part of the electrochromic ionogel. **(b)** the UV/Vis absorbance spectra obtained for both oxidised and reduced states of $[P_{V,8,8,8}][3X]$ as part of the electrochromic ionogel.

From figure 4.3 (a), the expected redox chemistry of a system containing di-quaternised pyridinium ions is observed (i.e., two reduction potentials observed at -0.84 and -1.21 V, respectively). These redox couples are the inherent electron mediated equilibria of di-substituted viologens as discussed previously.

As the sol-gel matrix can be viewed as an insulating material, ion movement typical of a solid-state electrolyte must then facilitate the current needed for these redox processes. However in this case, the electrochrome *is also the electrolyte.*

When the applied potential to the electrochromic device is maintained at (-0.84 V), a dark navy blue colour with a λ_{max} at 610 nm is generated (figure 4.3 (b)) due to the generation of the monocationic radical. When compared to the initial published results on electrochromic IL's (18,000 seconds) [19], this result is approximately two orders of magnitude faster (figure 4.5 (a)).

As the MAV starting material contains a pyridinium site it is capable of reduction and redistribution of electrons through the hetrocycle, which will alter its optical properties. A second device was prepared (Device II), based on an ionogel comprising the unmodified IL. The viologen moiety (MAV) is physically entrapped rather than covalently attached to the phosphonium cation.

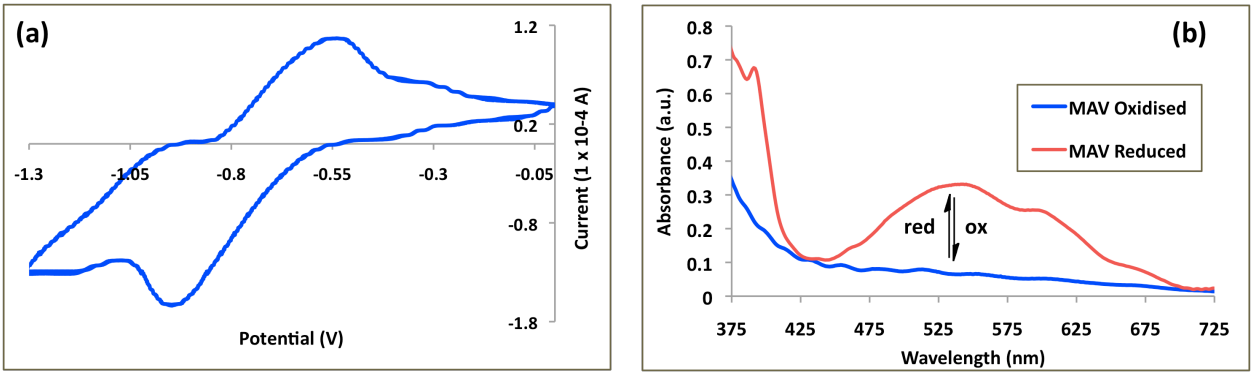

Figure 4.4: (a) Cyclic voltammogram (Scan rate: 50 mV/Sec) obtained for MAV physically entrapped within a $[P_{6,6,6,14}][Cl]$ based ionogel, **(b)** the absorbance spectra obtained for both oxidised (V^{2+}) and reduced states ($V^{\cdot+}$) of MAV as part of $[P_{6,6,6,14}][Cl]$ ionogel.

The control experiments involving MAV exhibited only one redox couple (Figure 4.4 (a)). By maintaining the potential throughout the device in the same manner as in the previous experiment (i.e. at the specific reduction potential, -0.91 V), a bright purple colour with a λ_{max} at 550nm was generated (Figure 4.4 (b)). In this case however, the redox chemistry of the MAV is facilitated by independent addition of $[P_{6,6,6,14}][Cl]$.

A summary of the optical properties of the devices and the viologen redox chemistry is presented in scheme 4.4.

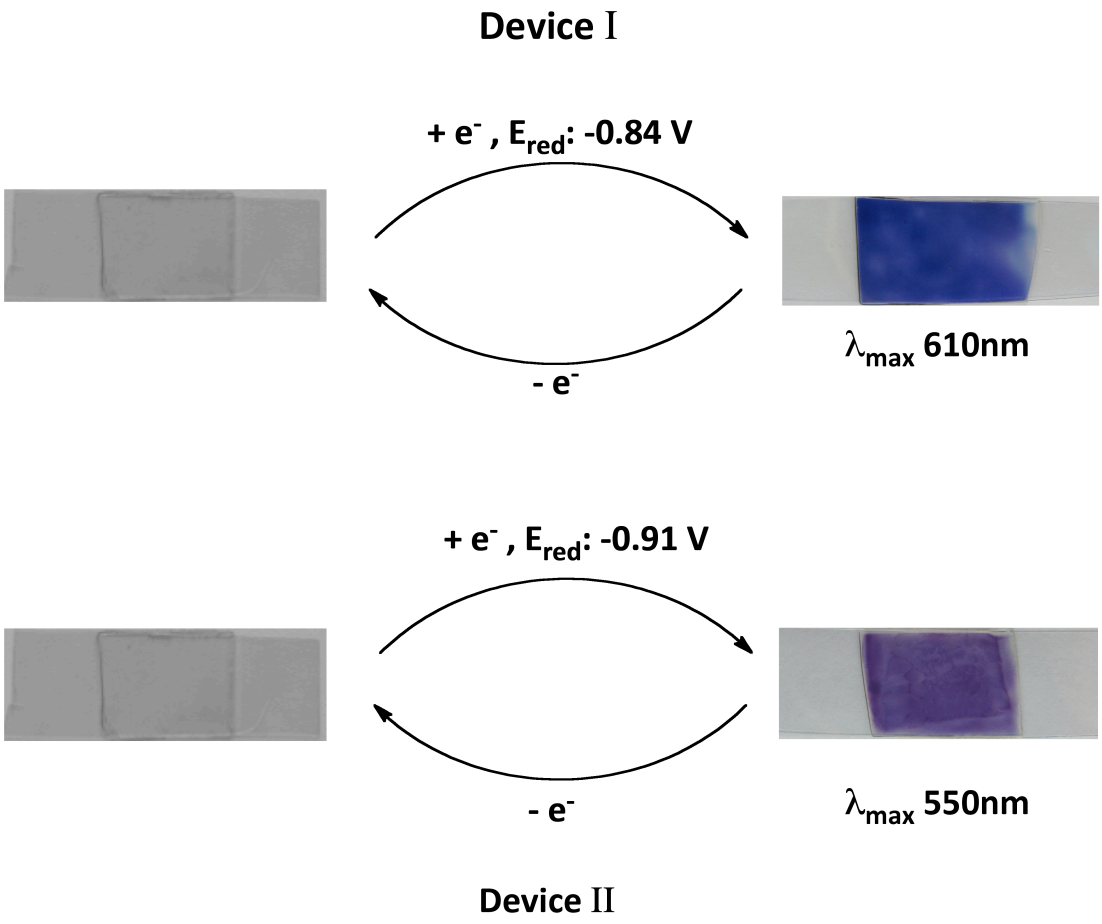

Scheme 4.4: Summary of the optical properties of solid-state devices I and II;

Top: Device I (λ_{max} 610 nm, E_{red} -0.84 V), with viologen chromophore bound to the phosphonium cation of the IL and encapsulated in the sol-gel. Device dimensions L: 4 cm, B: 1.5 cm and thickness 53 µm ± 2 µm (average of 4 devices, Figure A2 (a)).

Bottom: Device II (λ_{max} 550 nm, E_{red} -0.91 V) with viologen chromophore is physically entrapped in the sol-gel along with a conventional phosphonium based IL ($[P_{6,6,6,14}][Cl]$). Device dimensions L: 4 cm, B: 1.5 cm and thickness 86 µm ± 22 µm (average of 4 devices, Figure A2 (b)).

4.4.4 Device Performance:

The colouration efficiency of an electrochromic device relates the change in its absorbance to the charge required to induce the change [27, 28], according to the equation:

$$\eta = \frac{\Delta OD}{Q_d} = \frac{\log \frac{T_c}{T_t}}{Q_d} \qquad \textbf{(4.2)}$$

Where η is the colouration efficiency at a given wavelength, ΔOD is the change in the optical density, T_c and T_t are the transmission levels of the coloured and transparent states respectively and ΔQ is the charge needed to induce this change.

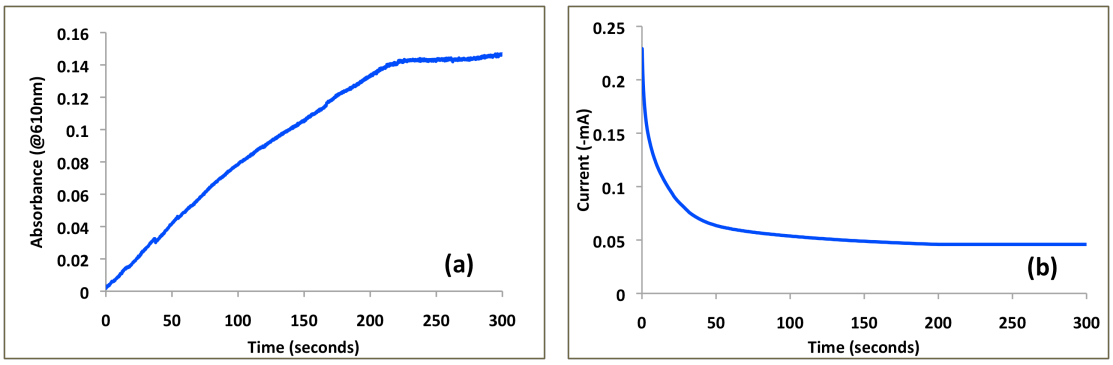

Figure 4.5: (a) Coloration response curve obtained for the simplified electrochromic device**,** and **(b)** the current maintained within the device during coloration.

Inputting the data from figure 4.5 into equation 1 allowed the colouration efficiency of Device I to be calculated at 10.72 cm^2C^{-1}, which is low in comparison to a similar solid-state device based on viologen functionalised nanoparticles (colour efficiency 205 cm^2C^{-1}). However, considering the very viscous nature of the ionogel, and the fact that the viologen is covalently integrated with the phosphonium cation, a low value is to be expected. Furthermore, nanoparticulate electrochromic materials have a large surface area and the porosity of thin films prepared from spherical electrochromic nanoparticles can enhance the electrochromic device response characteristics because of improved ionic conductivity[29].

In order to further investigate the low coloration efficiency of the device, EIS was employed to quantify the conductivity of the oxidised and reduced states of device I. From figure 4.7 (a) the conductivity of the ionogel was found to be 4.08 x 10^{-7} S/cm^2.

For comparative purposes, the result obtained in **section 6.4.1.2** where the conductivity of a viologen physically entrapped in an ionogel based on a low viscosity IL ($[C_2mIm][FAP]$, 75 cP at 25 ^0C) was found to be 1.54 x 10^{-4} S/cm^2. This difference in the ionic conductivity of the ionogels can be attributed to the viscosity of the ionic liquid in question. $[P_{V,8,8,8}][3X]$ is a highly viscous yellow wax-like liquid, meaning its ability to carry current through ion flow is greatly reduced compared to that of a less viscous liquid in which the ions are more mobile such as $[C_2mIm][FAP]$[30, 31].

4.4.5 Device Calibration and Optical Memory

Experiments were then designed to calibrate the colour generated as a function of a D.C potential applied. To do this a series of devices were exposed to increasing applied voltages for 60 seconds, and the absorbance at 610 nm measured.

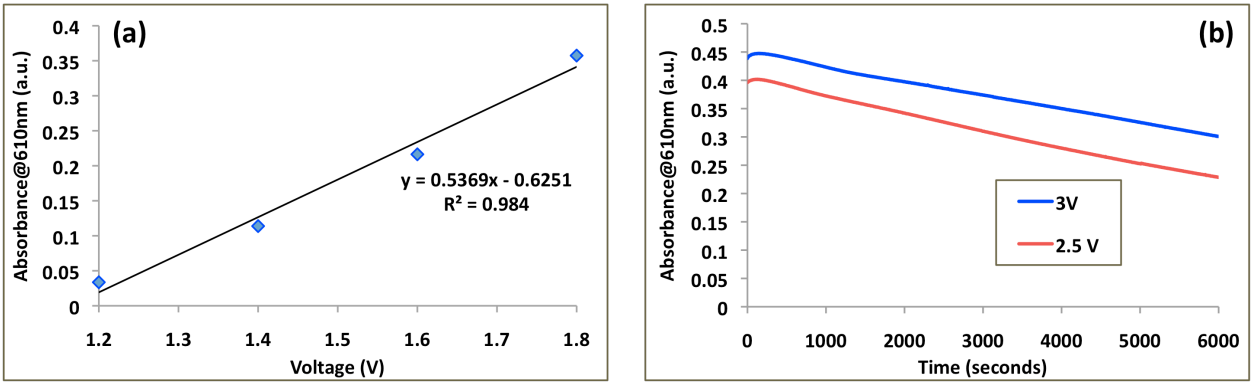

Figure 4.6: (a) Calibrated response obtained for the simplified electrochromic ionogel and **(b)** the optical memory recorded for the simplified electrochromic ionogel after 100 minutes.

It can be seen from figure 4.6 (a) that the optical response of Device I is linearly correlated with the applied potential. Throughout the course of the these experiments it was noted that the devices exhibited a prolonged optical memory, meaning the colour generated is significantly maintained under open circuit conditions[27]. To investigate this behaviour, devices were first brought to a coloured state by polarising at 2.5 V and 3 V (60 seconds), and monitoring the de-colouration process for a period of over 100 minutes under open circuit conditions.

Figure 4.6 (b) shows when an applied voltage is 2.5 V the absorbance at 610 nm increases to 0.396 a.u., 57.7% of which is maintained after 100 minutes.

When the applied voltage is 3 V the absorbance at 610 nm increases to 0.438 a.u., 68.5% of which is retained after 100 min. It is interesting that the rate of decrease in absorbance is relatively constant with time for both experiments at ca. $1.5x10^{-3}$ a.u./s. This is related to the leakage current of the device, which suggests it can be increased or reduced by varying the device insulation, or providing a more effective discharge pathway (see discussion below).

EIS proved to be a valid tool to explain why the reduced state is maintained under open circuit conditions. By amperometrically maintaining a current at the first reduction potential for 160 seconds, the direct impedance of the reduced monocationic radical form of the ionogel was estimated (figure 4.7 (a) and (b)).

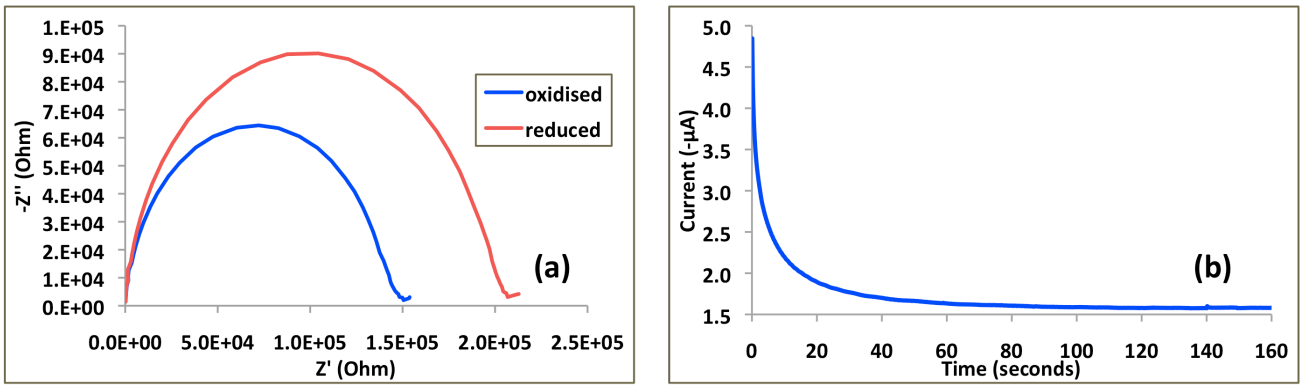

Figure 4.7: (a) Nyquist plots obtained for $[P_{V,8,8,8}][3X]$ in the oxidised (V^{2+}) and reduced state ($V^{\cdot+}$); **(b)** amperometric i-t curve used to generated the reduced state ($V^{\cdot+}$).

The resultant Nyquist plot exhibits an increase in impedance due to the loss of a cationic site. Furthermore the shape of the semicircle arc also increases; which is indicative of a capacitance effect. This explains the prolonged optical memory; as the presumed unstable monocationic radical is preserved due to an increased capacitance within the gel. This effect could be used to exploit a prolonged darkened state in electrochromic applications should the need arise.

4.4.6 Device Switching

The final device performance experiment involved attempts to reversibly switch between the coloured and transparent forms of the device using a potentiostat to repeatedly switch between the redox forms of viologen. For this experiment a 2-electrode set up was employed with the device placed in the optical pathway of the UV spectrometer to enable changes in absorbance to be simultaneously monitored. In order to take advantage of the stable electrochemical window endowed on the system by the IL, the voltage was allowed to cycle from -3 V to +3 V and the absorbance was monitored over time (sweep rate = 100 mV/s).

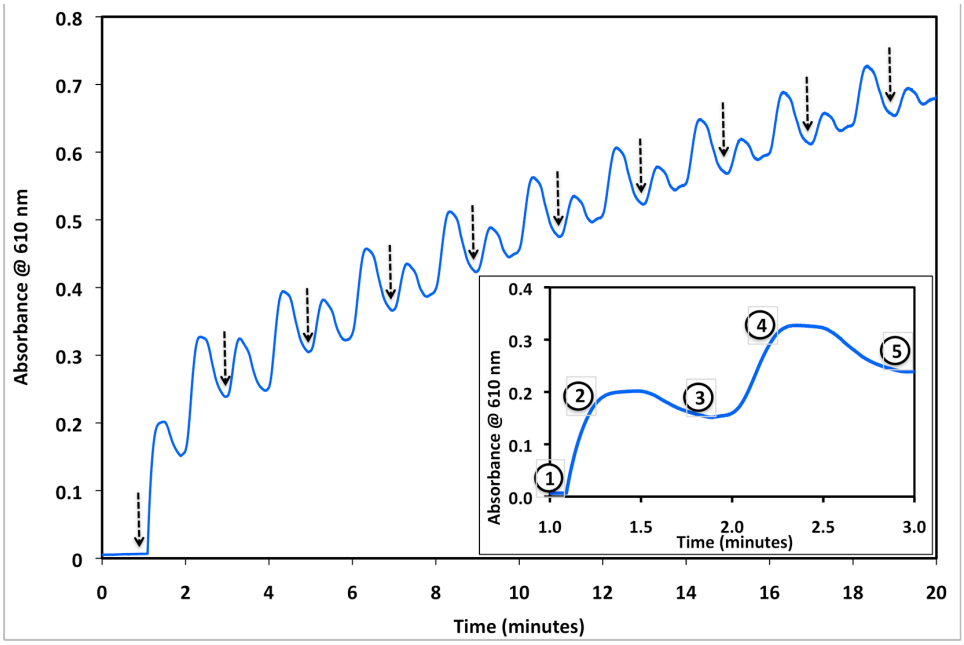

Figure 4.8: Changes in absorbance (610 nm) as a result of the $[P_{V,8,8,8}][3X]$ redox processes.

Figure 4.3 (a) shows the electrochemistry of the viologen system and figure 4.8, changes in absorbance over time as the cell is cycled repeatedly from 0 V (initial voltage) through -3 V to +3 V, and back to 0 V. The inset (right) shows absorbance changes over the time 1-3 minutes (the first CV), with distinct regions labelled 1-5.

Initially, at 0 V (1, inset), viologen exists in the colourless V^{2+} form, and the absorbance is low. As the voltage approaches and passes through -0.85 V, the reduction current increases as the viologen is reduced to blue coloured $V^{\bullet+}$ radical, and there is a simultaneous increase in the absorbance (2, inset). However, as the voltage passes through ca. -1.25 V, the coloured $V^{\bullet+}$ radical is converted to the colourless V form (quinoid) and the absorbance decreases (3, inset).

The voltage continues through -1.35 V to -3.0 V and then sweeps back in the positive direction. At ca. -1.0 V oxidation of V to the $V^{\bullet+}$ radical occurs and the absorbance increases again (4, inset). At -0.45 V oxidation of $V^{\bullet+}$ to V^{2+} occurs and the colour decreases again as voltage increases through 0 V to +3.0 V (5, inset); with a sweep rate of 100 mV/s, and a voltage range of +/- 3 V, each cycle takes 2 min, and the repeating pattern for each of the 9 indicated cycles (Figure 4.3 (a)), in which the two coloured regions caused by formation of $V^{\bullet+}$ are clearly visible. It is notable that the absorbance does not return to baseline after each cycle, indicating that residual $V^{\bullet+}$ remains in place, and gradually builds up over time. This is probably due to the rather sluggish kinetics of the redox chemistry within the cell, which also manifests as a dampened absorbance/time signal, with considerable broadening of the absorbance peaks.

The secondary absorbance cycle seen in the kinetic profile is assigned to subsequent oxidation of V back to $V^{\cdot+}$ as the potential cycles back to -0.95 V and the absorbance again increases. The final redox transition occurs at -0.46 V ($V^{\cdot+}$ to V^{2+}) and the absorbance again decreases. The effects of the individual redox equilibria on the absorbance are reproducible over time and a gradual staircase effect is seen in the final kinetic profile.

Figure 4.9 was constructed by taking individual segments from the decay response (600 – 1600 seconds under open circuit conditions, and between 150 and 175 seconds under anodic conditions). The initial time of each segment was redefined as t_0. This allows the effects of the absorbance decay under open circuit and anodic perturbations to be seen.

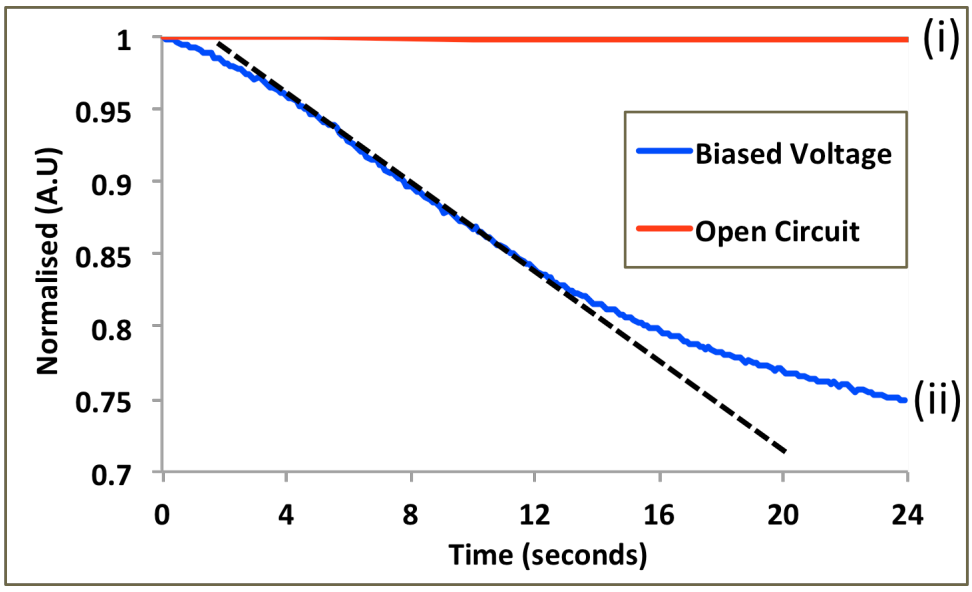

Figure 4.9: Normalised response decay obtained under **(i)** open circuit (abs 0.44 at 610 nm, t = 0) and **(ii)** positive biased voltage conditions (+3 V, abs 0.32 at 610 nm, t = 0). Slope of the line is calculated from the inflection point, shown by the dotted line.

Under open circuit conditions (Figure 4.9), the absorbance is stable in the timeline shown (24 sec) and the slope of the decay is relatively constant at ca. 3.27 x 10^{-5} a.u./s. Under anodic conditions, oxidation of the chromophore is induced and the decay is ca. 100 times more rapid (slope: 3.37 x 10^{-3} a.u./sec). This shows that rate of decoloration can be controlled to a significant degree by changing from a floating voltage (in which leakage current from the capacitive charge is the decoloration process) to a polarising voltage in which the redox chemistry of the coloured viologen monocationic radical is actively driven to the colourless V^{2+} form (in this case V = + 3 V and $V^{\cdot+} \rightarrow V^{2+} + e^-$). In addition, if the device is considered as a capacitor, improving the insulation would further reduce the leakage current, enabling the coloured state to be maintained for longer durations, which the decoloration process

(as it is actively driven) should remain unaffected. This means that one could maintain the coloured state until a pre-set time at which the device is connected to a polarising voltage and rapidly decolorises.

4.5 Conclusion

The synthesis of a novel phosphonium electrochromic IL has been described and the resulting material successfully incorporated into a solid-state electrochromic device. One major advantage of the electrochromic device is the fact that the viologen is inherently part of the IL and therefore no leaching occurs. The ease of its encapsulation within the inert polymer matrix and subsequent photo-polymerisation between two ITO electrodes formed the basis of a simple electrochromic device.

The inherent electrochromic nature of the MAV starting material provided the ideal control and validation experiment to authenticate the synthesis, as its electro-optical properties are significantly different to the $[P_{V,8,8,8]}][3X]$ IL.

Device 1 exhibited coloration kinetics close to two orders of magnitude faster (221 seconds for 95 % absorbance) compared to a previously reported electrochromic IL (18,000 seconds). The dynamics of colour change are determined by the ability to get charge into and out of the device, as this drives the redox chemistry of the coloration; therefore coloration can be controlled by alternatively insulating the device to prevent leakage current (which maintains the colour) or actively driving current into or out of the device, which gives much faster changes (100 times quicker). It is likely that the device characteristics can be further improved by improving the charge transport capability, for example by adding a high conductivity material such as carbon nanotubes to the gel and examine the colouration efficiency.

4.6 References

1. J. P. Coleman, J. J. Freeman, P. Madhukar and J. H. Wagenknecht, *Displays*, 1999, **20**, 145-154.
2. D. R. Rosseinsky and R. J. Mortimer, *Advanced Materials*, 2001, **13**, 783-793.
3. R. Vergaz, D. Barrios, J. M. Sanchez-Pena, C. Pozo-Gonzalo, M. Salsamendi and J. Pomposo, *Displays*, 2008, **29**, 401-407.
4. G. Chidichimo, M. De Benedittis, J. Lanzo, B. C. De Simone, D. Imbardelli, B. Gabriele, L. Veltri and G. Salerno, *Chemistry of Materials*, 2007, **19**, 353-358.
5. S. Dai, M. E. Sigman and E. L. Burch, *Chemistry of Materials*, 1995, **7**, 2054-2057.
6. K. C. Ho, Y. W. Fang, Y. C. Hsu and L. C. Chen, *Solid State Ionics*, 2003, **165**, 279-287.
7. X. Tu, X. Fu, Q. Jiang, Z. Liu and G. Chen, *Dyes and Pigments*, 2011, **88**, 39-43.
8. L. A. Godinez, R. Castro and A. E. Kaifer, *Langmuir*, 1996, **12**, 5087-5092.
9. F. Campus, P. Bonhote, M. Gratzel, S. Heinen and L. Walder, *Solar Energy Materials and Solar Cells*, 1999, **56**, 281-297.
10. R. J. Mortimer, A. L. Dyer and J. R. Reynolds, *Displays*, 2006, **27**, 2-18.
11. T. Sakano, F. Ito, T. Ono, O. Hirata, M. Ozawa and T. Nagamura, *Thin Solid Films*, 2010, **519**, 1458-1463.
12. C. L. Bird and A. T. Kuhn, *Chemical Society Reviews*, 1981, **10**, 49-82.
13. C. A. Melendres, P. C. Lee and D. Meisel, *Journal of the Electrochemical Society*, 1983, **130**, 1523-1527.

14. R. Cinnsealach, G. Boschloo, S. N. Rao and D. Fitzmaurice, *Solar Energy Materials and Solar Cells*, 1999, **57**, 107-125.

15. J. A. Barltrop and A. C. Jackson, *Journal of the Chemical Society-Perkin Transactions 2*, 1984, 367-371.

16. S. C. Dorman, R. A. O'Brien, A. T. Lewis, E. A. Salter, A. Wierzbicki, P. W. Hixon, R. E. Sykora, A. Mirjafari and J. H. Davis, Jr., *Chemical Communications*, 2011, **47**, 9072-9074.

17. S. G. Zhang, S. M. Liu, Q. H. Zhang and Y. Q. Deng, *Chemical Communications*, 2011, **47**, 6641-6643.

18. L. C. Branco and F. Pina, *Chemical Communications*, 2009, 6204-6206.

19. A. Branco, L. C. Branco and F. Pina, *Chemical Communications*, 2011, **47**, 2300-2302.

20. A. Kavanagh, R. Copperwhite, M. Oubaha, J. Owens, C. McDonagh, D. Diamond and R. Byrne, *Journal of Materials Chemistry*, 2011, **21**, 8687-8693.

21. S. Ahmad and M. Deepa, *Electrochemistry Communications*, 2007, **9**, 1635-1638.

22. R. E. Del Sesto, C. Corley, A. Robertson and J. S. Wilkes, *Journal of Organometallic Chemistry*, 2005, **690**, 2536-2542.

23. K. J. Fraser and D. R. MacFarlane, *Australian Journal of Chemistry*, 2009, **62**, 309-321.

24. K. J. Fraser, E. I. Izgorodina, M. Forsyth, J. L. Scott and D. R. MacFarlane, *Chemical Communications*, 2007, 3817-3819.

25. C. Lee, Y. M. Lee, M. S. Moon, S. H. Sang, J. W. Park, K. G. Kim and S. J. Jeon, *Journal of Electroanalytical Chemistry*, 1996, **416**, 139-144.

26. S. H. R. Brienne, P. D. W. Boyd, P. Schwerdtfeger, G. A. Bowmaker and R. P. Cooney, *Journal of the Chemical Society-Faraday Transactions*, 1993, **89**, 3015-3020.

27. D. Cummins, G. Boschloo, M. Ryan, D. Corr, S. N. Rao and D. Fitzmaurice, *Journal of Physical Chemistry B*, 2000, **104**, 11449-11459.

28. A. A. Argun, P. H. Aubert, B. C. Thompson, I. Schwendeman, C. L. Gaupp, J. Hwang, N. J. Pinto, D. B. Tanner, A. G. MacDiarmid and J. R. Reynolds, *Chemistry of Materials*, 2004, **16**, 4401-4412.

29. V. Jain, M. Khiterer, R. Montazami, H. M. Yochum, K. J. Shea and J. R. Heflin, *Acs Applied Materials & Interfaces*, 2009, **1**, 83-89.

30. P. Hapiot and C. Lagrost, *Chemical Reviews*, 2008, **108**, 2238-2264.

31. D. R. MacFarlane, M. Forsyth, E. I. Izgorodina, A. P. Abbott, G. Annat and K. Fraser, *Physical Chemistry Chemical Physics*, 2009, **11**, 4962-4967.

Chapter 5

Photopatternable, photoswitchable surface chemistry in organic/inorganic sol-gels

5.1 Abstract:

This chapter describes the synthesis and characterisation of hybrid sol-gel materials co-polymerised with a monomer based on the light responsive chromophore Spiropyran (SP). The hybrid materials contain a silane centre chemically tethered to an acrylate monomer via a propyl linker which are co-polymerised with a varying metal propoxide/methacrylate complex. These hybrid materials are of the optimum mechanical stability for patterning under incident light. This chapter therefore provides the reader with an in-depth discussion of the chemistries required for sol-gel preparation and the area of photopatterning of sub-micron 3-D structures.

Initial studies showed that sol-gels containing d-block (Zr,Ti) propoxides exhibited irreversible chelation to SP, resulting in a change in their absorption properties from colourless to red (for Zr gels) and yellow to orange (Ti gels). The effects of chelation were characterised principally by molecular spectroscopy, whilst the change in surface chemistry of the polymerised film is characterised by their direct contact angle with a water droplet.

Sol-gels based on aluminium *iso*-propoxide permit the light responsive chemistry of SP and were chosen for photofabrication based on multi-photon polymerisation techniques. Spiral structures, that are patterned in the style of the chromophore were fabricated with precise geometries and sub-micron resolutions. The new, light responsive materials exhibited minimal-shrinkage after fabrication, and possess the mechanical stability to be patterned as free standing structures without a supporting perimeter.

5.2 Introduction:

Hybrid sol-gels are a subclass of polymers that combine the classical hydrolysis/condensation reactions of metal alkoxide groups with organic functional moieties[1]. Based on the interaction between the components, they have been categorised into class I and class II hybrid sol-gels respectively[2]. Class I hybrids are subdivided on the basis that both organic and inorganic components exhibit exclusive non-covalent interactions, i.e. they exist as two individual components within the same matrix[3].

Class II differ in that in these materials the metal alkoxides are chemically tethered to the organic moiety via a stable linker. The linker therefore must be stable under the conditions required for condensation of the metal alkoxide in order to preserve the covalent interaction[4].

Both sub classes of sol-gels are very attractive canditates for materials research as they combine the individual features of both components within the same material. These include the low refractive index and mechanical stability of glassy materials with the ease of film formation typical of organic systems.

Efforts aimed at tuning the optical properties of these materials involve the addition of a second metal-alkoxide group. As the first group is typically based on silicon, alkoxides of titanium, aluminium and zirconium are the most popular secondary alkoxide used[5, 6]. The reactivity of the secondary alkoxide is dictated by the relative dipole moment of the oxide bond, which is usually much higher than that of Silicon. In order to control this reactivity Ti, Al and Zr are usually complexed with a suitable ligand in order to prevent precipitation of the fully condensed material[4, 7].

Varying the stoichiometric ratio of the secondary alkoxide alters the optical properties of the resultant film which is produced via free radical methods. Materials of this type have therefore found application in optical waveguides[8] and sensors[9].

Arguably the most novel aspect of these materials is that they are of the required mechanical stability to be patterned under application of irradiated light. Direct photopatterning techniques allow the formation of structures with precise dimensions[10, 11]. The high concentration of inorganic groups allows 3-D structures to be fabricated which exhibit non-shrinkage properties after etching[12]. The precise geometry of the polymerised structures are a direct function of the exposure time and the focal point of the light source, both of which are controlled by the user[13, 14].

In this chapter the aim is to co-polymerise a monomer based on the optical chromophore Spiropyran (SP) with these photoreactive class II hybrid sol-gels in order to **(a)** demonstrate that these SP functionalised can be photo-patterned into complex 3-D structures and **(b)** exploit the photoswitchable properties of the dye embedded within.

Spirocyclic compounds and their merocyanine (MC) isomers exist in a photodynamic equilibrium, controlled by the application of visible and ultraviolet light respectively[15, 16]. Such a phenomenon is known as *Photochromism*, as the application of light causes a change in the optical properties of the molecule[17]. The equilibrium between two photochromic isomers **A** and **B** can be summarised according to equation 5.1.

$$\mathbf{A} \underset{\lambda_2}{\overset{\lambda_1}{\rightleftharpoons}} \mathbf{B} \qquad \textbf{(5.1)}$$

Where λ_1 and λ_2 are two light incidences of distinct frequencies. Irradiation of species **A** with light of wavelength λ_1 causes a molecular re-orientation within the molecule producing species **B.** The molecular reorientation can be reversed under application of light of wavelength λ_2.

Previous works utilising SP and MC have seen them behave in systems capable of user controlled transition metal ion uptake and release[18, 19], as effective solvatochromic probes[20, 21] and as hybrid materials that exhibit user controlled multi-switchable optical properties[22].

Most importantly for this work, the SP or closed isomer is "non-polar", UV irradiation results in cleavage of the C_{spiro} bond, heterocylic ring opening and a large change in dipole moment yielding the "polar" MC isomer[17, 23].

It is this property that allows the SP/MC equilibrium to be utilized in materials that can undergo a change in their surface energy upon application of light of the appropriate frequency[24-26].The ability to modify the surface energy of a given substrate has been the subject of a concerted amount of research, resulting in applications of this phenomenon in areas such as drug delivery[27], controlled cell growth[28] and in the control of fluid movement in microfluidic devices[29, 30]. To date, systems have been shown to undergo a reversible change in surface energy in response to pH[31], metal ions[24], applied voltages[32, 33] and irradiation with light[34, 35].

An interesting approach to improve the difference in contact angle between the hydrophillic and hydrophobic state has been to enhance or modify the structure of the surface[36, 37]. The difference is amplified as the treated surface creates voids on the surface which – upon switching to the hydrophillic state – allowing the probing liquid to enter the void.

Herein this chapter describes the progress into the integration of SP into these hybrid photopatternable materials, with a view to switching the optical and surface properties of the photopatterned materials using light. SP undergoes chelation with d-orbital based hybrid materials and the chemistry is subsequentially charactersied using UV/Vis and IR spectroscopy.

Al based materials facilitate the ring opening process, allowing the optical difference btween SP and MC states to be visualised within a polymerised surface. Contact angles of all incidences involving the interaction of SP with metal alkoxides are also presented. Finally, mechanically stable 3-D structures patterned using a 2-photon polymerisation technique according to the theme of the research are also presented.

5.3 Experimental:

5.3.1 Chemicals and Materials:

MAPTMS, ZrPO, TiPO, AlPO MAAH were all used as purchased from Sigma-Aldrich® Ireland Ltd.

Igracure® 184 (generously donated by Ciba® chemicals) and diethylaminobenzophenone were used as the photoinitiators for the single and multi-photon polymerisation techniques respectively.

5.3.2 Synthesis of Hybrid Sol-Gels:

The sol-gel synthesis was based on the formation of a stable and homogeneous material obtained from the reaction between a photosensitive organically modified precursor MAPTMS, and a methacrylate based complex of the various metal alkoxides.

The first step (as denoted in scheme 5.1) involved pre-hydrolysis of MAPTMS with an aqueous solution (HCl, pH2), employing a 1.00: 0.75 water to alkoxide molar ratio. As MAPTMS and water are not miscible, the hydrolysis was performed in a heterogeneous way. After 20 min of stirring, the production of methanol became sufficient to allow the miscibility of all species leading to a transparent solution. The reaction was then allowed to stir for a further 25 minutes.

In order to control the hydrolysis–condensation kinetics and the formation of unwanted agglomerates of the various metal propoxides (MPO); a parallel reaction involving MAAH as a chelating agent was employed as it forms a complex through displacement of the ether based propoxide chains (step 2, scheme 5.1).

After 45 minutes of the parallel reaction the pre-hydrolysed MAPTMS solution was added dropwise to the methacrylate complex, characterised by an exothermic reaction (step 3, scheme 5.1).

Following another 45 minutes of reaction, in order to improve the homogeneity of both molecular systems, the 4th step involved a second hydrolysis reaction using water (pH 7). The final water concentration used was 1.5: 1 (H_2O: alkoxide), which ensured complete condensation of all reactive moieties. The final sol was then left stirring for 24 hours before use. All sol-gels were prepared in this fashion, and are listed below:

MAPTMS: ZrPO: MAAH (10: 4: 4)	**(1)**
MAPTMS: TiPO: MAAH (10: 4: 4)	**(2)**
MAPTMS: AlPO: MAAH (10: 4: 4)	**(3)**
MAPTMS	**(4)**

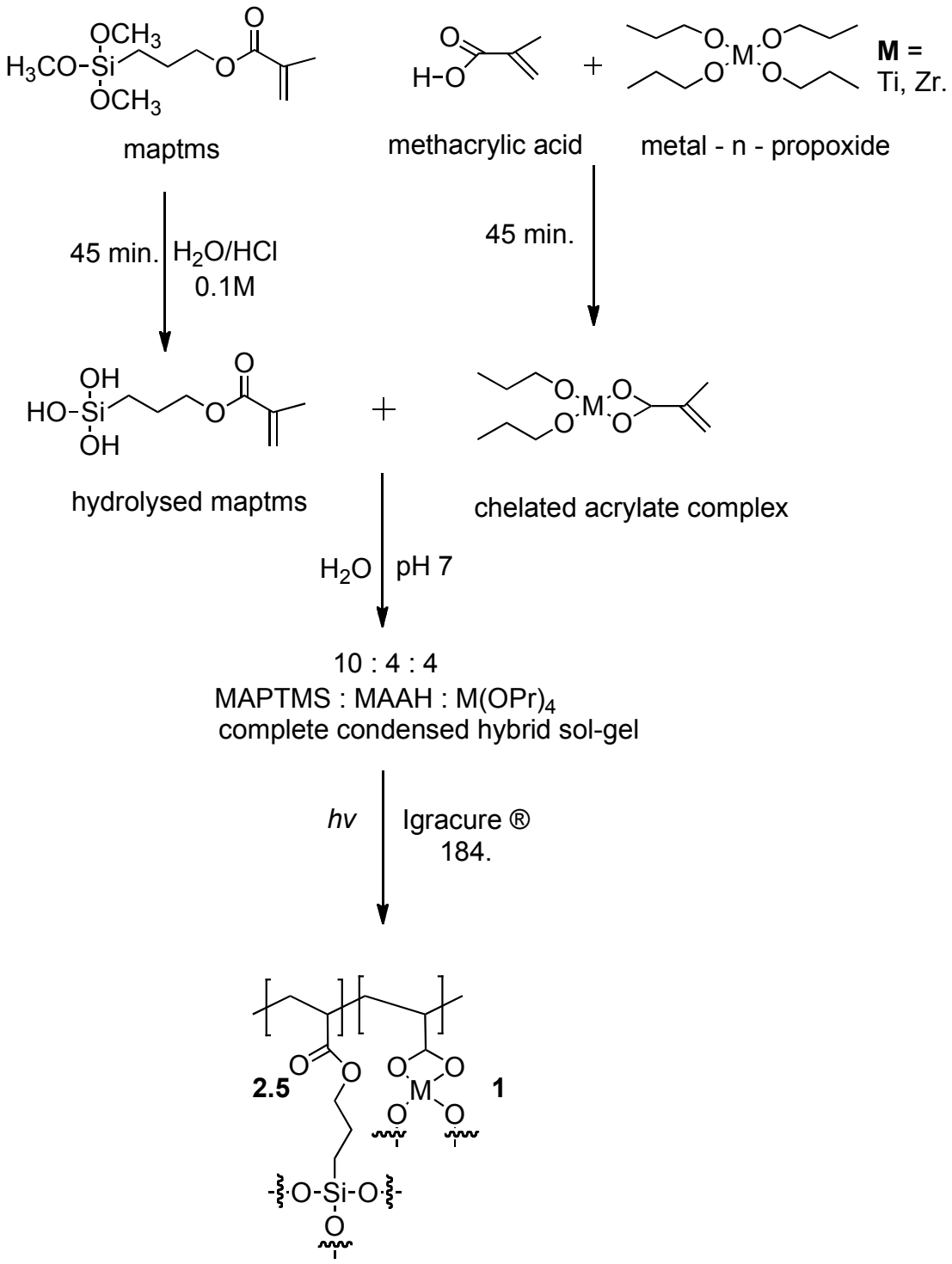

Scheme 5.1: The parallel synthetic route employed to produce the sol-gels used in this work.

5.3.3 Synthesis of the SP monomer:

The synthesis of the SP monomer **[***1' ,(9-decenyl)-3' ,3' -dimethyl-6-nitrospiro[2H-1]-benzopyran-2,2' -(2H)-indoline***]** derivative was performed as described in a previous work[38].

This involved a two-step synthesis involving first the precursor 2,3,3 – trimethylindoline. It was allowed to undergo nucleophilic attack using 10-bromo-1-decene as the electrophile under basic condtions at 80^0C.

Next the product from the first step underwent coupling with nitrosalicylaldehyde under the same conditions to yield the monomeric SP product.

5.3.4 Preparation of the SP functionalised sol-gels:

In order to prepare the photo responsive sol-gel; 1 mol% of the SP monomer was dissolved in the condensed sol-gel precursors. The photoinitiator concentration was kept constant at 5wt.% for all sol-gels prepared.

All of the surfaces analysed for their contact angle were prepared by spin coating under saturated alcohol conditions onto 22 x 22 mm microscope glass slides.

Ultraviolet photo-polymerisation was then performed using the UV light source for 5 minutes. A summary of the preparation and polymerisation of the Al gel can be seen in scheme 5.2.

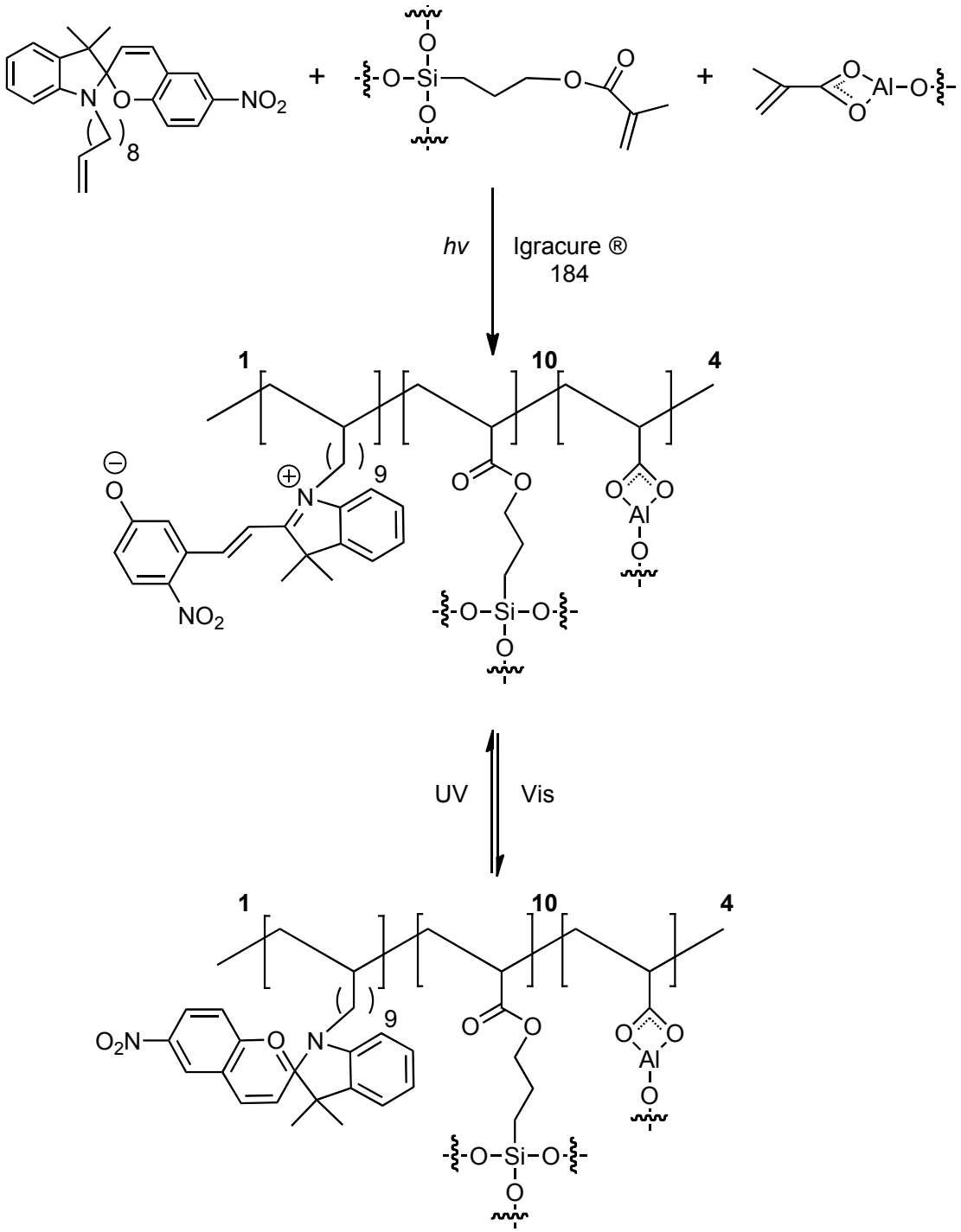

Scheme 5.2: Synthesis of SP functionalised sol gel based on photo-induced co-polymerisation of the hybrid precursors MAPTMS, AlPO/MAAH complex and the SP monomer. The photodynamic equilibrium between SP and MC is also depicted.

5.4 Results and Discussion:

5.4.1 Vibrational analysis of synthesised sol-gels

Given the nature of the materials studied, IR spectroscopy was employed to assign the various molecular stretching that originate within them. In order to form a valid comparative the spectra presented are the gels in their final condensed liquid form.

The IR spectrum of MAPTMS (figure 5.1) was found to contain aliphatic C-H stretching at ~2900 cm^{-1} which we attribute to contributions arising from the tethered acrylate moiety. Methanol produced as a by-product is evident via a broad stretch at ~3200 cm^{-1}, whilst the carbonyl and the siloxane contributions can be seen at 1700 and 1000 cm^{-1} respectively. The stretch at 1640 cm^{-1} is the unpolymerised double bond of the acrylate moiety.

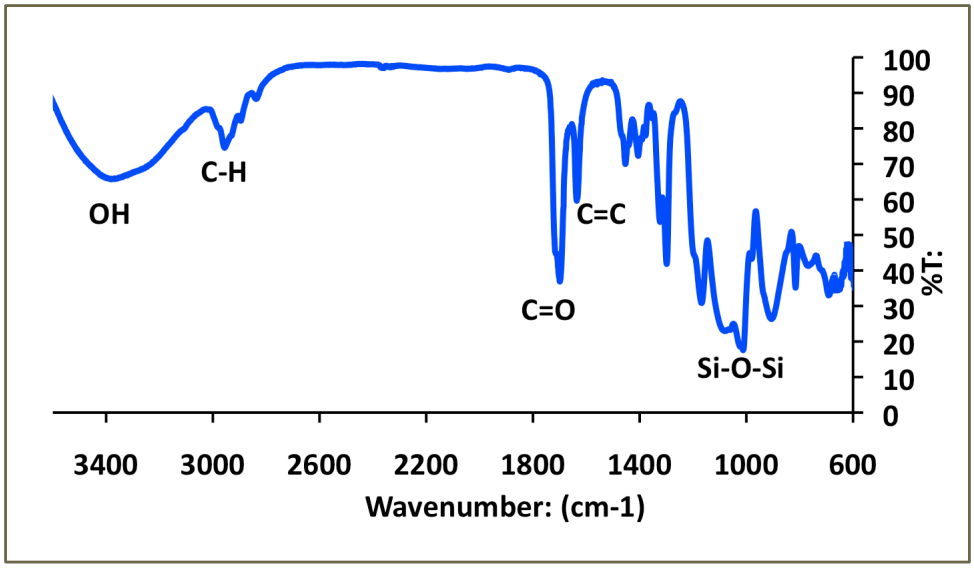

Figure 5.1 IR spectrum obtained for complete condensed MAPTMS solution.

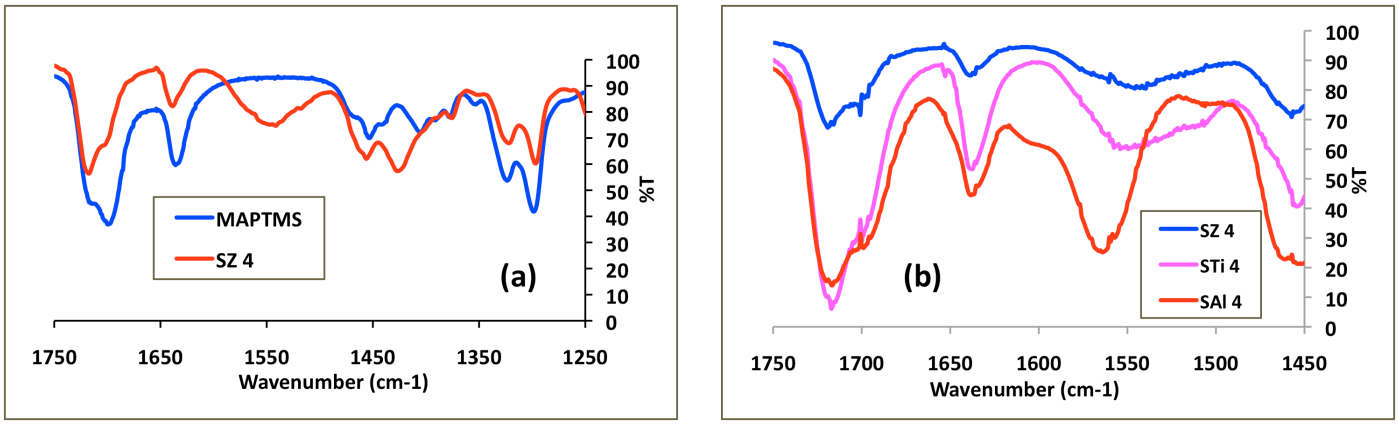

Figure 5.2: (a) IR spectra obtained for MAPTMS vs. SZr 4 gel and **(b)** spectral overlay of Zr, Ti and Al based gels confirming the methacrylate complex formation.

As expected the same contributions are evident in the SZr 4 spectrum (figure 5.2(a)). Complexation of ZrPO with MAAH results in the formation of a new stretch at 1545 cm^{-1}, which has been attributed to a carboxylate contribution as part of a bridging co-ordinate geometry[39].

This stretch can therefore be used to confirm the complexation of MAAH with the Al and Ti alkoxides (figure 5.2 (b)). This figure was baseline corrected in the regions from 1900 – 2400 cm^{-1} where no spectral activity was seen, and normalised according to the aliphatic C-H content. It can be seen from this figure that the trend in transmission values of the acrylate complex is of the order Al > Ti > Zr. The carboxylate stretch was observed at 1569 cm^{-1} and 1554 cm^{-1} for both Al and Ti based sol-gels respectively.

5.4.2 Contact angle determination

Given that the metallate is the only variant in the analysis we sought out to see if it would dictate the surface chemistry of the polymerised sol-gel. Table 5.1 below summarises the results across all three polymerised films, and are the averages of 5 individual measurements.

Propoxide Variant:	**Contact Angle:**
Zr	68.23^0 (3.01^0)
Ti	65.6^0 (1.66^0)
Al	62.97^0 (0.75^0)

Table 5.1: Measured contact angles for the initial sol-gels prepared based on the alteration of the metal propoxides (errors in parentheses).

The transmission trend of the carboxylate stretch does indeed correlate with the surface chemistry of the polymerised sol-gels. The same trend is repeated as before, the Zr-O bond exhibits the weakest dipole moment of the three and therefore is the most hydrophobic. Al-O based sol-gels are therefore the most hydrophilic whilst Ti-O gels are again in between the two relative extremes.

5.4.3 Characterisation of SP functionalised materials:

5.4.3.1 Spectroscopic Analysis

In order to examine the effects of adding the SP material to the sol-gels, equivalent sol-gels were prepared with 1mol% SP incorporated. The first striking effect noted was the generation of red and orange colours within the Zr and Ti based materials respectively, which can be ascribed to chelation of the chromophore by the metallate complex. We have credited the generation of new colours within Zr and Ti based sol-gel solutions to be a result of charge-transfer complexes involving the d-orbital of the transtion elements. Subsequent characterisation of this consequence was performed using UV/Vis and IR spectroscopy.

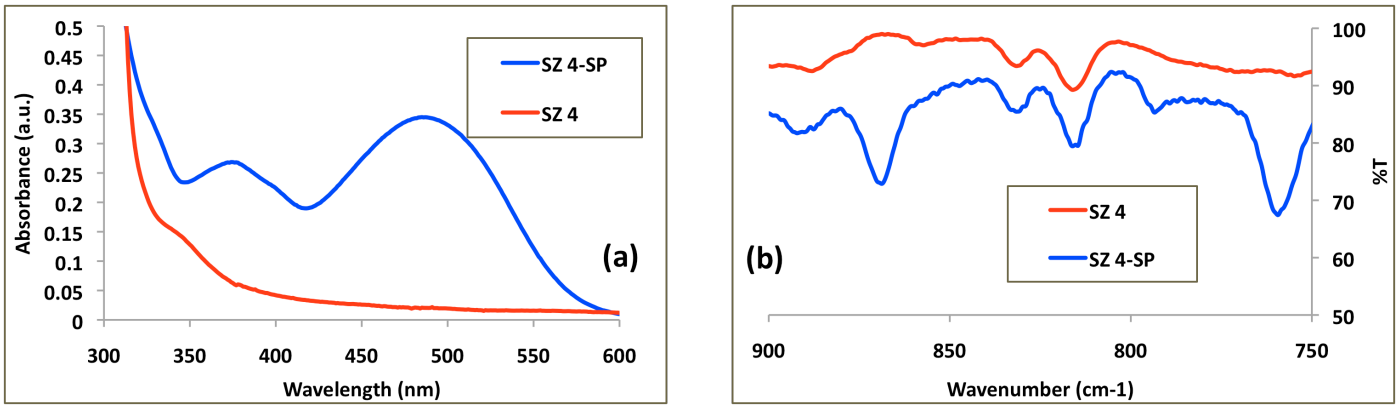

Figure 5.3: (a) UV/Vis spectra obtained for the addition of SP to the SZr 4 sol-gel, **(b)** the corresponding IR spectra.

Figure 5.3 (a) shows the visible spectra obtained upon addition of SP to SZr 4. The sol-gel solution undergoes a change in its optical properties from colourless to red, resulting in two new distinct absorption maxima at 383 and 493nm respectively. The colour of the solution could not be reversed under white light; a trait not expected for SP based chelation.

By plotting an overlay of the fingerpint IR region of the two materials (i.e. colourless vs. red), three new stretches appear for the complexed spectrum at 871, 794 and 760 cm^{-1} respectively (Figure 5.3(b)). The two new individual stretches observed serve to validate that complexation has occurred. Given the region involved, this points toward the formation of a transduction complex between Zr and the electron rich indoline and pyran elements of SP.

This irreversible trait is not favourable for applications involving the photodynamic control of surfaces. The first efforts to overcome this feature involved the synthesis of sol-gels with incrementally decreasing molar concentration of the initial Zr/methacrylate complex. Sols were prepared with with Zr/MAAH ratios of two and one respectively (SZ1, SZ2). The results are displayed in Figure 5.4 below show that despite lowering the Zr concentration, complexation still occurred.

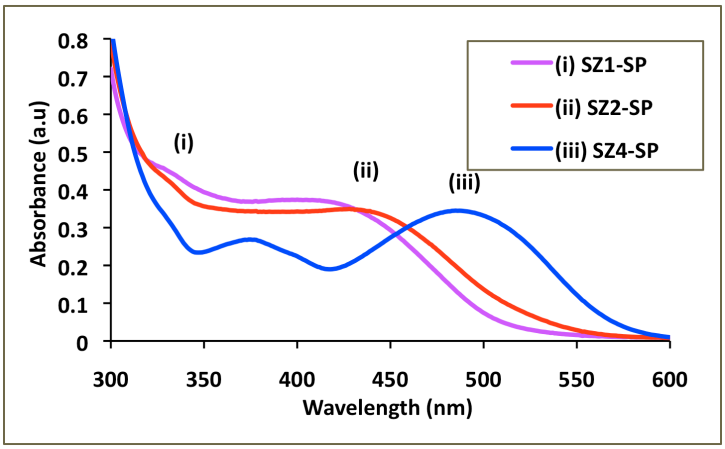

Figure 5.4: Effect of decreasing Zr concentration (from SZr 4 to SZ2 and SZ1) on the absorption maxima of SP containing sol-gels.

Decreasing the Zr concentration shifted the absorption maxima hypsochromically. The colour formed within the sol-gel still proved irreversible under application of white light. It should be noted that the Zr content in gels of this nature has been proven to co-ordinate with other constituents of the monomer solution. In previous works Zr underwent irreversible chelation to the amino based photoinitiators used for polymerisation, resulting in the same change in optical properties of the solution as observed in this work[40].

A control experiment involved removing the acrylate complex from the synthetic route altogether, to see if the silane based material MAPTMS could facilitate the photoequilibrium. Addition of SP to MAPTMS yielded no optical evidence of complexation and optical switching to MC was achieved using UV light. The MC isomer was stabilised due to the high polarity of the condensed MAPTMS solution (figure 5.5 (a)).

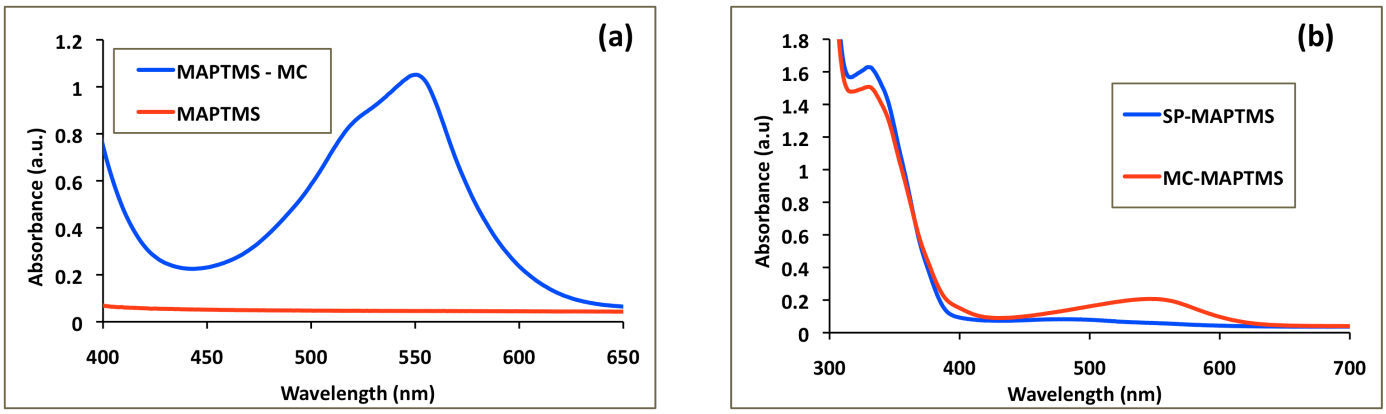

Figure 5.5: (a) UV/Vis spectra obtained for MAPTMS, and MC in MAPTMS and **(b)** UV/Vis spectra obtained for SP and MC as part of MAPTMS based film.

Once a film based on MAPTMS alone was photopolymerised (figure 5.5 (b)), it was possible to manipulate and control the SP/MC equilibrium. Unfortunately however, MAPTMS is defined extensively in the literature as a precursor for polymer gel formation with films described as "tacky" in one particular report[41]. Even under extreme conditions, the film does not dry fully rendering it invalid for applications involving surface chemistry.

It was decided therefore that a new strategy should be employed which involved variation of the central metallic element that undergoes complexation with MAAH in the original synthesis. For this TiPO and AlPO were employed in the same stoichiometric ratio as SZr 4.

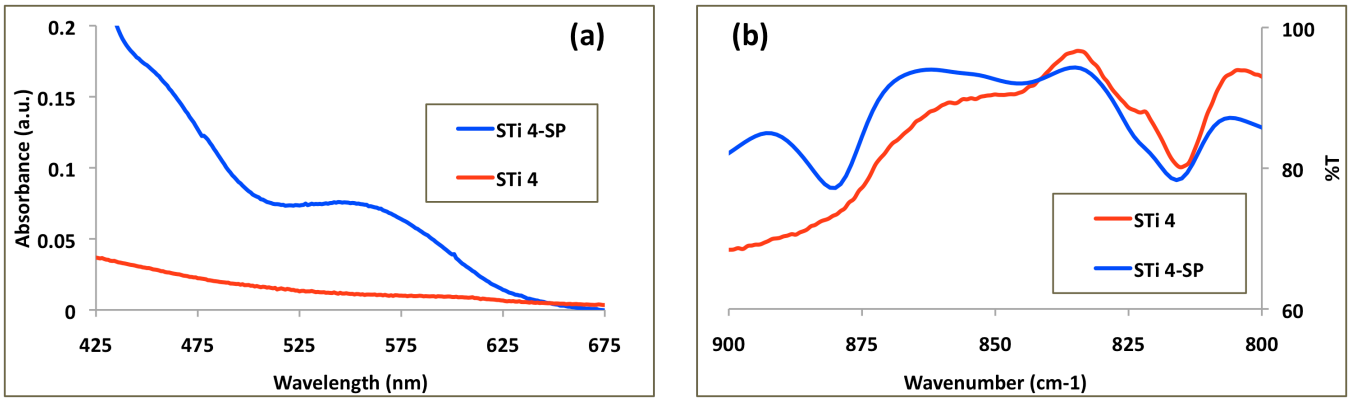

Figure 5.6: (a) UV/Vis spectra obtained for the complexation of STi 4 gel with SP and **(b)** the corresponding IR spectra.

Figure 5.6 (a) shows the spectra obtained after addition of SP to the STi 4. In this instance a dark orange colour is generated and new absorption maxima produced at 461 and 567 nm respectively. It should be noted that the original TiO/MAAH complex is yellow and so accounts for the orange colour of the complex formed. IR analysis reveals only one new stretch (Figure 5.6(b)), at 882 cm^{-1}. This points toward differing co-ordination geometry in this case, but again most likely through the electron rich heterocycles. The new Ti stretch attributed to complexation occurs at 12 wavenumbers higher when compared to Zr, which is due to the higher electronegativity of Ti over Zr.

The final metallic sol-gel prepared was based on AlPO, it was anticipated that this atmosphere would prove favourable to the SP – MC equilibrium due to the lack of d-orbitals in Al. This proved true to a degree, as addition of SP to the gel resulted in a faint yellow colour (Figure 5.7).

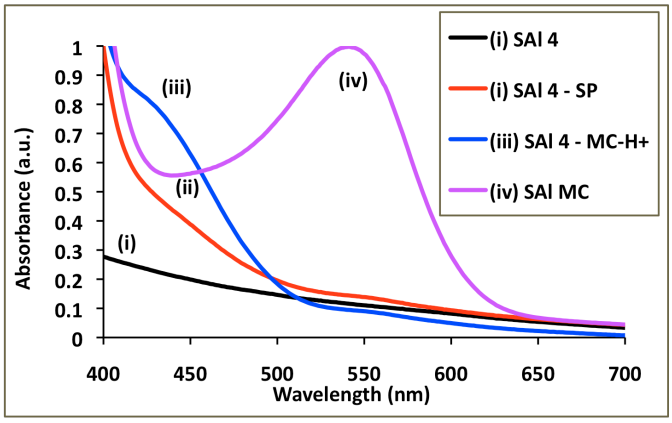

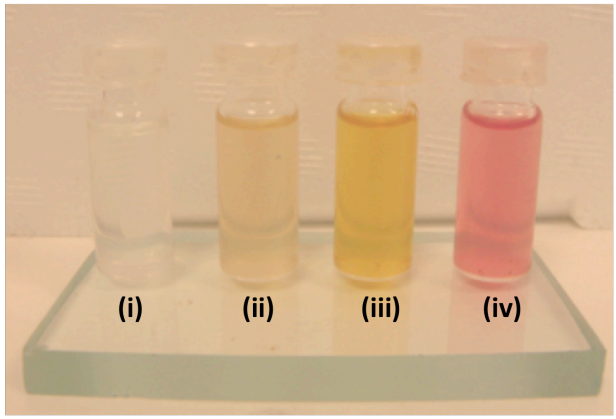

Figure 5.7: Optical properties of SP in SAl 4 sol-gel. **(i)** is used to denote the optical spectra of the original SAl 4 material, **(ii)** upon addition of SP, **(iii)** after irradiaton with UV light for 60 seconds and **(iv)** upon titration with a base.

Spirocyclic structures are influenced by the pH of the local environment[42]. This acidochromic effect means that in the presence of residual acid, ring opening is induced and protonation of the phenolate anion occurs with a characteristic yellow colour formed in solution[43]. The yellow colour obtained when SP is introduced into SAl 4 is therefore attributed to the acidic environment of this gel.

Irradiation of the faint yellow solution for 60 seconds with UV light yielded a strong dark yellow colour, indicating that the concentration of the protonated structure has increased. This process is reversible under white light; titration with a small volume of base gave the characteristic violet/purple colour of MC. The MC isomer was then preserved within the monomer solution as the acid became neutralised in the polar (short chain alcohol) environment.

It was decided therefore to reduce the acidic nature of the Al gel by preparing a sol of the stoichiometry: 10/4/0.5 (MAPTMS/AlPO/MAAH) under much milder acid catalyst conditions (HCl, pH 3.5). The same acidochromic behaviour was observed for this sol, rendering it easy to conclude that the acid nature is inherent to the material studied. Al based gels are therefore the most optimum to facilitate the SP to MC ring opening process.

5.4.3.2 Contact Angle determination

5.4.3.2.1 Photodynamic studies

As the behaviour of the SP was now fully understood in the differing sol-gel formulations, experiments were then undertaken to examine its affect on the surface chemistry. The first experiments undertaken were to prepare films via spin-coating of the optimised SAl 4 gels.

Isomer:	**Contact Angle: (error)**
SP	67.73^0 (2.59^0)
MC – H^+	65.66 (2.73^0)

Table 5.2: Contact angle values obtained for SP to MC-H^+ switching in SAl 4 sol-gels.

Table 5.2 shows that the initial introduction of SP results in an increase in hydrophobicity vs. the original SAl 4 material. As SP contains a dec-1-ene chain and is polymerised in relatively high concentrations, one can therefore conclude that this feature is a result of the unsaturated chain.

Application of UV light for 60 seconds induces the ring opening and colour change in the film, and the contact angle was again measured. Switching back to the closed form was achieved using white light for the same time and the contact angle again measured. Switching experiments were repeated a total of 5 times, resulting in a change in contact angle of ~2^0. This negligible change in contact angle occurs as the acidic nature of the gel prevents the generation of the unprotonated MC isomer. The MC isomer is essential in order to yield a significant change in the chemistry of the surface, as it is this structure that contains much more extensively π-delocalised electrons and ionic sites.

5.4.3.2.2 Effect of Complexation

The final experiments of the unpatterned surfaces were to examine the effects of complexation of SP with Ti and Zr. The results across 5 measurements are shown below in Table 5.3.

SP sol:	**Contact Angle:**
STi 4	70.2^0 (1.73^0)
SZr 4	70.77^0 (1.66^0)

Table 5.3: Contact angle values obtained for complexed films of SP with STi 4 and SZr 4 (errors in parentheses).

It can be seen in both circumstances that metal chelation causes an increase in the hydrophobicity of the polymerised surface. Chelation of Ti induces a 5-degree increase whilst chelation of Zr induces a 3-degree change.

This goes against the convention for SP systems, wherein complexation usually occurs after the ring opening process resulting in a more hydrophilic surface[24]. The surface chemistry therefore becomes more hydrophilic as the complex is usually between the metal ion and the phenolate base of the MC isomer[44].

In the cases studied the complexation of the ligand proved irreversible after irradiation of white light, and resulted in an increase in hydrophobicity of the polymerised surface. One can conclude from these results that the complexation does not follow the conventions described for SP based studies.

5.4.4 Photopatterning of SP functionalised materials:

A particularly attractive feature of these materials is the ability to be photopatterned into structures of precise dimensions. Experiments to demonstrate the compatibility of the SP functionalised systems involved the use of direct UV laser writing and 2-photon polymerisation based techniques.

5.4.4.1 Direct UV laser writing

For the direct laser written sample of varying distances between the lines, contact angles were taken to see if the line distance could influence the photochromic equilibrium.

Line distance: (μm)	**Contact Angle:**	
50	*SP*	*MC*
	75.78^0	72.94^0
100	*SP*	*MC*
	72.37^0	68.98^0
200	*SP*	*MC*
	72.54^0	69.88^0

Table 5.4: Contact angles obtained for 50, 100 and 200 μm distance between UV laser written lines. Visible light irradiated samples are on the left whilst UV irradiated samples are on the right.

Direct laser writing allows the distance between individual lines written to be selected by the user. In order to test the hypothesis discussed individual line distances were varied incrementally from 50 to 100 and 200 μm between individual lines.

It was found however, that varying the distance between the individual lines altered the contact angle very little.

The initial contact angle is increased however, which can be attributed to an effect of patterning the surface known as the *Cassie-Baxter* model[45]. Under this model air first fill the voids generated by the pattern, which effectively stabilises the liquid droplet on the surface causing an increase in hydrophobicity. Switching the chromophore between the polar and non-polar states caused the contact angle to reversibly change by ~4^0 in all cases.

5.4.4.2 2PP polymerised structures:

In keeping with the chemical nature of SP; experiments to demonstrate the 3-D compatibility of the novel materials involved patterning them into repeating spiral structures in sequence. Figure 5.8 (a) below first shows the complete surface area patterned, whilst Figure 5.8 (b) details the individual repeating structures. The spiral diameter was 1.3 µm, the height was 6 µm (3 pitches of 2 µm), and the gaps in-between the spirals was 0.7 µm, which were patterned into an array of a 50x50 µm area.

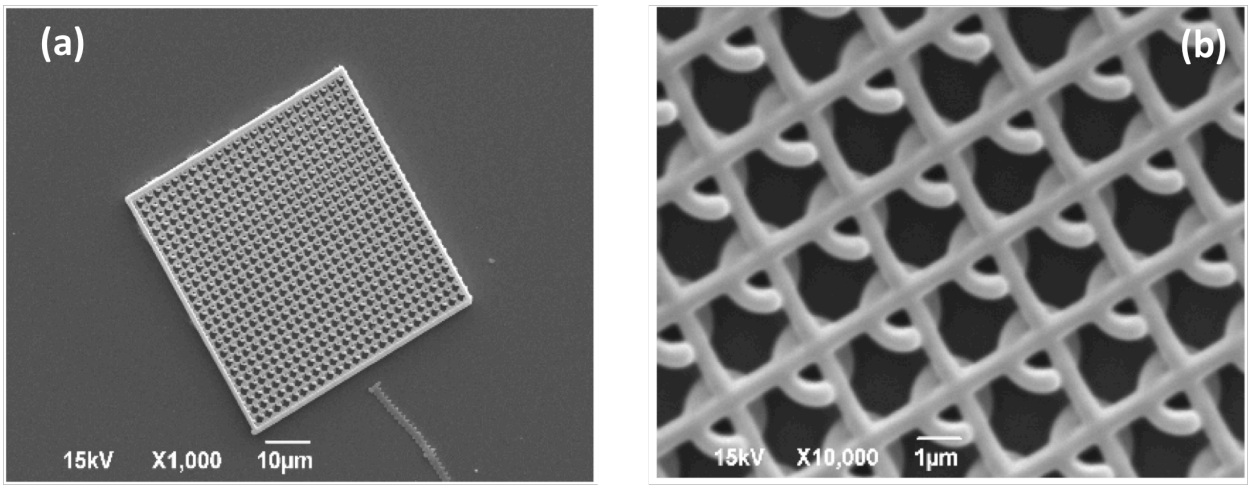

Figure 5.8: 2PP spiral patterning structures of Aluminium based SP sol-gel.

These images effectively demonstrate the complete compatibility of the materials for photopatterning. The microstructures shown exhibit minimal-shrinkage qualities after fabrication, meaning they avoid mechanical deformation over time.

As the first structure was first created using a supporting structure across the entire perimeter of the patterns, it was decided to test the mechanical stability of the new material even further by patterning them into freestanding spiral structures without the supporting perimeter wall. The spirals were patterned to the same dimensions as before.

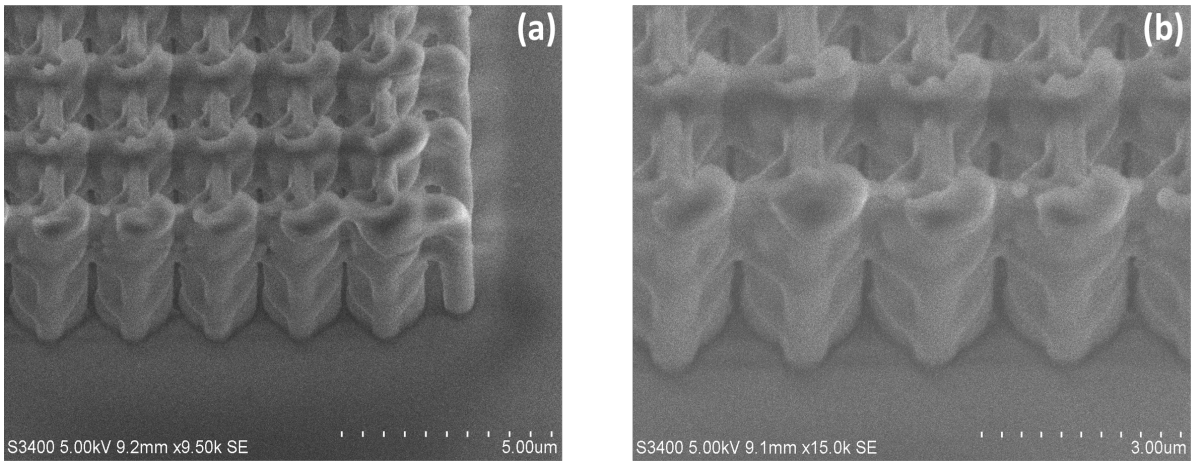

Figure 5.8: (a) and **(b)** Free-standing SP functionalised SAl 4 2PP produced spiral structures.

Figure 5.8 (a) and (b) effectively demonstrate the increased mechanical stability of the SP functionalised sol-gels. The complex structures are patterned to exact repeating dimensions with sub-micron resolutions without the need for a supporting perimeter.

5.5 Conclusion:

In summary this chapter focused on integrating and fully characterising how the optical chromophore SP behaves in a variety of sol-gel environments. The nature and the concentration of the metallate strongly influenced the optical properties of SP.

UV and IR spectroscopy convincingly show that SP undergoes irreversible chelation to sol- gels containing d-block elements. Complexation was found to influence strongly the surface energy of the resultant polymerised film. Irreversible complexation is undesirable for applications involving a user-controlled energy of a surface and therefore a new environment was needed.

Al containing gels were found to be the most optimum to facilitate the SP to MC interconversion. Direct laser writing of these materials into pillar structures increased the hydrophobicity over the untreated material. SP was reversibly switched to its protonated MC isomer as part of these patterned films, which in turn reversibly altered their surface energy moderately. 2PP demonstrated that these novel photochromic hybrid materials are suitable for fabrication in three dimensions. 3-D repetitive stand-alone spirals were patterned on a sub-micron scale to effectively demonstrate this feature.

SP functionalised patterned systems have been shown in the literature to undergo a reversible change in wettability as high as 21 degrees[45]. As the photopatternability of these systems has now been demonstrated, future work must now be aimed at optimising the sol-gel environment to improve on current switching parameters.

Tremendous ability now lies in the possibility of developing sub-micron patterned structures that can alter their optical properties as a function of the incident light source.

5.6 References:

1. F. Ribot and C. Sanchez, *Comments on Inorganic Chemistry*, 1999, **20**, 327-371.
2. J. J. E. Moreau and M. W. C. Man, *Coordination Chemistry Reviews*, 1998, **178**, 1073-1084.
3. J. Liu, Y. Gao, F. D. Wang, D. C. Li and J. Xu, *Journal of Materials Science*, 2002, **37**, 3085-3088.
4. O. Soppera, C. Croutxe-Barghorn and D. J. Lougnot, *New Journal of Chemistry*, 2001, **25**, 1006-1014.
5. M. Oubaha, R. K. Kribich, R. Copperwhite, P. Etienne, K. O'Dwyer, B. D. MacCraith and Y. Moreau, *Optics Communications*, 2005, **253**, 346-351.
6. D. Blanc, S. Pelissier, K. Saravanamuttu, S. I. Najafi and M. P. Andrews, *Advanced Materials*, 1999, **11**, 1508-1511.
7. A. Kavanagh, R. Copperwhite, M. Oubaha, J. Owens, C. McDonagh, D. Diamond and R. Byrne, *Journal of Materials Chemistry*, 2011, **21**, 8687-8693.
8. D. L. Versace, M. Oubaha, R. Copperwhite, C. Croutxe-Barghorn and B. D. MacCraith, *Thin Solid Films*, 2008, **516**, 6448-6457.
9. R. Copperwhite, M. O'Sullivan, C. Boothman, A. Gorin, C. McDonagh and M. Oubaha, *Microfluidics and Nanofluidics*, 2011, **11**, 283-296.

10. J. Liu, J. M. O'Reilly, T. W. Smith and P. N. Prasad, *Journal of Non-Crystalline Solids*, 2005, **351**, 2440-2445.

11. H. X. Zhang, D. Lu, T. Liu, M. Mansuripur and M. Fallahi, *Applied Physics Letters*, 2004, **85**, 4275-4277.

12. A. Ovsianikov, J. Viertl, B. Chichkov, M. Oubaha, B. MacCraith, I. Sakellari, A. Giakoumaki, D. Gray, M. Vamvakaki, M. Farsari and C. Fotakis, *Acs Nano*, 2008, **2**, 2257-2262.

13. R. J. Narayan, A. Doraiswamy, D. B. Chrisey and B. N. Chichkov, *Materials Today*, 2010, **13**, 42-48.

14. C. Molina, P. J. Moreira, R. R. Goncalves, R. A. S. Ferreira, Y. Messaddeq, S. J. L. Ribeiro, O. Soppera, A. P. Leite, P. V. S. Marques, V. D. Bermudez and L. D. Carlos, *Journal of Materials Chemistry*, 2005, **15**, 3937-3945.

15. R. J. Byrne, S. E. Stitzel and D. Diamond, *Journal of Materials Chemistry*, 2006, **16**, 1332-1337.

16. R. Byrne and D. Diamond, *Nature Materials*, 2006, **5**, 421-424.

17. B. Schaudel, C. Guermeur, C. Sanchez, K. Nakatani and J. A. Delaire, *Journal of Materials Chemistry*, 1997, **7**, 61-65.

18. A. Radu, S. Scarmagnani, R. Byrne, C. Slater, K. T. Lau and D. Diamond, *Journal of Physics D-Applied Physics*, 2007, **40**, 7238-7244.

19. A. Radu, R. Byrne, N. Alhashimy, M. Fusaro, S. Scarmagnani and D. Diamond, *Journal of Photochemistry and Photobiology a-Chemistry*, 2009, **206**, 109-115.

20. S. Coleman, R. Byrne, S. Minkovska and D. Diamond, *Physical Chemistry Chemical Physics*, 2009, **11**, 5608-5614.

21. R. Byrne, S. Coleman, K. J. Fraser, A. Raduta, D. R. MacFarlane and D. Diamond, *Physical Chemistry Chemical Physics*, 2009, **11**, 7286-7291.

22. K. Wagner, R. Byrne, M. Zanoni, S. Gambhir, L. Dennany, R. Breukers, M. Higgins, P. Wagner, D. Diamond, G. G. Wallace and D. L. Officer, *Journal of the American Chemical Society*, 2011, **133**, 5453-5462.

23. C. Schomburg, M. Wark, Y. Rohlfing, G. Schulz-Ekloff and D. Wohrle, *Journal of Materials Chemistry*, 2001, **11**, 2014-2021.

24. R. Byrne, C. Ventura, F. B. Lopez, A. Walther, A. Heise and D. Diamond, *Biosensors & Bioelectronics*, 2010, **26**, 1392-1398.

25. K. Arai, Y. Shitara and T. Ohyama, *Journal of Materials Chemistry*, 1996, **6**, 11-14.

26. D. Dattilo, L. Armelao, G. Fois, G. Mistura and M. Maggini, *Langmuir*, 2007, **23**, 12945-12950.

27. D. A. LaVan, T. McGuire and R. Langer, *Nature Biotechnology*, 2003, **21**, 1184-1191.

28. B. Garner, A. J. Hodgson, G. G. Wallace and P. A. Underwood, *Journal of Materials Science-Materials in Medicine*, 1999, **10**, 19-27.

29. B. Zhao, J. S. Moore and D. J. Beebe, *Analytical Chemistry*, 2002, **74**, 4259-4268.

30. B. Zhao, J. S. Moore and D. J. Beebe, *Science*, 2001, **291**, 1023-1026.

31. E. Stratakis, A. Mateescu, M. Barberoglou, M. Vamvakaki, C. Fotakis and S. H. Anastasiadis, *Chemical Communications*, 2010, **46**, 4136-4138.

32. L. B. Xu, W. Chen, A. Mulchandani and Y. S. Yan, *Angewandte Chemie-International Edition*, 2005, **44**, 6009-6012.

33. J. Isaksson, C. Tengstedt, M. Fahlman, N. Robinson and M. Berggren, *Advanced Materials*, 2004, **16**, 316-+.

34. S. Samanta and J. Locklin, *Langmuir*, 2008, **24**, 9558-9565.

35. K. Fries, S. Samanta, S. Orski and J. Locklin, *Chemical Communications*, 2008, 6288-6290.

36. R. Rosario, D. Gust, A. A. Garcia, M. Hayes, J. L. Taraci, T. Clement, J. W. Dailey and S. T. Picraux, *Journal of Physical Chemistry B*, 2004, **108**, 12640-12642.

37. R. Rosario, D. Gust, M. Hayes, F. Jahnke, J. Springer and A. A. Garcia, *Langmuir*, 2002, **18**, 8062-8069.

38. Z. Walsh, S. Scarmagnani, F. Benito-Lopez, S. Abele, F.-Q. Nie, C. Slater, R. Byrne, D. Diamond, B. Paull and M. Macka, *Sensors and Actuators B-Chemical*, 2010, **148**, 569-576.

39. U. Schubert, E. Arpac, W. Glaubitt, A. Helmerich and C. Chau, *Chemistry of Materials*, 1992, **4**, 291-295.

40. M. Oubaha, R. Copperwhite, C. Boothman, A. Ovsianikov, R. Kiyan, V. Purlys, M. O'Sullivan, C. McDonagh, B. Chichkov, R. Gadonas and B. D. MacCraith, *Journal of Materials Science*, 2011, **46**, 400-408.

41. D. L. Versace, O. Soppera, J. Lalevee and C. Croutxe-Barghorn, *New Journal of Chemistry*, 2008, **32**, 2270-2278.

42. A. Garcia, M. Marquez, T. Cai, R. Rosario, Z. B. Hu, D. Gust, M. Hayes, S. A. Vail and C. D. Park, *Langmuir*, 2007, **23**, 224-229.

43. H. F. Gong, C. M. Wang, M. H. Liu and M. G. Fan, *Journal of Materials Chemistry*, 2001, **11**, 3049-3052.

44. K. H. Fries, J. D. Driskell, G. R. Sheppard and J. Locklin, *Langmuir*, 2011, **27**, 12253-12260.

45. A. Athanassiou, M. I. Lygeraki, D. Pisignano, K. Lakiotaki, M. Varda, E. Mele, C. Fotakis, R. Cingolani and S. H. Anastasiadis, *Langmuir*, 2006, **22**, 2329-2333.

Chapter 6

Photopatternable, electro-responsive ionogels

6.1 Abstract

This chapter is focused on the photopatterning of electro-active hybrid sol-gels that are based on the chemical composition (MAPTMS,ZrPO,MAAH) as introduced in chapter 4. For these studies however, the hybrid materials are based solely on Zr metallate complexes. The electroactive species that become encapsulated within the polymer matrix are both phosphonium and imidazolium based IL's, dispersed graphene sheets and the electrochromic dye EV.

Initial studies were based on varying the IL content alone and were characterised by EIS and Raman spectroscopy. The latter confirmed the non-destructive encapsulation of the ILs whilst EIS was used to investigate the resultant conductivity trends as a result of the variation experiments. Incorporation of a graphene dispersion within the sol matrix greatly improved the conductivity of an ionogel based on $[P_{6,6,6,14}][DCA]$, whose subsequent physical properties were characterised by EIS, XRF and UV/Vis spectroscopy.

1 and 2 photon patterned, sub-micron structures were fabricated, and again proved to be of the right mechanical stability to exhibit minimal shrinkage and non-distortion after etching. In order to demonstrate that these materials can facilitate a prospective current, electrochromic ionogels were prepared by addition of EV to an ionogel based on $[C_2mim][FAP]$. The optical chemistry of the co-encapsulated dye allowed a patterned, electrochromic device to be fabricated that switched between both the coloured and transparent states of EV.

6.2 Introduction:

Of their many advantageous properties, perhaps the application with the most potential for ionogels is in the development and fabrication of solid-state electrolytes[1, 2]. This chapter is based on that premise, particularly on the *in-situ* method of preparing ionogels, so that the IL becomes encapsulated as the polymer develops. Ionogels offer many advantageous properties for solid-state electrolytes, including ionic conductivities similar to that of the IL itself, transparency, mechanical robustness, flexibility, and thermal stability over wide temperature ranges[3, 4].

An interesting approach to improve on the existing conductivity properties of solid-state electrolytes is in the addition of co-encapsulants that exhibit electronic conductivity[5]. Arguably the avenue of choice for many are materials derived from the carbon allotrope *graphite,* which is multiple stacked sheets of aromatic sp^2-hybridised atoms that exist in the third dimension[6]. Graphite can exist as *single* two-dimensional sheets (graphene)[7], which can subsequentially be rolled up to form one-dimensional nanotubes[8]. The mechanical strength, optical transparency and electronic conduction properties of materials based on graphite make them good candidates for electro-chemical research, particularly in the development of new electrodes[9, 10].

When combined with ionogels, so called *"bucky gels"* therefore unite the electron conducting properties of graphite-based materials with the ionic conducting ILs in the solid state[11].

Composites based on ILs and materials derived from graphite are easily prepared[12]. Simple mixing and sonicating of the two independent liquid phases[13], or by mixing and grinding graphene powder with an IL in an agar plate, produces the gel-like material[14].

In both these instances the two distinct chemical moieties exhibit negligible chemical interactions with one another and exist as one homogenous material. An interesting alternate approach has been to exploit the reactive chemistry of some ILs to produce the composite material. ILs that possess polymerisable vinyl groups have been show to undergo polymerisation in the presence of carbon nanotubes to produce physical gels[15], whilst another report used the inherent wide electrochemical window of an IL to facilitate the electrochemistry required to produce the composite material. The resultant composite was used to dramatically improve the colorimetric switching kinetics of a π- conjugated electrochromic polymer film[16].

The aim of this work is two fold: (a) To develop on the knowledge of photopatterning techniques gained in chapter 5 to explore new ways of fabricating ionogels; and (b) to explore new ways of synthesising and fabricating bucky gels, by allowing an acidified aqueous graphene dispersion to undergo the chemistry required to produce new, photopatternable ionogels.

Herein, this chapter describes the synthesis and characterisation of phosphonium and imidazolium based ionogels and shows impressive 2- and 3D photo-patternable ionogel structures with sub-micron resolution. In order to demonstrate that these materials can facilitate a current, the fabrication of a [C_2mim][FAP] based ionogel device containing the electrochromic dye *ethyl viologen dibromide* is also described.

6.3 Experimental:

6.3.1 Chemicals and Materials

$[P_{6,6,6,14}][DCA]$ and $[P_{6,6,6,14}][NTf_2]$ were obtained compliments of Cytec® Industries, the ILs were purified in the same manner as detailed previously.

$[C_2mim][FAP]$ was obtained compliments of Merck® industries and used without further purification. ITO coated polyethylene, Graphite powder, POT, MAPTMS, ZrPO, MAAH, DMPA and EV were used as purchased from Sigma-Aldrich® Ireland.

Igracure® 369 was obtained compliments of Ciba® chemicals and used as the photoinitiator for all experiments involving graphene dispersed ionogels.

6.3.2 Ionogel preparation

e.g. SZr 4: $[P_{6,6,6,14}][DCA]$ 60:40 w/w

600 mg of SZr 4 was mixed thoroughly with 400 mg of $[P_{6,6,6,14}][DCA]$ and 5 wt% of photoinitiator (DMPA). SZr 4 was prepared in the same manner as in section 5.3.2. The ionogel solution was sonicated for 5 minutes to ensure the photoinitiator was dissolved fully. It was then transferred to the relevant substrate for analysis and photopolymerized with a UV BondWand (20 W, 365 nm) for 10 minutes. All ionogel combinations, as described in table 6.1 were prepared in accordance to the above procedure, with adjustments only to the hybrid organic sol-gel and IL proportions.

6.3.3 Graphene dispersed ionogel preparation

For the analyses involving the preparation of graphene-dispersed ionogels, Zr based sol-gels of stoichiometry 10/4/4, 10/6/6 and 10/8/8 (MAPTMS/ZrPO/MAAH) were first prepared. However to incorporate the electroactive material, an aqueous graphene dispersion (0.22 mg/ml, stabilised by NaDBSA (0.5 mg/ml)) was used as the hydrolysis agent (Step 1, Scheme 5.1). The dispersion was acidified to pH 2.3 using HCl (5×10^{-2} M). Once this step was complete, the reaction followed the same manner found in Scheme 5.1.

After 24 hours of stirring, the ionogel was prepared according to section 6.3.2 by adding $[P_{6,6,6,14}][DCA]$ (40 wt.%) to the sol-gel solution.

6.3.4 Electrochromic device fabrication:

The construction of the electrochromic device slightly differs in this chapter in that the ionogel solution was doped with an ethyl quaternised viologen derivative. The ionogel containing EV was first photopolymerised into square patterns for 10 minutes onto ITO using a specialised UV filter mask.

Once polymerised the resultant patterns were etched with ethanol and allowed to dry for a further 10 minutes (figure 6.12 (left)). The original ionogel material (without dye) was then applied around the electro-active patterns to facilitate the prospective current being passed through the device.

An electrical seal was generated in the same manner as before by placing the top ITO layer atop of the liquid supporting ionogel, and photo-polymerising through it for a further 10 mins.

6.4 Results and Discussion

6.4.1 Phosphonium and Imidazolium ionogel characterisation

6.4.1.1 Raman spectroscopy

Raman spectroscopy was first used as a technique that could confirm the compatibility of both liquid systems (IL and SZr 4) as part of a polymerised structure. As in the previous chapter, the initial hybrid material SZr 4 excluding the IL was initially characterised, to identify the specific functional groups that arise within it (figure 6.1).

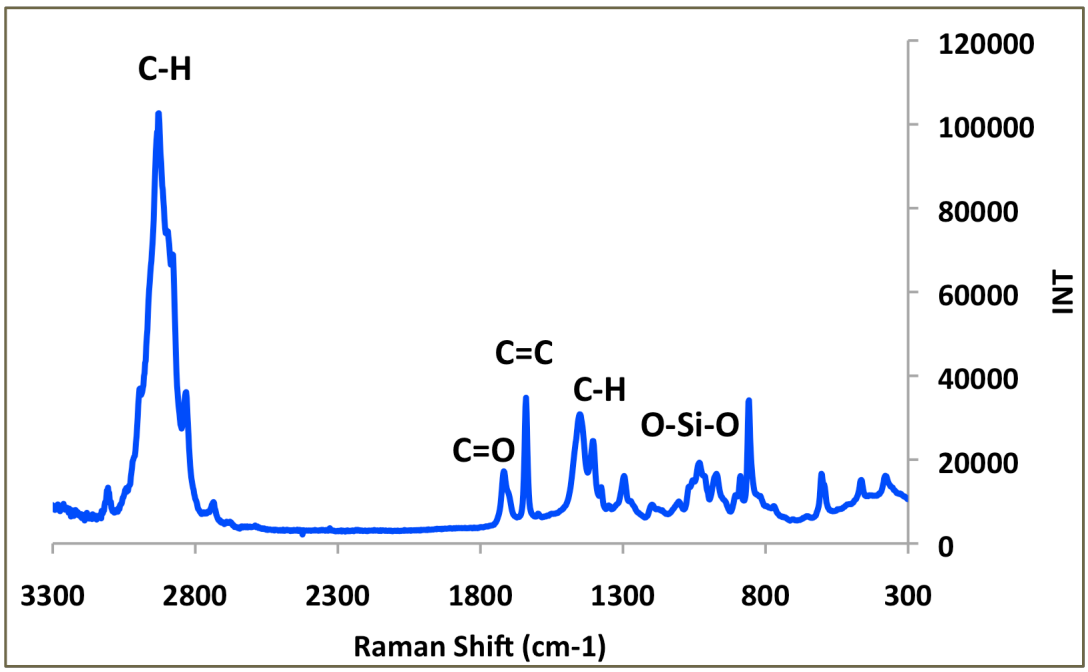

Figure 6.1: Raman spectrum obtained for the hybrid SZr 4 sol-gel.

As expected, the signature groups present of the SZr 4 from the IR analysis are also prevalent in the Raman spectrum. The strongest contributions to the spectrum are those arising from the polymer backbone (C-H) at ~2900 and 1480 cm^{-1}, which confirm that polymerisation has occurred. Residual alkenes stretching at 1640 cm^{-1} can be attributed to unreacted methacrylate, while the condensed siloxane groups contribute at 1000 cm^{-1}. The carbonyl stretch of the MAPTMS moiety is seen as 1700 cm^{-1} whilst contributions from the zirconate complex are seen in the region spanning from 400 – 900 cm^{-1}.

In order to confirm the encapsulation of the IL within SZr 4, individual overlays were constructed of the ionogel in question vs. the SZr 4 sol-gel.

Figure 6.2 (a) shows the Raman spectrum of the SZr 4 hybrid material, and the 40 wt% based [$P_{6,6,6,14}$][DCA] ionogel overlayed. This spectrum clearly shows the incorporation of [$P_{6,6,6,14}$][dca] within the ionogel structure, as the signature nitrile (-C≅N) stretch originating from the $[DCA]^-$ anion in the IL is now located at 2188 cm^{-1}. This is similar to the reported nitrile stretch in liquid [$P_{6,6,6,14}$][DCA].[17]

Figure 6.2 (b) represents an overlay based on the 40 wt.% [$P_{6,6,6,14}$][NTf_2] ionogel. In this case, the first assignable vibration from the [NTf_2] anion is the SO_2 symmetric stretching located at 1136 cm^{-1}. The terminal trifluoromethane groups of the anion exhibit a clear signature stretch at 740 cm^{-1}. Based on this spectral overlay, one can conclude that no significant vibrational deviations for [$P_{6,6,6,14}$][NTf_2] were observed when immobilised within the SZr 4 matrix.

Figure 6.2 (c) presents the Raman spectrum obtained for the 50 wt.% [C_2mim][FAP] ionogel. This spectrum again clearly shows the non-invasive encapsulation of the IL, as indicated by the presence of the signature C-F stretching again at 740 cm^{-1}.

The characteristic C=N contributions of the imidazolium cation to the spectrum are located at both 1596 cm^{-1} and 744 cm^{-1}. Similar to the phosphonium based ionogels, [C_2mim][FAP] vibrational bands were not strongly influenced by the hybrid silicato-zirconate material ionogel matrix.

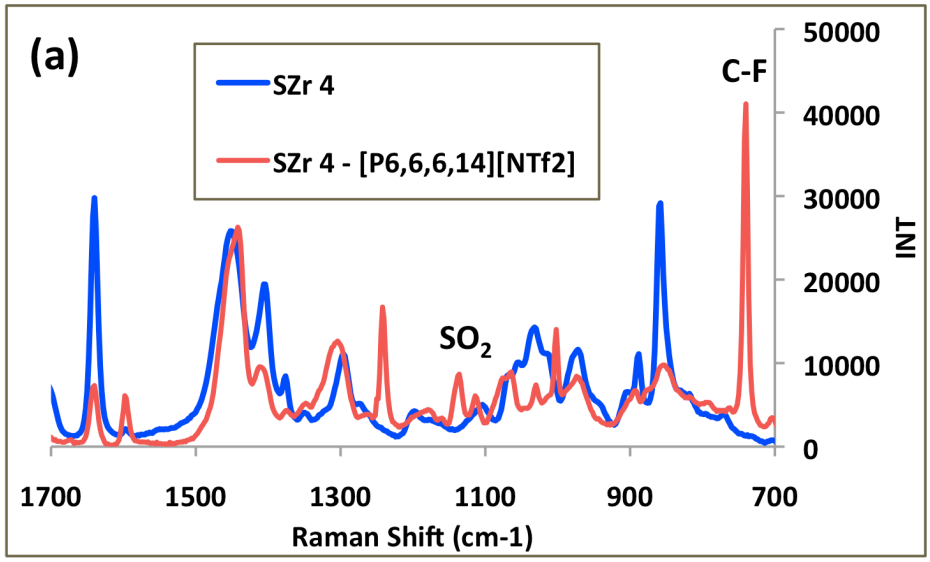

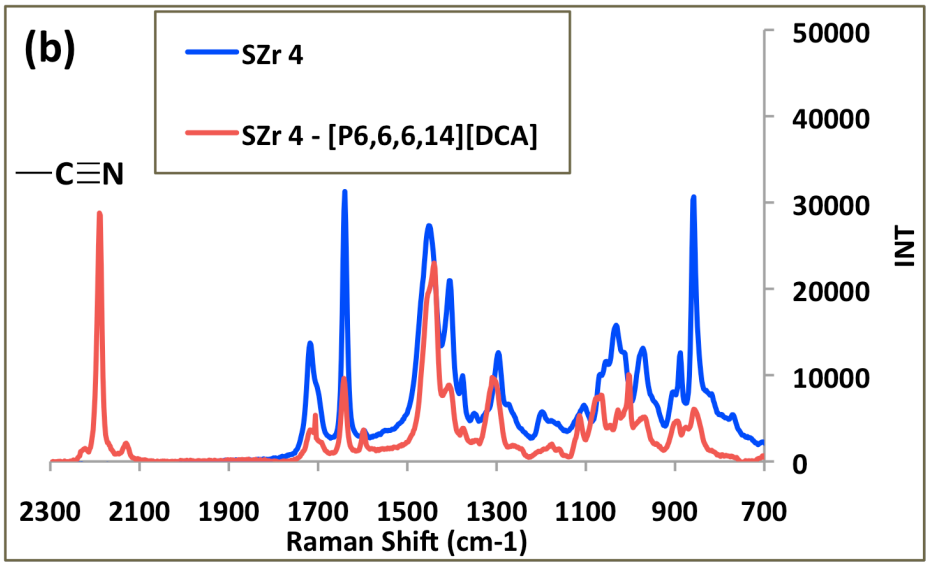

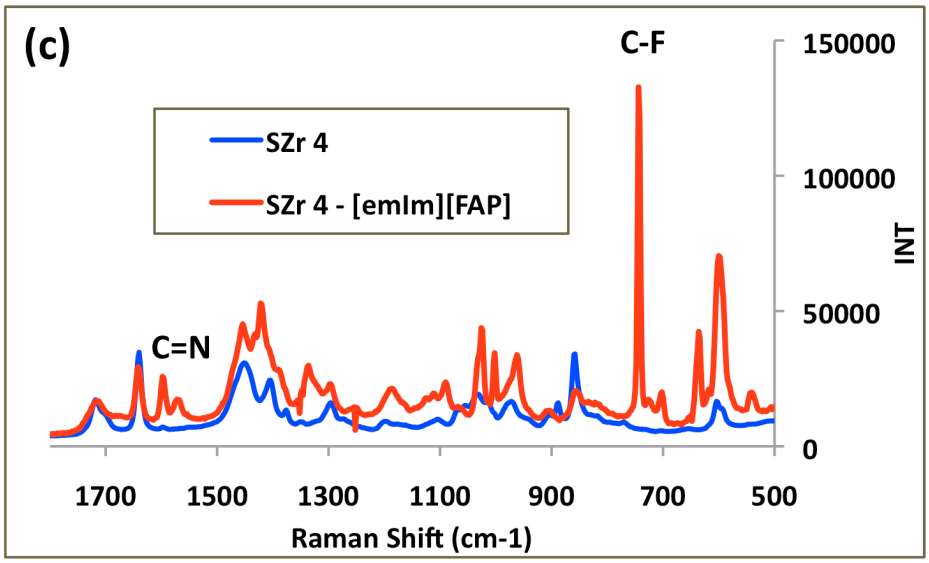

Figure 6.2: Raman spectra obtained for (a) $[P_{6,6,6,14}][DCA]$, (b) $[P_{6,6,6,14}][NTf_2]$ and (c) $[C_2mim][FAP]$ based ionogels (red) vs. the original sol-gel (blue).

6.4.1.2 EIS Spectroscopy

EIS was first used to determine the effects of increasing the concentration of the phosphonium IL within the SZr 4 ionogel. This is best analysed via the *"Bode"* plot (Figure 6.3 (a) and (b)) which depicts the relationship between the impedance of the sample and the frequency scanned.

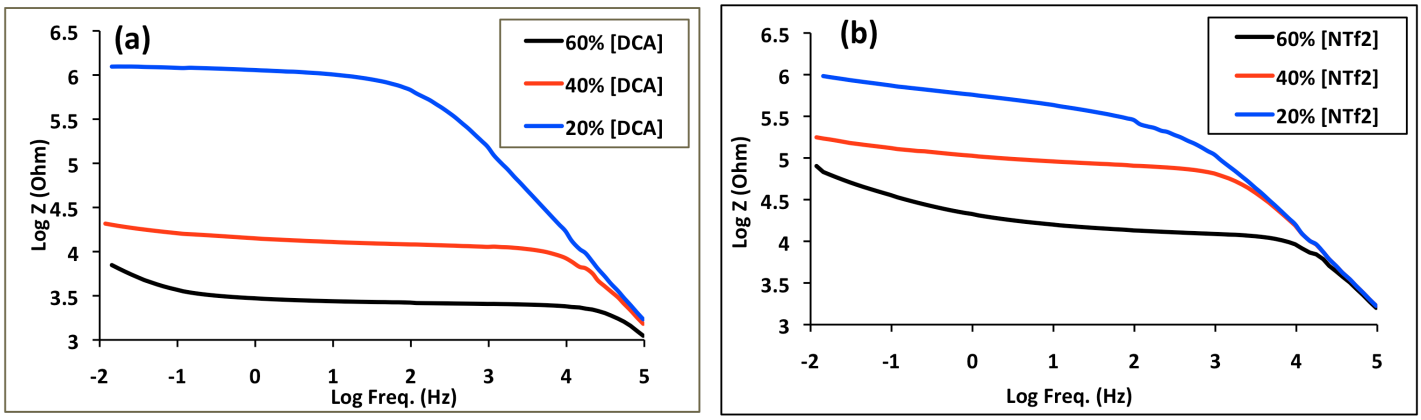

Figure 6.3: Bode plots obtained for increasing concentrations of $[P_{6,6,6,14}][DCA]$ and $[P_{6,6,6,14}][NTf_2]$ incorporated in SZr 4 matrix.

By increasing the concentration of the IL in the SZr 4 matrix, the expected complementary decrease in impedance was observed across the whole frequency range for all IL concentrations. The ionogels display stable ionic conductivity, given that a linear increase in impedance is seen at both the high (electronic) and low (proton) frequency extremes.

The Nyquist plot was used to graphically illustrate the difference in conductivity of the phosphonium based ionogels as a function of the IL anion. Figure 6.5 shows an overlay of the two Nyquist plots obtained; whilst the calculated conductivity values can be seen in table 6.1. These values were again calculated according to equations 3.4 and 3.5. The results of the thickness analyses used for these equations can be seen in figures A8 – A11.

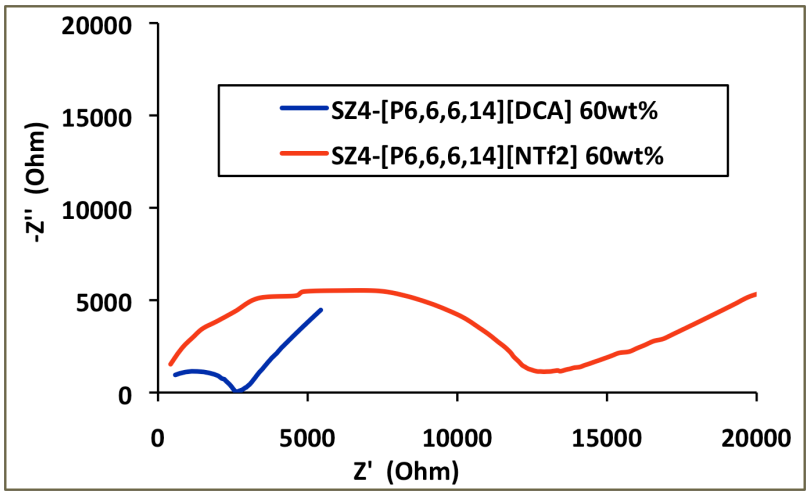

Figure 6.4: Nyquist plots obtained for $[P_{6,6,6,14}][DCA]$ and $[P_{6,6,6,14}][NTf_2]$ (60 wt.%) ionogels.

This clear difference in conductivity as a function of the IL anion can be seen from both table 6.1 and figure 6.4. It was found that ionogels containing the $[DCA]^-$ anion were of higher conductivity than their $[NTf_2]^-$ counterparts, which is in agreement with previous studies[18]. The viscosities for $[P_{6,6,6,14}][DCA]$ and $[P_{6,6,6,14}][NTf_2]$ are quoted in the literature as 490 cP and 450 cP at 20 ^{0}C respectively[19].

Viscosity obviously does not completely govern conductivity in this case, the lower value obtained is most likely due to extensive electron delocalisation present in the $[DCA]^-$ ion and it being a comparably smaller ion than $[NTf_2]^-$.

In order to improve the conductivity of the ionogels further, a lower viscosity IL $[C_2mim]$ [FAP] (75 cP at 20 ^{0}C) was added at 50 and 80 wt% concentrations and analysed again by EIS.

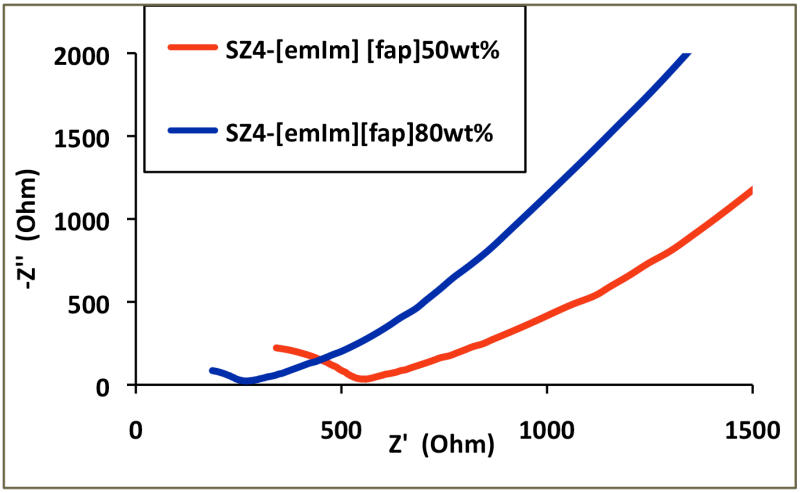

Figure 6.5: Nyquist plots obtained for (a) 50wt% $[C_2mim][FAP]$ and (b) 80wt% $[C_2mim][FAP]$ in SZr 4 gel.

The resultant Nyquist plots from the $[C_2mim][FAP]$ ionogel analysis can be seen in figure 6.5, and the conductivity values are again quoted above in table 6.1. The conductivity of both films dramatically increased when compared to previous results, which is most likely due to mainly the comparatively low viscosity but also due to increased charge distribution.

The cationic charge distribution in imidazolium based IL's is much increased as the whole heterocycle contains delocalised electrons. Contrarily, the cationic charge of the phosphonium cation is much more centered and shielded by extensive alkylation.

Ionogel Composition:	**R_{CT}: (Ω)**	**σ : (S/cm^2)**
[$P_{6,6,6,14}$][DCA]		
40 wt.%	12,100 (445)	7.2 x 10^{-6}
60 wt.%	2664 (23)	3.27 x 10^{-5}
[$P_{6,6,6,14}$][NTf_2]		
40 wt.%	84,730 (976)	1.03 x 10^{-6}
60 wt.%	13,106 (535)	6.65 x 10^{-6}
[C_2mim][FAP]		
50 wt.%	576 (24)	1.51 x 10^{-4}
80 wt.%	258 (2)	3.38 x 10^{-4}

Table 6.1: Ionogel w/w composition, R_{CT} (errors in parentheses) and conductivity values obtained from EIS for IL's in SZr 4 gel.

6.4.2 Graphene encapsulated ionogels characterisation

6.4.2.1 Raman Spectroscopy

Raman spectroscopy was again employed to confirm the co-encapsulation of the electroactive materials within the same hybrid sol-gel matrix. In order to form a valid comparison the spectra obtained for the original ionogel material (10/4/4; 40 wt.% IL) was overlayed against the new ionogel containing the same stoichiometry and IL content plus graphene (figure 6.6). The figure was first baseline corrected using the 1800-2000 cm^{-1} region where no spectral activity was seen, and normalised according to the C-H contributions of both samples at ~2900 cm^{-1}.

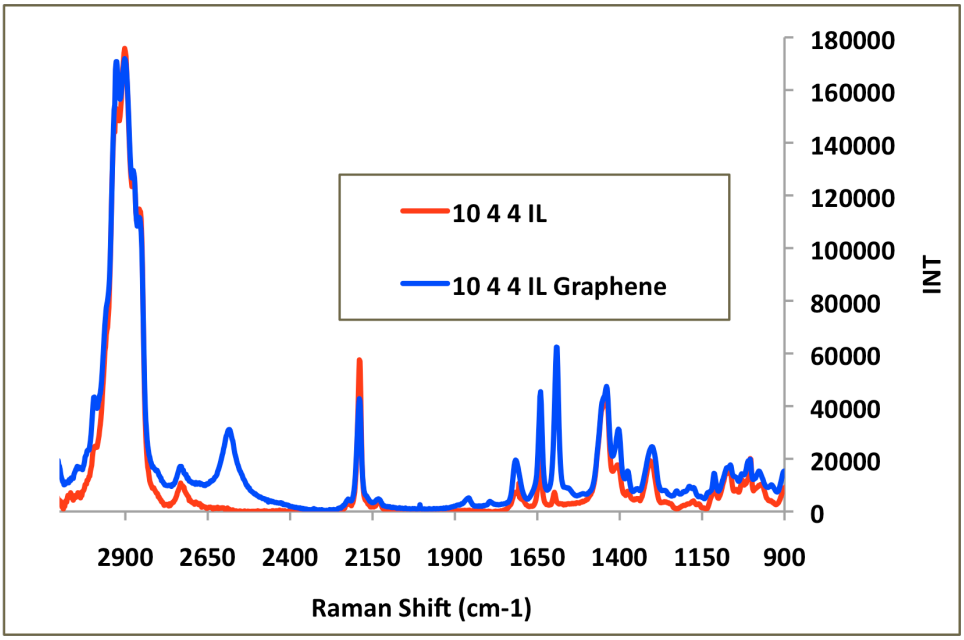

Figure 6.6: Raman spectra obtained for 10/4/4 ionogel containing 40 wt% $[P_{6,6,6,14}][DCA]$ **(red)** and 10/4/4 ionogel containing 40 wt% $[P_{6,6,6,14}][DCA]$ and graphene **(blue).**

This allows the spectral contributions of the graphene dispersion to be fully analysed. The raman spectroscopy of, and the underlying physics behind the raman spectroscopy of graphene are quiet well understood and are the subject of a previous reviews[20, 21].

The encapuslation of graphene within the sol-gel matrix is confirmed via the presence of the G' band at 2590cm^{-1} arising from a two phonon inelastic scattering process; and the disorder induced D' band at 1572cm^{-1} . An increase in intensity of the band at 1592cm^{-1} can be attributed to the doubly degenerate G phonon mode. All spectral bands arising from the sol-gel matrix and the IL (as highlighted in previous sections) appear unperturbed and at the same frequencies.

Similiar to the original ionogel experiments therefore, one can then conclude that the encapsulation of the conducting materials occurs undisturbed within the sol-gel matrix.

6.4.2.2 EIS Spectroscopy

It was anticipated that the introduction of graphene sheets dispersed within the ionogel matrix would increase the conductivity of the ionogels, which were again investigated using EIS. For these analyses the concentration of both $[P_{6,6,6,14}][DCA]$ and the graphene dispersion were kept constant across all samples.

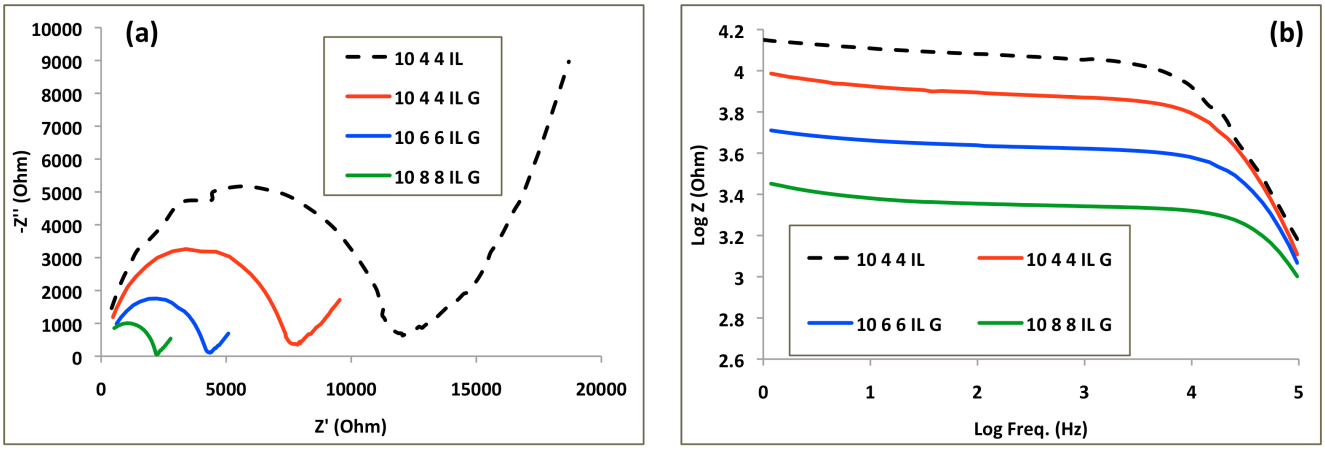

Figure 6.7: (a) Nyquist plot and **(b)** Bode plot analysis of graphene encapsulated ionogels. In both cases the black dashed line represents the original $[P_{6,6,6,14}][DCA]$ 40wt% ionogel, the graphene encapsulated ionogels are in red (10/4/4), blue (10/6/6) and green (10/8/8).

This anticpation was based on the electronic conductive properties of graphene, which have been well documented in the literature[22]. By first analysing the initial Nyquist and Bode plot results for 10/4/4 IL and 10/4/4 IL G (Figure 6.7 (a) and (b)); one can see the initial change in (a) the R_{CT} x-axis intercept and (b) the uniformal decrease in impedance across all frequencies scanned. The introduction of graphene causes a 37.46 % decrease in x-axis intercept and a 59.9 % improvement in the calculated conductivity (table 6.2).

In order to study the effects of increasing the metallate complex of Zr on the conductivity endowed on the ionogel, ionogels of stiochiometry 10/6/6 and 10/8/8 (MAPTMS/ZrPO/MAAH) were next prepared and analysed.

In both cases the conductivity of the ionogels is increased by 189 % and 455 % respectively (table 6.2). The remarkable increase in conductivity is therefore a combination of the graphene content and the increased elements of the sol which undergo condensation reactions. The increased concentration of condensed material serves to encapsulate the electro-active materials more and more efficiently, which causes the conductive network encapsulated within to operate more efficiently. Ionic conductivity as a result of these measures therefore increases in tandem.

Sample:	R_{CT}: (Ω)	R_{CT} decrease: (%)	σ: (S/cm^2)	σ increase: (%)
10/4/4 IL	12,100		5.21 x 10^{-6}	
10/4/4 IL G	7567 (± 312)	37.4	8.34 x 10^{-6}	59.9
10/6/6 IL G	4185 (± 21)	65.4	1.5 x 10^{-5}	189.1
10/8/8 IL G	2180 (± 19)	81.9	2.89 x 10^{-5}	455

Table 6.2: Ionogel composition, R_{CT} values (errors in parentheses) and conductivity values obtained from EIS for graphene encapsulated ionogels.

6.4.2.3 XRF and UV/Vis analysis

As the effects of increasing the Zr content had now been effectively documented by EIS, it was decided to exhibit the increasing Zr concentration further using XRF. XRF is a suitable technique to exhibit this as Zr is a heavy metal element which exhibits the photo-electronic effect under x-ray irradiation. The results of the XRF analysis are shown in figure 6.8 (a).

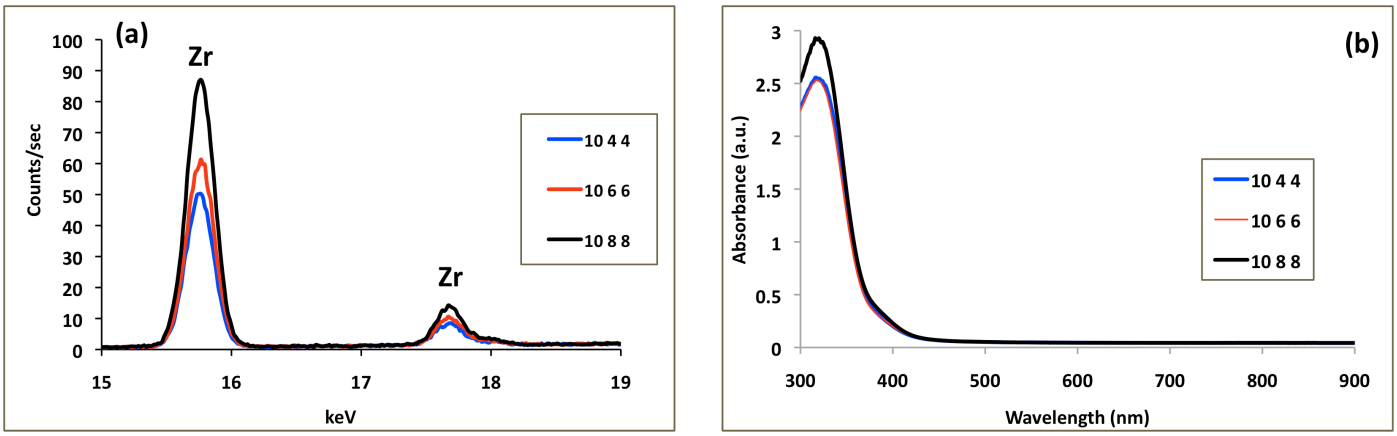

Figure 6.8: (a) XRF analysis and **(b)** UV/Vis spectra of 10/4/4, 10/6/6 and 10/8/8 graphene/IL encapsulated ionogels.

It can be seen from these results that increasing the Zr content from 10/4/4 to 10/6/6 and 10/8/8 causes the intensity of the photon count attributed to Zr at the XRF detector to increase accordingly. This effectively exhibits that the concentration of the Zr content does increase from ionogel to ionogel, and so ratifies the trend observed previously using EIS.

The UV/Vis spectra of all three graphene encapsulated ionogels can be seen in figure 6.8 (b). All three ionogels exhibit optical transparency in the visible region spanning from 900 nm to ~430 nm, meaning the graphene content does not affect the optical properties of the ionogels in this region. The broad shoulder centered at 395 nm is attributed to the photoreactivity of the initiator, as this shoulder is only evident after polymerisation was performed. The absoption maximum at 325 nm is due to unreacted photoinitiator.

6.4.3 One and two photon patterning of ionogel structures

Experiments to demonstrate the photopatternability of these novel materials were carried out using the SZr 4 material containing 20 wt.% $[P_{6,6,6,14}][DCA]$ in conjunction with a direct laser writing process. The microstructures shown (figure 6.9 (c) and (d)), exhibit both a cross-sectional and top-down view of the photopatterned ionogel thin films. It can be seen from these images that as the UV exposure dose is decreased (from left to right in Figure 6.9(c)), that the size of the resulting microstructures also decreases. This demonstrates that the dimensions of these microstructures are sensitive to the UV exposure dose as is the case for standard photocurable hybrid sol-gel materials. These results clearly demonstrate the potential of these conductive materials to be exploited in high resolution photopatterning processes.

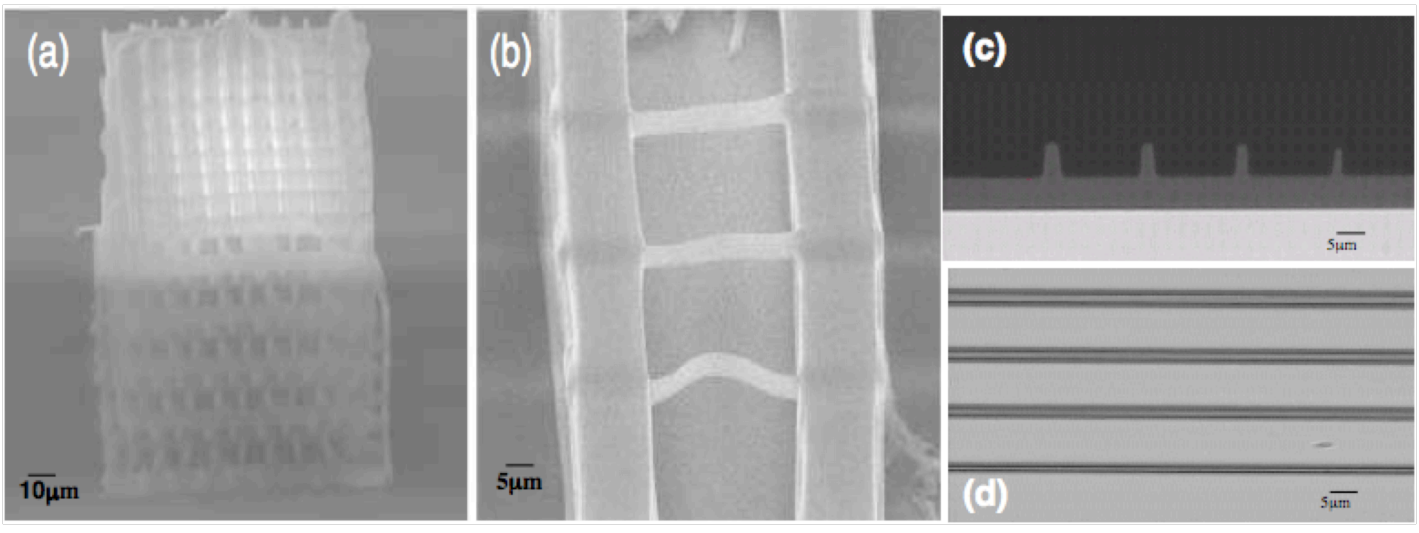

Figure 6.9: (a) and **(b)** SEM images of three-dimensional crystals fabricated from SZr 4 - 20 wt.% $[P_{6,6,6,14}][DCA]$ **(c)** and **(d)** Photopatterning of SZr 4 - 20 wt% $[P_{6,6,6,14}][DCA]$ with photolithography.

A three-dimensional woodpile structure fabricated employing the 2PP technique is presented in figure 6.9 (a) and (b). In comparison with commonly used liquid resins in 2PP processing, this material allows the fabrication of a woodpile type structure exhibiting negligible shrinkage, which avoids any further mechanical compensation. This is attributable to the particular molecular structure of the hybrid ionogel, in which both organic and inorganic moieties can form interconnected networks leading to high molecular cohesion. First, the hydrolysis and condensation reactions taking place during the sol-gel synthesis allow the formation of polycondensable M-OH (M = Si, Zr) groups capable of forming strong and irreversible covalent bonds (Si-O-Si, Zr-O-Zr, and possibly Si-O-Zr). Upon 2PP irradiation, the pendant methacrylate groups contained in the MAPTMS are crosslinked, resulting in the formation of irreversible and fully saturated aliphatic C-C covalent bonds, which penetrate throughout the irradiated region of the film. It is thought, in agreement with a recently reported study[23], that this has the effect of confining the other constituents of the sol (in this case the IL and the graphene sheets). Figure 6.10 shows the graphene-dispersed ionogels 2PP patterned to mimic the crystal lattice structure of graphene. Similar to the previously patterned ionogels, the graphene-dispersed materials were found to be of the optimum mechanical stability to be stable in the 3rd dimension after etching.

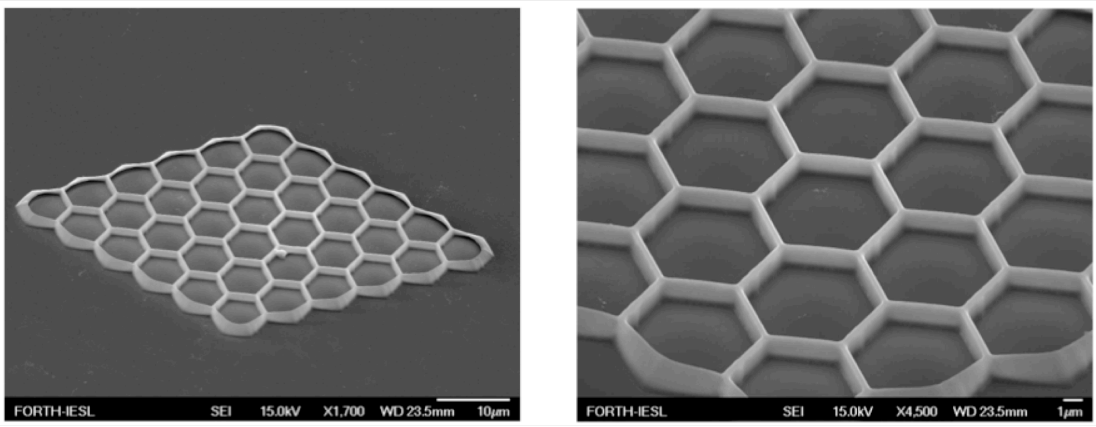

Figure 6.10: 2PP graphene - dispersed phosphonium ionogels, patterned to mimic the crystal lattice structure of graphene. Honeycomb diameter: 8μm.

6.4.4 Viologen spectroelectrochemistry and device fabrication:

In order to demonstrate the conductive nature of the novel photopatternable materials, it was decided to encapsulate an electrochromic dye using the same methods that form the basis of chapter 4. In keeping with the EIS data obtained, an ionogel containing 50wt% [C_2mim][FAP] and SZr 4 was chosen as it displayed the highest conductivity value. The viologen derivative chosen was EV, as its increased polarity over MAV ensured its miscibility within the [C_2mim][FAP] ionogel solution.

EV exhibits the same equilibria as the viologen derivatives discussed in section 4.4.6, in that one electron reduction of the colourless dicationic state produces a coloured monocationic radical. This radical can also be reduced further to the quinoid state. The concentration of EV was kept at 5 x 10^{-2} M for the spectroelectrochemical experiments.

The initial experiments based on SZr 4 proved invalid as electroplating under cathodic conditions was observed. The high concentrations of Zr leached out of the ionogel and coated the electrode under negative potentials, which hindered the optical properties of the gel. In order to prevent this effect a sol containing 10/0.5/0.5 (MAPTMS/ZrPO/MAAH) was synthesised, and was prepared for electrochromic experiments in the same manner as previously described, the results of which are shown in figure 6.11.

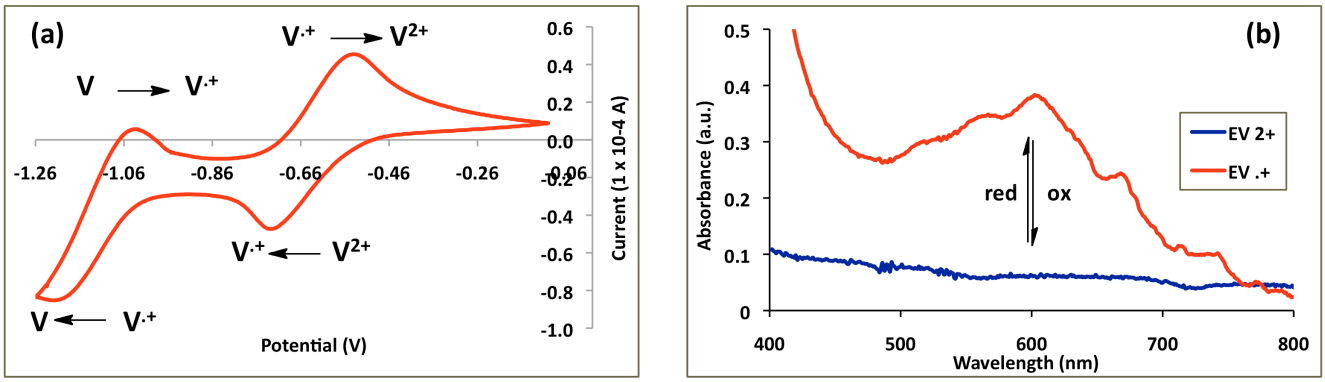

Figure 6.11: (a) Cyclic Voltammogram obtained of EV in [C_2mim][FAP]/SZr 4 gel, and **(b)** UV/Vis redox spectra of EV in [C_2mim][FAP]/SZr 4 gel.

The CV (figure 6.11 (a)) was obtained by scanning in the potential range from -1.6 V – 0.1 V at a scan rate of 1 mV/sec. It can be seen from this figure that it exhibits the classical two reduction steps expected for viologen based devices[24, 25]. This ensures that the equilibrium of the viologen derivative can be facilitated as part of a solid-state photopatternable ionogel. The radical cationic state was generated by maintaining the voltage potential on the working electrode at the first reduction point in the CV (in this case -0.7 V). This resulted in the generation of a dark blue colour, and a strong absorbance at 610 nm (figure 6.11 (b)).

The next step was the construction of the electrochromic device, where the photopatternable ionogel was expected to act as a solid electrolyte for the reversible viologen redox process. The fabrication process for the patterned electrochromic device is described above in section 6.3.5. Once the device was complete it was connected to a power supply, the perturbation voltage was 1 V, which resulted in the patterned squares turning blue (figure 6.12 (right)).

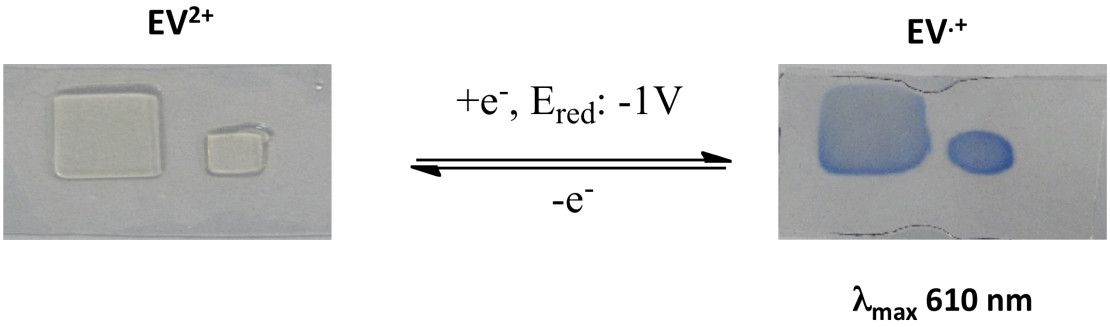

Figure 6.12: Patterned electrochromic ionogel exhibiting both viologen redox states.

This device exhibited the same stabilisation of the coloured form as the devices in chapter 4. Some strategies to quantify and optimise this effect are suggested in **section 7.2.3.** It can also be noted from figure 6.12 that the viologen doped, patterned squares change their morphology after the initial voltage was applied. This is an interesting phenomenon as the material appears to actuate as a function of the voltage applied. This feature is however outside the scope of the present study and will be the subject of future work investigating this effect.

6.5 Conclusion

In summary, this chapter provided a facile method to photo-pattern ionogel materials containing phosphonium and imidazolium based ILs. The Ionogels have been characterised by EIS and Raman spectroscopy, from these results the organic-inorganic matrix does not seem to affect the physical or chemical behaviour of the encapsulated IL.

Once an appreciation of the effect of IL encapsulation had been gained, experiments aimed at improving the conductivity of an ionogel based on $[P_{6,6,6,14}][DCA]$ were then undertaken, which involved the use of an aqueous graphene dispersion as the hydrolysis agent for sol-gel preparation. The addition of this electronic conductor - coupled with the incremental increase of condensing agents within the sol – resulted in a dramatic improvement in the resultant conductivity of the ionogel as characterised by EIS.

XRF analysis documented the increase in Zr content whilst UV/Vis spectroscopy showed these materials exhibited good optical transparency in the visible region.

A particularly attractive quality of these ionogels is the ability to spatially define their precise location and structure by optical exposure. Tremendous potential lays in the ability to photopattern flexible opto-electronic materials with high precision. The incorporation of an electrochromic dye also highlights further future potential applications in the development of a patternable electrochromic display those functions under a comparatively low voltage perturbation signal.

6.6 References

1. R. Goebel, P. Hesemann, J. Weber, E. Moeller, A. Friedrich, S. Beuermann and A. Taubert, *Physical Chemistry Chemical Physics*, 2009, 11, 3653-3662.
2. F. Gayet, L. Viau, F. Leroux, S. Monge, J. J. Robin and A. Vioux, *Journal of Materials Chemistry*, 2010, 20, 9456-9462.
3. T. Ueki and M. Watanabe, *Macromolecules*, 2008, 41, 3739-3749.
4. J. Le Bideau, L. Viau and A. Vioux, *Chemical Society Reviews*, 2011, 40, 907-925.
5. K. T. Lee, J. C. Lytle, N. S. Ergang, S. M. Oh and A. Stein, *Advanced Functional Materials*, 2005, 15, 547-556.
6. F. Tuinstra and J. L. Koenig, *Journal of Chemical Physics*, 1970, 53, 1126-&.
7. K. S. Novoselov, A. K. Geim, S. V. Morozov, D. Jiang, Y. Zhang, S. V. Dubonos, I. V. Grigorieva and A. A. Firsov, *Science*, 2004, 306, 666-669.
8. E. Lahiff, C. Lynam, N. Gilmartin, R. O'Kennedy and D. Diamond, *Analytical and Bioanalytical Chemistry*, 2010, 398, 1575-1589.
9. X. Wang, L. Zhi and K. Muellen, *Nano Letters*, 2008, 8, 323-327.
10. M. Hilder, B. Winther-Jensen, D. Li, M. Forsyth and D. R. MacFarlane, *Physical Chemistry Chemical Physics*, 2011, 13, 9187-9193.
11. J. B. Ducros, N. Buchtova, A. Magrez, O. Chauvet and J. Le Bideau, *Journal of Materials Chemistry*, 2011, 21, 2508-2511.
12. T. Fukushima, *Polymer Journal*, 2006, 38, 743-756.
13. I. Ahmad, U. Khan and Y. K. Gun'ko, *Journal of Materials Chemistry*, 2011, 21, 16990-16996.
14. J. Lee and T. Aida, *Chemical Communications*, 2011, 47, 6757-6762.

15. T. Fukushima, A. Kosaka, Y. Yamamoto, T. Aimiya, S. Notazawa, T. Takigawa, T. Inabe and T. Aida, *Small*, 2006, 2, 554-560.

16. A. P. Saxena, M. Deepa, A. G. Joshi, S. Bhandari and A. K. Srivastava, *Acs Applied Materials & Interfaces*, 2011, 3, 1115-1126.

17. R. Byrne, S. Coleman, S. Gallagher and D. Diamond, *Physical Chemistry Chemical Physics*, 2010, 12, 1895-1904.

18. D. R. MacFarlane, M. Forsyth, E. I. Izgorodina, A. P. Abbott, G. Annat and K. Fraser, *Physical Chemistry Chemical Physics*, 2009, 11, 4962-4967.

19. R. E. Del Sesto, C. Corley, A. Robertson and J. S. Wilkes, *Journal of Organometallic Chemistry*, 2005, 690, 2536-2542.

20. A. C. Ferrari, *Solid State Communications*, 2007, 143, 47-57.

21. L. M. Malard, M. A. Pimenta, G. Dresselhaus and M. S. Dresselhaus, *Physics Reports-Review Section of Physics Letters*, 2009, 473, 51-87.

22. U. Khan, I. O'Connor, Y. K. Gun'ko and J. N. Coleman, *Carbon*, 2010, 48, 2825-2830.

23. A. Vioux, L. Viau, S. Volland and J. Le Bideau, *Comptes Rendus Chimie*, 2010, 13, 242-255.

24. C. A. Melendres, P. C. Lee and D. Meisel, *Journal of the Electrochemical Society*, 1983, 130, 1523-1527.

25. M. De Leo, L. M. Moretto, O. Buriez and P. Ugo, *Electroanalysis*, 2009, 21, 392-398.

Chapter 7

Conclusions and future work

7.1 Thesis Conclusions

The main topics discussed in this thesis are the design of polymer gels with novel and stimuli responsive materials encapsulated within. This conclusion section aims at summarising the highlights of the thesis under the two main research themes. The future work section outlays some experiments that are designed to generate new information that could lead to exciting future developments.

7.1.1 Sensor component simplification

Chapters 3 and 4 discussed the many positive outcomes that arose out of the use of IL's as multifunctional agents encapsulated within solid-state platforms.

Chapter 3 started this premise by discussing the novelty of using the IL as the ligand in a charge transfer metal complex (and thereby producing an optical response). The multifunctionality of the IL provided the foundation for very simplified yet functional optodes. Whilst ILs have found use within the literature as plasticisers for PVC, this has mainly been put to use within electrochemical sensing platforms. Indeed in some cases the inherent charge of the membrane eliminated the need for an ion-exchanging salt. To our knowledge further simplification by using the IL as the optical responsive agent within this and other sensing platforms has been explored very little.

Incorporating $[P_{6,6,6,14}][DCA]$ with PVC fulfilled multiple roles within the optode template. The IL functioned as an effective platiciser yielding a transparent flexible film.

It also acted as a diverse ligand for the analytes studied, the transducer dye yielding the optical response; whilst the binding mechanism eliminated the need for an ion-exchanger.

When exposed to a solutions containing various mixtures of the two analytes, $[P_{6,6,6,14}][DCA]$ simplified optodes were able to behave as dual analyte recognition platforms. The great importance of this finding is that this two-component system is effectively self-indicating. It clearly shows whether ions of interest are present as individual or as a mixture without the need to add a dye.

Of equal importance is the idea of developing sensors with multiple detection channels, which ultimately allows for greater freedom when choosing the detection method. The inherent conducting properties of the membranes gave a measured sensor response across three distinct instruments. In this case the instrumentation used were XRF, EIS and WRF.

The latter's response was principally based on the inherent ionic conductivity of $[P_{6,6,6,14}][DCA]$ - which upon co-ordination to Cu^{2+}, Co^{2+} and a mixture of the two – gave a discriminatory increase and decrease in the documented EIS and WRF responses respectively.

Chapter 3 therefore is an effective demonstration of two-component ionogels behaving as mixed opto/electronic functional materials. This raises the possibility to develop single use platforms that work under simplified conditions, that are capable of detecting multiple species via multiple detection channels with acceptable limits of detection (depending on the application).

In fact the main obstacle to the realization of this vision are the current detection limits. This can be addressed if a good understanding of the complexation process is achieved. Equally, ILs allow great freedom and variation in their design, and it is this exciting prospect that forms the basis of future work for this chapter (**section 7.2.1)**.

This idea of a multifunctional agent that will simplify the design template of a given platform provided the basis for the topics discussed in chapter 4. However this time a synthetic approach was used to produce a new novel material for this purpose. Going backward one step in the phosphonium IL synthetic route allowed the design of an IL with multiple traits at the final synthetic step.

^{1}H and ^{31}P NMR served to validate the products obtained at both stages within the synthetic route, whilst DSC and TGA thermal analyses verified that the $[P_{V,8,8,8}][3X]$ behaves in similarly to conventional phosphonium based ILs. Encapsulation of the novel IL material within an ionogel formed the basis of a simplified device that produced a change in optical properties of the gel upon voltage reduction.

The simplified template was then scrutinised according to classical performance parameters for devices of its kind. The device exhibited colouration kinetics that were almost two orders of magnitude faster than the initial documented kinetics for electrochromic ILs published recently.

The simplified device exhibited a prolonged optical memory under open circuit conditions, but poor colouration efficiency as the charge maintained within the device was low. EIS related the low charge within the device to the low conductivity of the ionogel; it also explained the prolonged optical memory as the capacitance of the device increases upon reduction of the chromophore.

The large, stable electrochemical window of the IL based device allowed reproducible absorbance switching experiments to be performed over a 20-minute time scale.

Chapter 4 therefore is equally effective at demonstrating the idea of employing ILs as multifunctional agents within solid-state platforms.

The main issue raised that is specific for this chapter is the physicochemical properties of the synthesised molecule. Fortunately enough the chemistry behind optimising the liquid properties of ILs are well understood. These chemistries are discussed in **section 1.2.1.2** and **7.2.2**, with a view to improving existing parameters.

The optical performance of electrochromic devices was observed and discussed in chapter 5, and forms the basis for experiments designated as future work to optimise these features for future platforms (**section 7.2.3)**.

7.1.2 Photopatterning of stimuli responsive sol-gels

Chapters 5 and 6 detailed the novelty of photopatterning electro- and photo-responsive materials within matrices whose chemical compositions were altered systematically. Photopatterning is an important technique that allows the user to design the polymer shape to intricate dimensions. The work was aimed at exploiting this technique in order to bring the chemistry of the stimuli responsive materials to the fore.

Chapter 5 discussed the idea of encapsulating electroactive materials within the photopatternable matrix. These included a diethyl substituted viologen derivative and an aqueous suspension of graphene. Subsequent characterisation via Raman spectroscopy confirmed their encapsulation within the medium, whilst EIS, CV and UV gave a good understanding of how to optimise the optoelectronic chemistry of these materials.

It was found that altering the composition of the IL within the photopatternable matrix affected the ionic conductivity of the resultant solid state. Ionogels that exhibited the most favourable conductivity were chosen to demonstrate the redox chemistry of the viologen analogue.

Addition of the electronic conductor graphene significantly improved the conductivity of a $[P_{6,6,6,14}][DCA]$ 40 wt% based ionogel. Another novel strategy employed to improve the conductivity of this ionogel was to incrementally the Zr/methacrylate complex within the initial sol-gel solution.

This complex acted as the condensing agent within the polymeric medium, incrementally increasing it therefore encapsulated the conductive materials within further and further. An increasing linear relationship was observed between ionic conductivity and the concentration of the condensation agent.

An improved understanding of how the electroactive materials behave within their respective hybrid sol-gel environments allowed sub-micron structures to be fabricated via optical exposure. These 3-D structures definitively encapsulate the electroactive materials within and exhibit minimal-distortion after etching.

Based on the knowledge gained from chapter 5 and the previous expertise of group members on photo responsive systems, the final experimental chapter discussed the advantages of co-polymerising a SP monomer within the same class of hybrid sol-gels. The variant in this chapter, unlike those within the first three experimental chapters, was the chemical nature of the polymer matrix and not the materials within.

Varying the concentration and nature of the metal alkoxide/acrylate complex allowed UV/Vis and contact angle trends to be elucidated. The trends were then effectively related to the molecular structure using IR spectroscopy.

Addition of a metal alkoxide that does not exhibit d-orbital phenomena (i.e the ability to participate in charge-transfer complexes) allowed the SP/MC equilibrium to dictate the surface energy of the resultant polymerised sol-gel. These findings made the Al based SP sol-gels ideal candidates for direct photopatterning.

Direct UV laser writing of pillar structures allowed the effects of the photodynamic equilibrium to be realized on the macro scale. Ultimately a new, novel, photoresponsive sol-gel was photopatterned. 2PP polymerisation produced spiral structures in tandem with the theme of the research.

The new photoresponsive material was of the optimium mechanical stability to be patterned as stand-alone structures without a supporting perimeter scaffold. Chapter 5 is therefore provides an insight into the behaviour of the photoresponsive SP dye within various photopatternable matrices, and relates macrocopic behaviour to molecular structure.

7.2 Future Work

7.2.1 Strategies to improve the limit of detection of two component optodes

Throughout the duration of the work on two component optodes, we discussed at length and concluded that the mode of ion transfer into the membranes was the co-extraction mechanism. In order to confirm this a quick, well defined experiment involving salts of Co^{2+} was conducted.

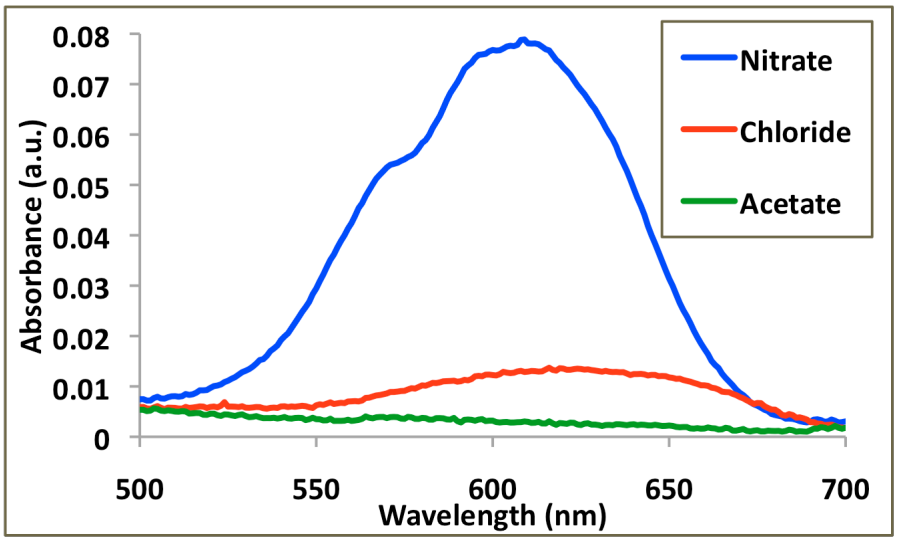

Figure 7.1: Absorption spectra obtained for Co-DCA complexation based on nitrate, chloride and acetate salts of Co^{2+}.

The spectra in Figure 7.1 were obtained by exposing three individual membranes to the Co^{2+} salt of the same concentration over the same time (0.1M, 10 minutes). It can be seen in the first instance that exposure of Co (II) acetate to the membrane yield no observable optical response. This is easily explained as the cobalt assumes tetrahedral geometry as part of a hydrated acetate salt. We can therefore conclude that the initial salt must be of octahedral geometry in order to recomplex within the membrane and produce a distinguished optical signal.

The co-extraction convention is experimentally established by looking at the response obtained for the chloride salt. A diminished response is seen over the same time period.

The polarity (relative to PVC) and the rate of transfer of the co-extracted anion therefore plays a crucial role in the detection process. There are some reports of a similar nature for electrochemical sensors based on PVC. In these the *Hofmeister* series plays a crucial role in the sensors response[1, 2].

The Hofmeister series was initially developed to study the solubility of proteins in solution, and relates to the relative hydration energy of the anions in question[3]. It is also well established for cations but for anions it follows the order:

$$ClO_4^- > SCN^- > I^- > \mathbf{NO_3^-} > Br^- > \mathbf{Cl^-} > HCO_3^- > CH_3COO^- > SO_4^{2-} > HPO_4^{2-}$$

The above list is by no means extensive but it does include some of the more conventional anions used in research. The anions on the extreme left are regarded as being more hydrophobic in nature opposed to the extreme right, which are more hydrophilic.

In this series the chloride and nitrate ions are of the same relative polarity, the latter being slightly more hydrophobic. From the experiment described, this suggests that tuning and optimising the polarity of the anion (relative to PVC) by following the series in the non-polar direction *should* increase the rate of ion transfer into the membrane. The limit of detection can therefore be decreased, as complexation should increase as a result.

Annealing is a process where a material is heated at elevated temperatures over time causing changes in its physical properties. It has found previous use in metallurgy for solids[4], and also in IL media where they were used as a stable solvent for the preparation of block copolymer dispersions at high temperatures[5].

At elevated temperatures (>310 ^{0} C) group 1 salts of dicyanamide have been shown to undergo trimerisation to form tricyanomelaminates[6, 7].

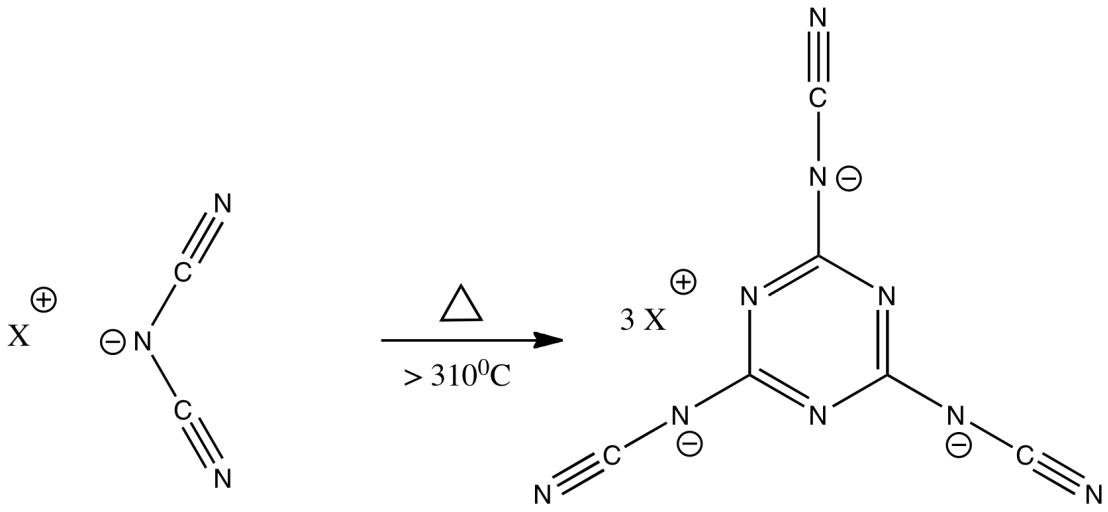

Figure 7.2: The trimerisation of the [DCA]$^{-}$ anion.

This unique property of $[DCA]^-$ salts allows the formation of anionic species with an increased conjugation and increased co-ordination sites. Once trimerised, the new species can be ion-exchanged according to the experimental conventions to form new IL's, that can simplify optodes in the same manner as discussed previously **(Section 2.4.3)**.

Experiments can then be designed to study the coordinating properties of the new IL species within optical sensing. If co-ordination occurs with either Cu^{2+} or Cu^{2+}, it is proposed that the increased conjugation of the anionic ligand will decrease the limit of detection below existing results.

7.2.2 Strategies to improve the liquid properties of electrochromic ionic liquids

7.2.2.1 Ion exchange metathesis

There are several strategies documented within the literature aimed at optimizing the physicochemical properties of IL's. Of these arguably the most popular method of choice to alter these properties is the use of π-electron delocalised anions that exhibit mere electrostatic interactions with the cation **(Section 1.2.1.2)**.

$[P_{V,8,8,8}][3X]$ is a trihalide, which can undergo ion-exchange metathesis with highly π-electron delocalised anions such as $[DCA]^-$ and $[NTf_2]^-$. Experiments can then be designed to understand how the ion-exchange reaction manifests itself in the liquids physical form.

7.2.2.2 Variation of the linker

$[P_{V,8,8,8}][3X]$ has a propyl linker between its phosphonium core and the pyridinium ion of the viologen moiety. This, coupled with the high density packing of the halides favours high viscosity and high melting point sytems. Modifying the structure of the linker will provide an effective study on relating chemical structure to IL liquidity.

Dihaloalkanes are readily available variants in both chain size and terminal halides. It is proposed that increasing the distance between the phosphonium and pyridinium centres will exhibit favourably in the liquid properties of the material.

Other reports on tuning the liquid properties of IL's involve the introduction of unsaturated aliphatic chains[8] and ethers[9] that induce "disorder" along the chain. In both cases the physicochemical interactions of the functionalised chains dominate over the previous structure. To this end the authors introduce unsaturated sites at specific points along the chain, with a decrease in melting point of 74.4^0C reported in one specific case.

For the case involving ethers, the authors reported an increased density and viscosity in most cases as the exclusive hydrogen bonding in compounds of this nature prevailed over previous interactions in the saturated systems.

Combining the strategies discussed will deliver electrochromic ILs with tailored liquid properties. They can be characterised via density, viscosity, thermal phase transitions, redox potentials and visible spectroscopy including the kinetics of the electrochromic equilibrium. It is anticipated that the latter experiments will be governed by the liquid properties of the parent molecule structure.

7.2.3 Strategies to quantify and optimize the capacitance effect of electrochromic device design

The electron-mediated equilibrium between the di- and monocationic states of a viologen molecule is shown above in figure 7.3.

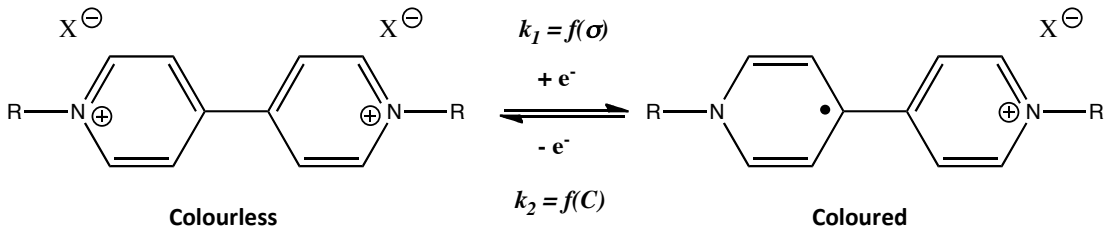

Figure 7.3: Equilibria of the viologen compounds.

In this instance the kinetics of the forward reaction *(k_1)* are a function of the conductivity of the ionogel; while the kinetics of reversion back to the colourless state *(k_2)* are a function of the capacitance of the device.

As the viologen equilibria are manipulated via potentiometry, the reactions that produce the change in optical density take place initially at the electrode interface. In order to produce a change within the film, charge diffusion must therefore migrate back out into the electrolyte phase. The rate of charge diffusion is therefore the limiting step under current experimental conditions.

It is proposed that this limitation can be improved via two routes:

(1) The forward reaction in figure 7.3 is governed by the ability of the electrolyte to facilitate a current i.e. its conductivity. The discussion in **section 4.4.4** relates the physical liquid properties of individual ILs to the conductivity of the solid-state device. It is anticipated that using a low viscosity, high conductivity IL will improve the kinetics of the forward, coloration reaction.

(2) Charge diffusion can be limited by simply making the ionogel layer between the tow electrodes thinner. As the current dropcasting technique produces acceptable reproducible devices thicknesses, decreasing the volume of the liquid used will make the ionogel layer thinner.

The ideal technique to monitor how these strategies will impart on the functionality of the new devices is EIS. The various electrochemical processes that govern the reactions taking place within the electrochromic devices can be individually quantified by fitting the EIS responses obtained to equivalent circuitry.

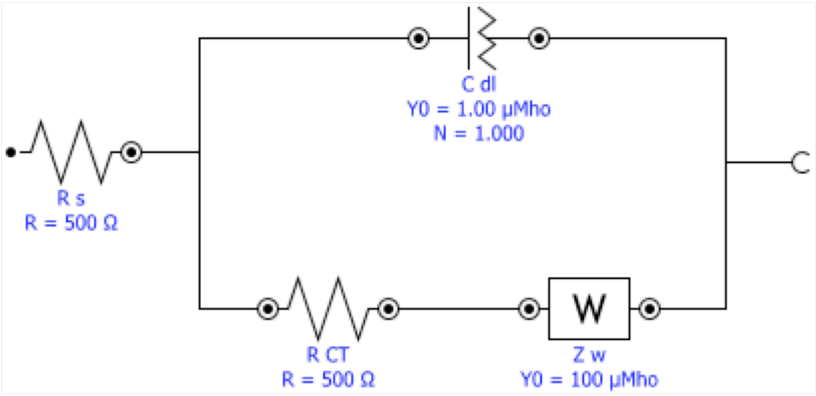

Figure 7.4: The Randles equivalent circuit used in EIS.

The *Randles* circuit is easily the simplest yet most popular circuit used in EIS, fitting it to the Nyquist plot obtained allows an independent estimation of the various electrochemical processes taking place within the cell (figure 7.4).

Here R_s is the solution resistance (KCl in the current system setup), R_{CT} is used to estimate the conductivity (as described, **section 3.4.10**), C_{dl} is the double layer capacitance and Z_w is the *Warburg* impedance.

A series of ionogels based on ILs of differing liquid properties can be scrutinised under the topic of device performance. Using this strategy device performance can be optimised to suit a particular purpose.

The kinetics of the forward reaction can be tuned by the use of ionogels with ILs of differing viscosities. If a prolonged optical memory is required then the use of a device with a relatively thick ionogel that possesses a high C_{dl} value should be used.

7.3 References

1. J. H. Shim, I. S. Jeong, M. H. Lee, H. P. Hong, J. H. On, K. S. Kim, H. S. Kim, B. H. Kim, G. S. Cha and H. Nam, *Talanta*, 2004, **63**, 61-71.
2. C. Coll, R. H. Labrador, R. M. Manez, J. Soto, F. Sancenon and M. J. Segui, *Chemical Communications*, 2005, 3033-3035.
3. Y. Zhang and P. S. Cremer, *Current Opinion in Chemical Biology*, 2006, **10**, 658-663.
4. C. A. Chang, A. Segmuller, H. C. W. Huang, B. Cunningham, F. E. Turene, A. Sugerman and P. A. Totta, *Journal of the Electrochemical Society*, 1986, **133**, 1256-1260.
5. L. Meli and T. P. Lodge, *Macromolecules*, 2009, **42**, 580-583.
6. E. Irran, B. Jurgens and W. Schnick, *Chemistry-a European Journal*, 2001, **7**, 5372-5381.
7. T. J. Wooster, K. M. Johanson, K. J. Fraser, D. R. MacFarlane and J. L. Scott, *Green Chemistry*, 2006, **8**, 691-696.
8. S. M. Murray, R. A. O'Brien, K. M. Mattson, C. Ceccarelli, R. E. Sykora, K. N. West and J. H. Davis, Jr., *Angewandte Chemie-International Edition*, 2010, **49**, 2755-2758.
9. T. Y. Wu, S. G. Su, K. F. Lin, Y. C. Lin, H. P. Wang, M. W. Lin, S. T. Gung and I. W. Sun, *Electrochimica Acta*, 2011, **56**, 7278-7287.

Appendix Experiments

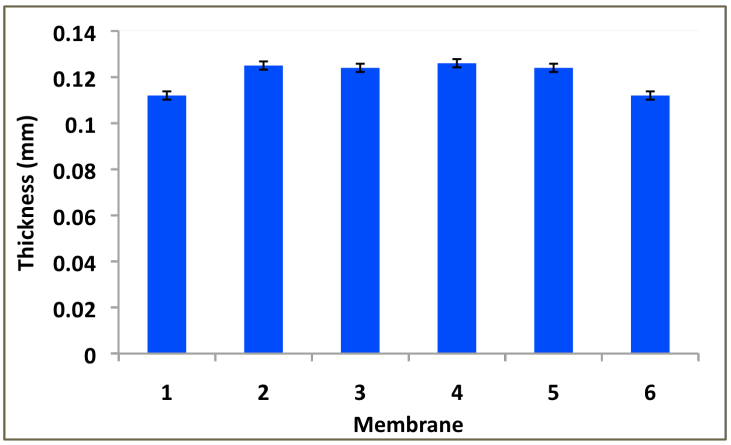

		mm			mm
membrane thickness	1	0.112	**glass slide thickness**	1	0.159
	2	0.125		2	0.161
	3	0.124		3	0.16
	4	0.126		4	0.161
	5	0.124		5	0.162
	6	0.112		6	0.157
	average	0.121		**average**	0.160
	stdev	0.007		**stdev**	0.002

Figure A1: Membrane thickness reproducibility analysis used to obtain results in sections **3.4.4** and **3.4.5.**

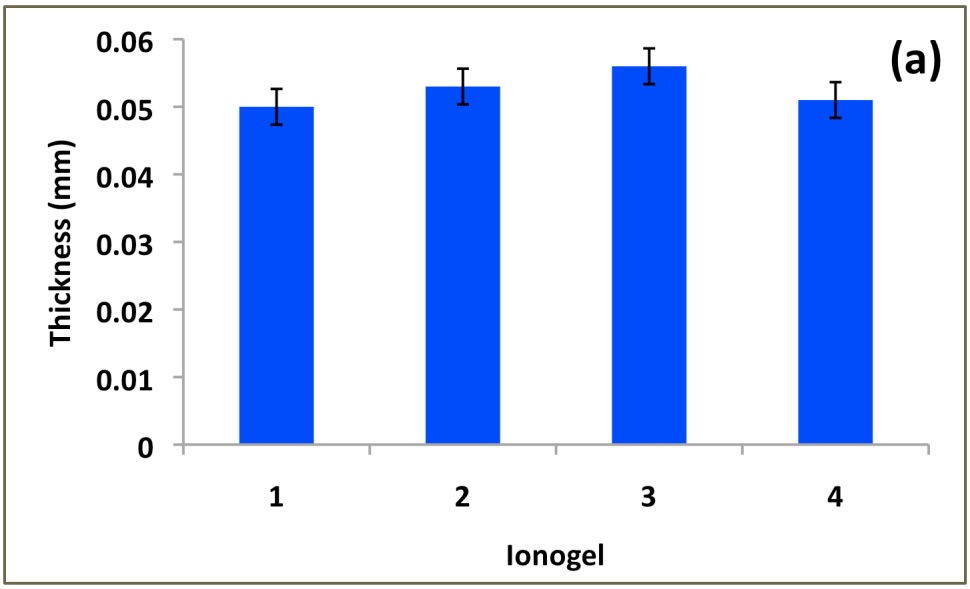

Device	*Ionogel + electrodes (mm)*	*Ionogel (mm)*
1	0.307	0.05
2	0.31	0.053
3	0.313	0.056
4	0.308	0.051
	average thickness (mm)	0.053
	SD	0.003

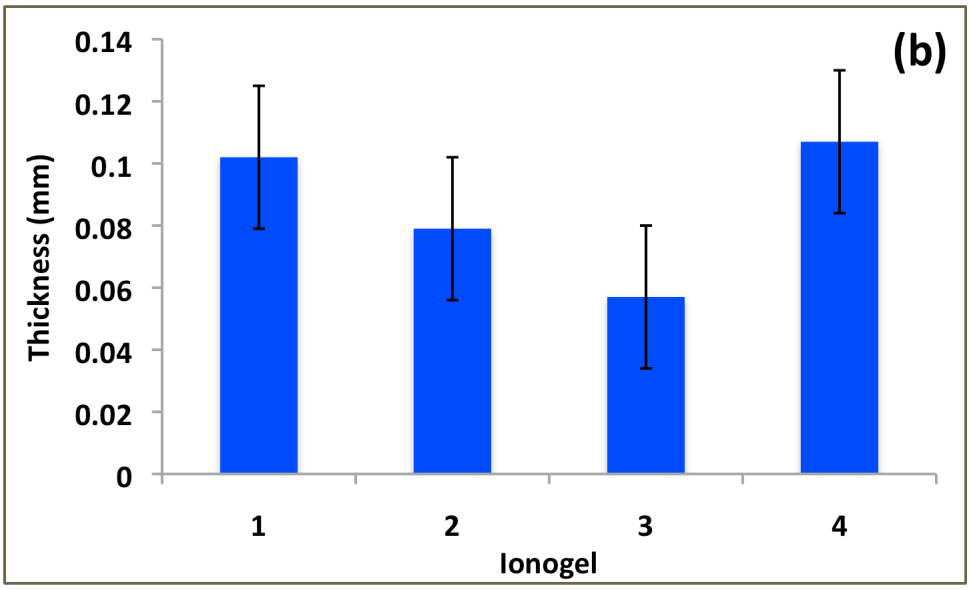

Device	*Ionogel + electrodes (mm)*	*Ionogel (mm)*
1	0.359	0.102
2	0.336	0.079
3	0.314	0.057
4	0.364	0.107
	average thickness (mm)	0.086
	SD	0.023

Figure A2: Electrochromic device thickness reproducibility analysis, (a) Device I and (b) Device II.

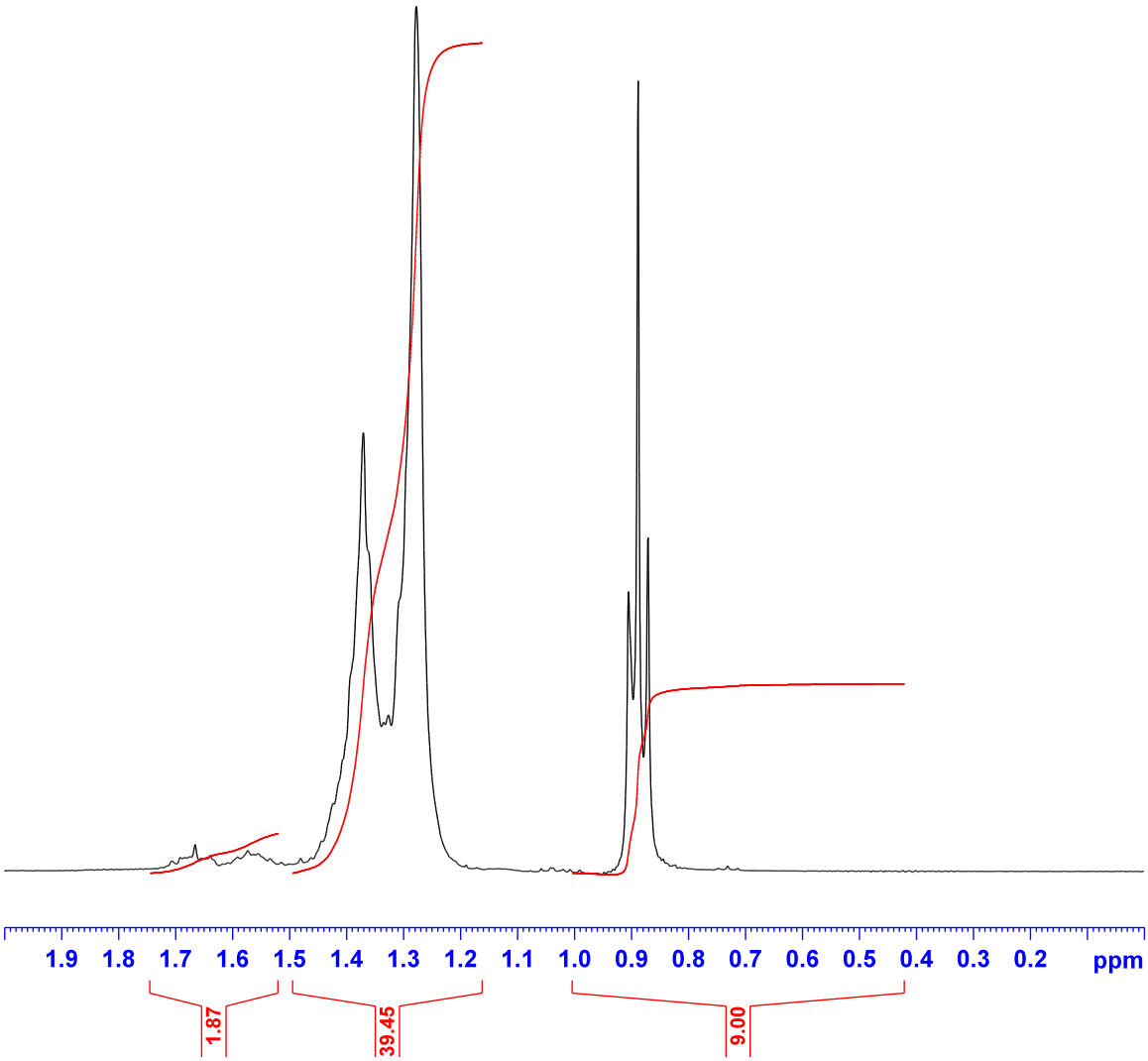

Figure A3 (i): ^{1}H NMR spectrum obtained for trioctylphosphine.

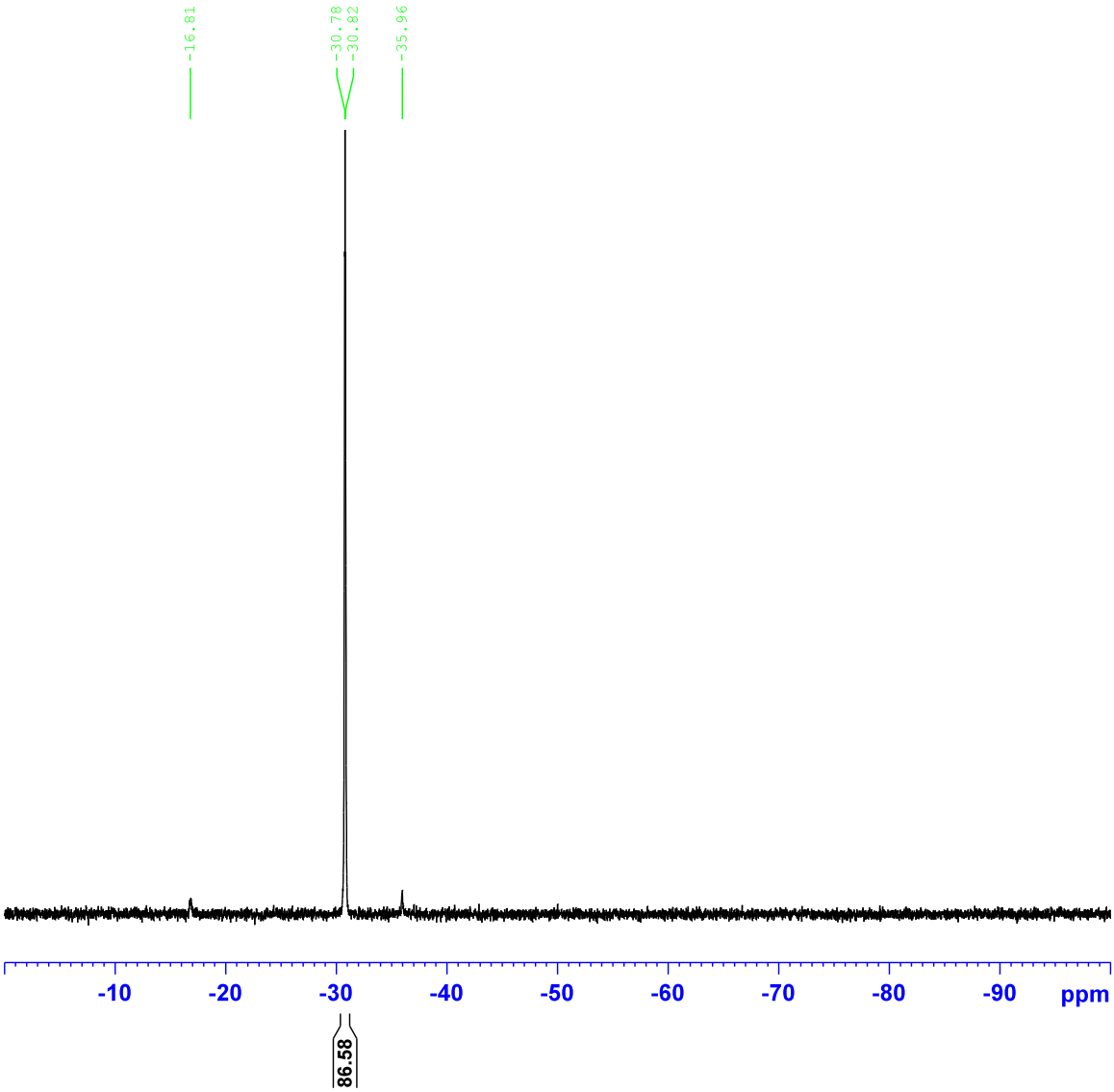

Figure A3 (ii): ^{31}P NMR spectrum obtained for trioctylphosphine.

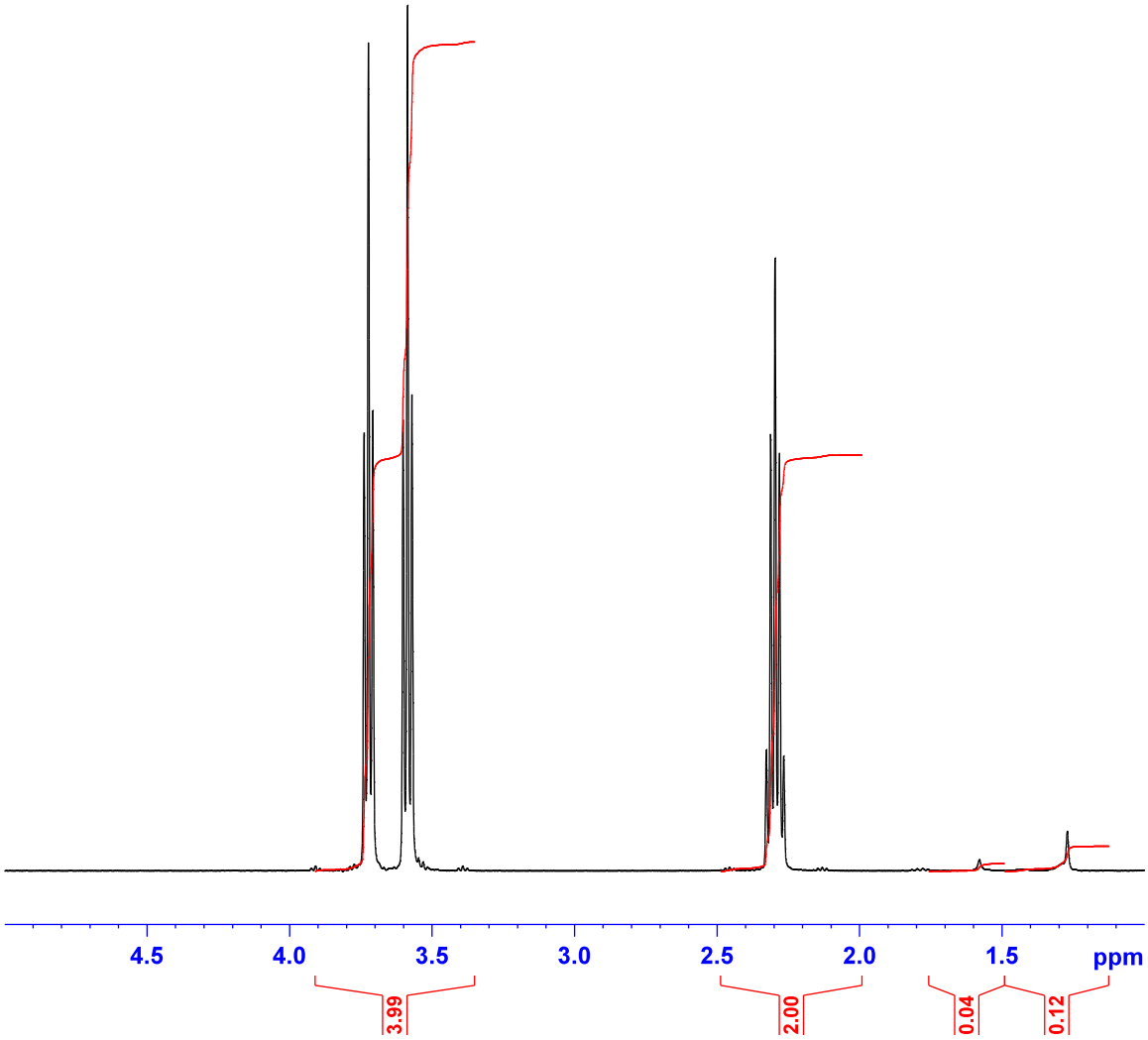

Figure A3 (iii): ^{1}H NMR spectrum obtained for C_3H_6BrCl.

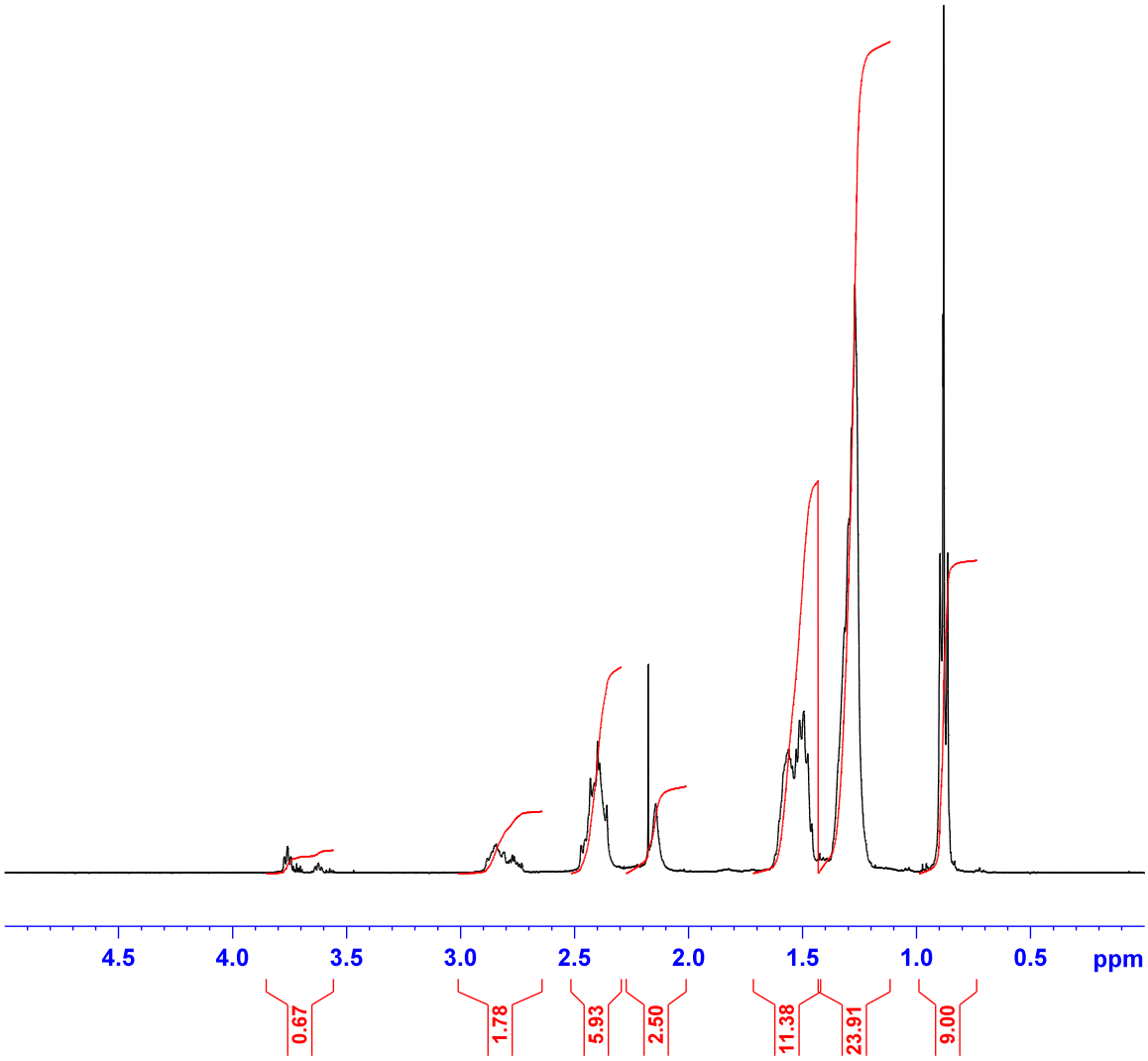

Figure A3 (iv): ^{1}H NMR spectrum obtained for [$P_{3Cl,8,8,8}$][Br].

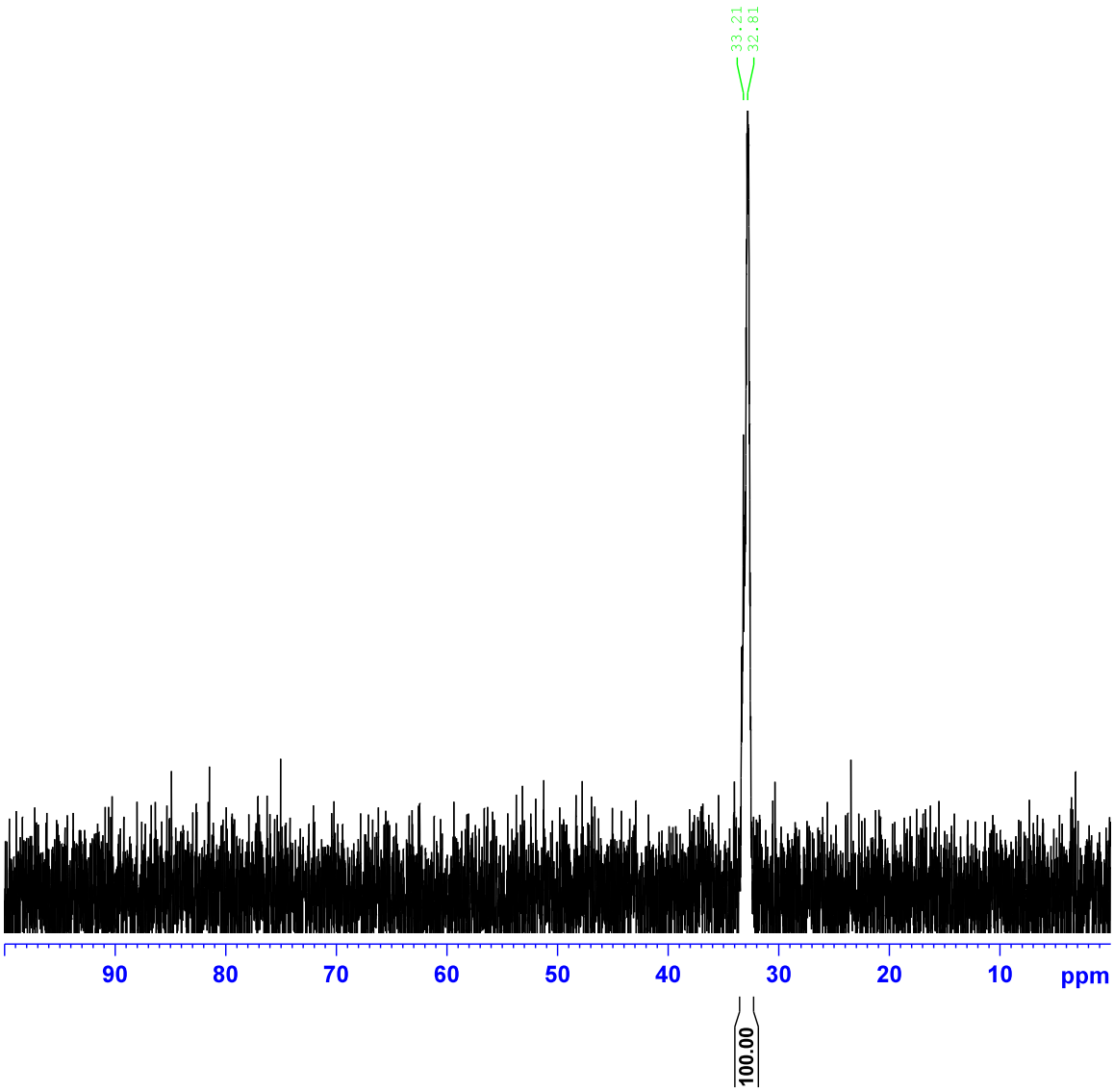

Figure A3 (v): ^{31}P NMR spectra of $[P_{3Cl,8,8,8}][Br]$.

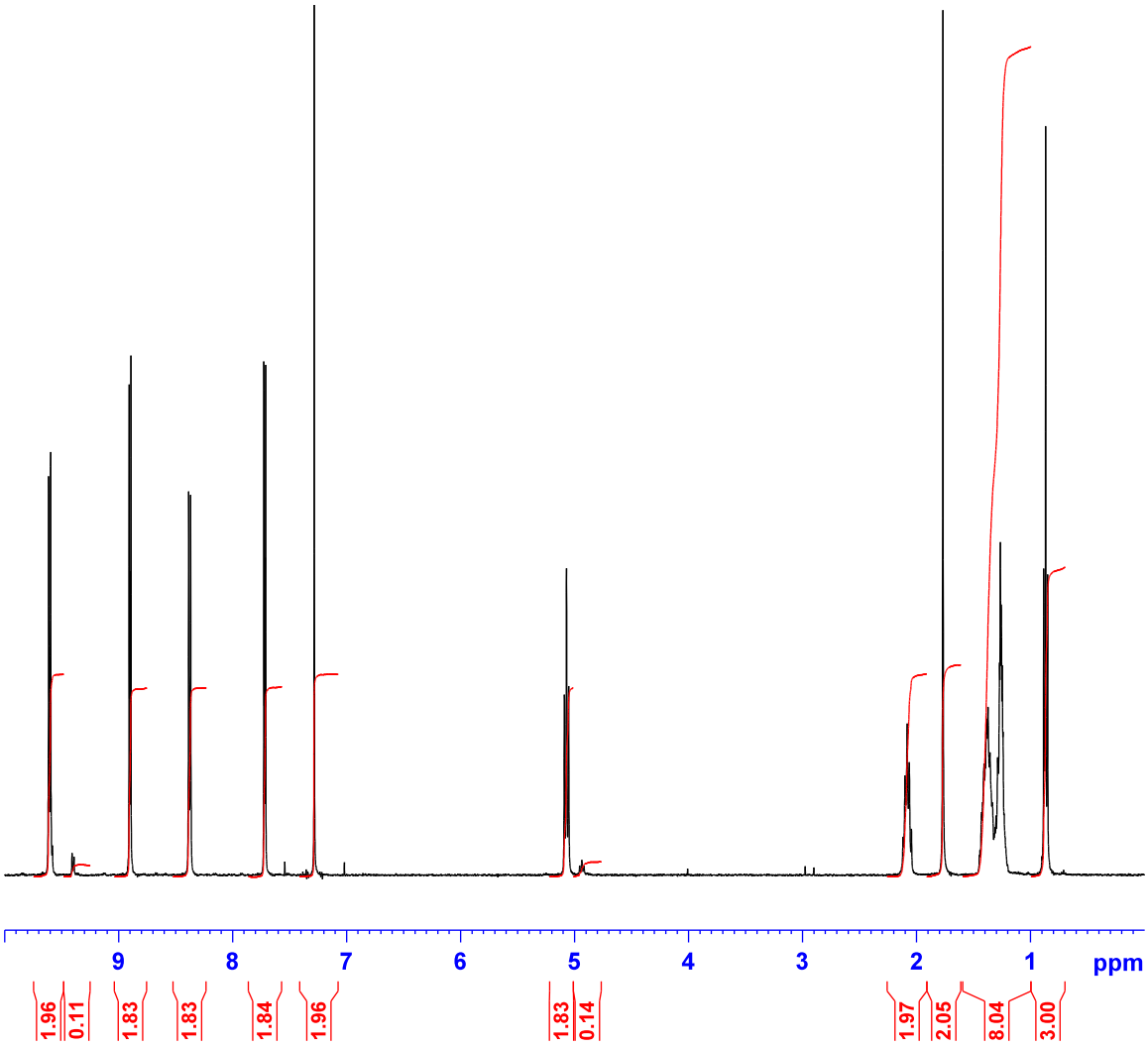

Figure A3 (vi): ^{1}H NMR spectrum obtained for MAV.

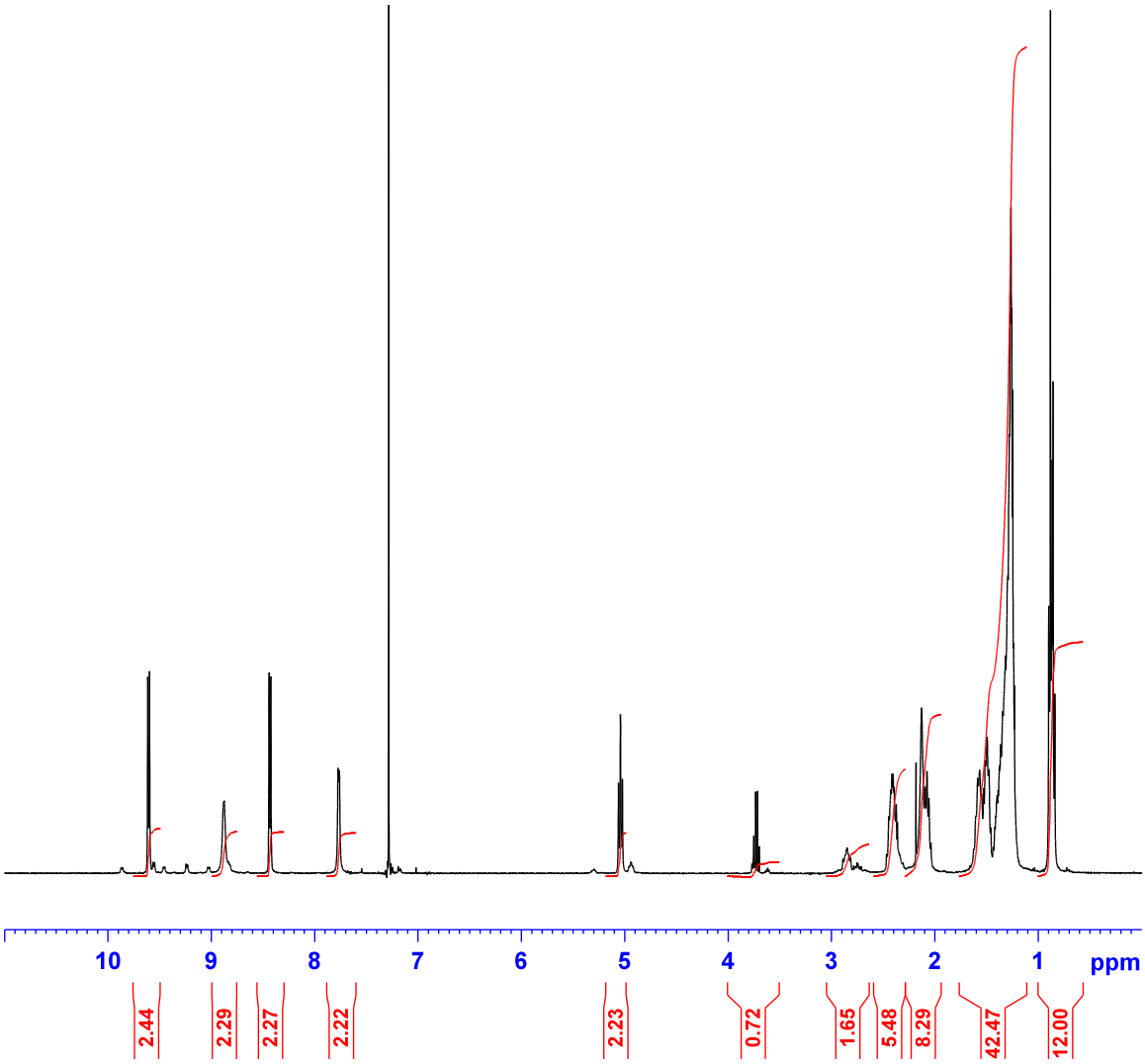

Figure A3 (vii): ^{1}H NMR spectrum obtained for the $[P_{V,8,8,8}][3X]$.

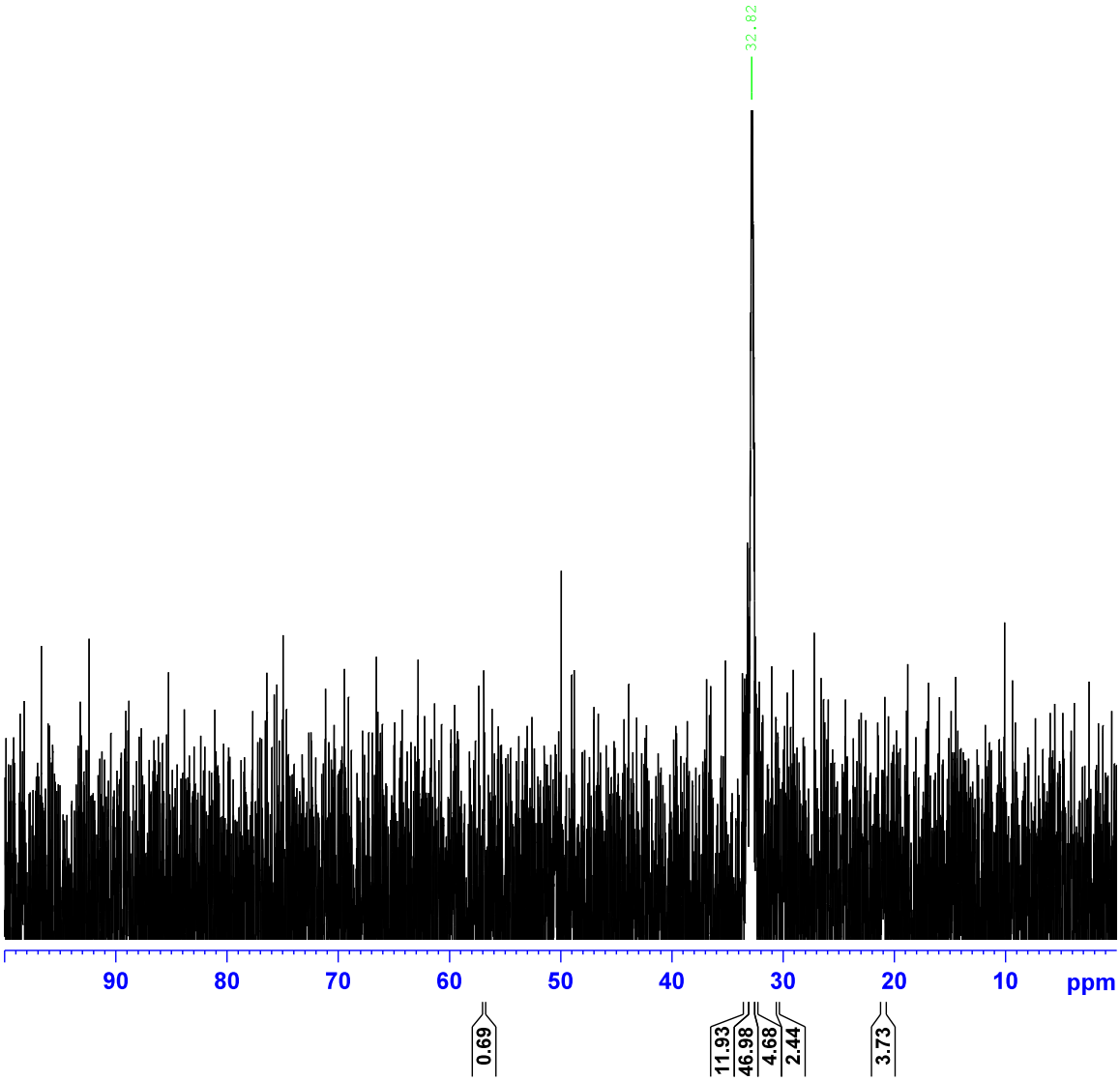

Figure A3 (viii): ^{31}P NMR spectrum obtained for the [$P_{V,8,8,8}$][3X] .

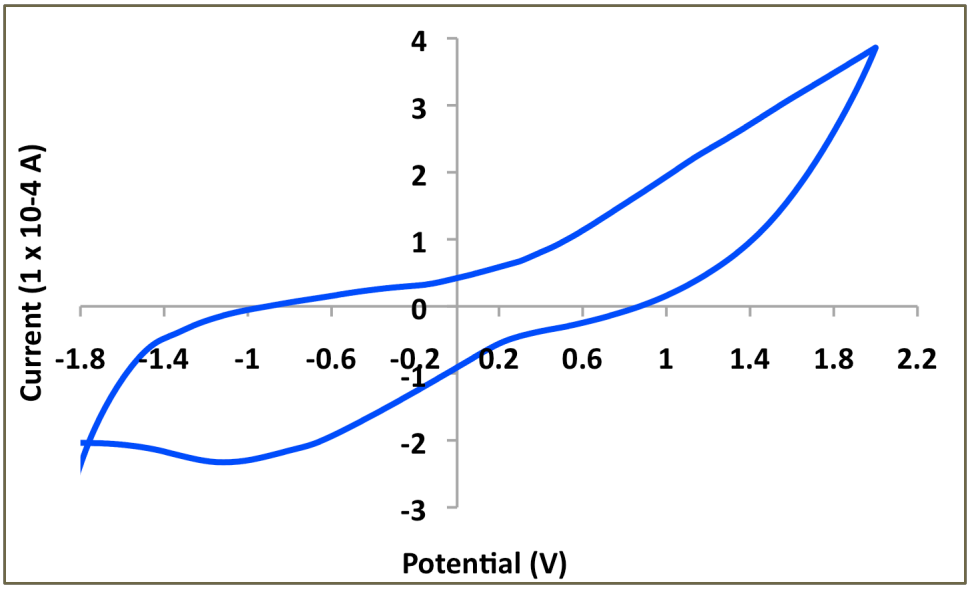

Figure A4: CV obtained for ionogel based on 2:1 PVC: $[P_{6,6,6,14}][DCA]$ on a screen-printed working electrode (Ag/AgCl reference electrode, Pt wire counter electrode, scan rate 0.05 V/sec).

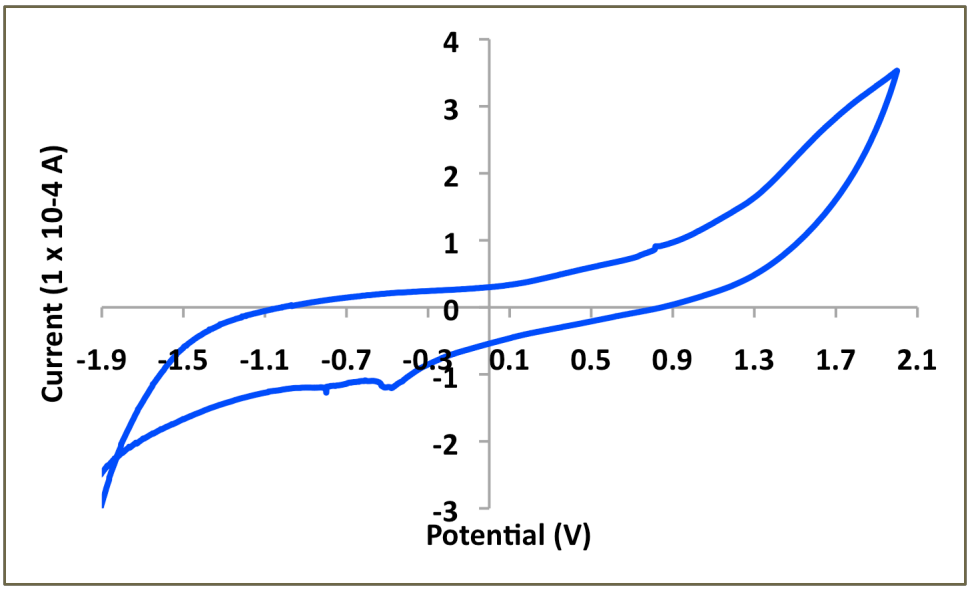

Figure A5: CV obtained for ionogel based on 40 wt.% $[P_{6,6,6,14}][DCA]$ and 60 wt.% SZr 4 on a screen-printed working electrode (Ag/AgCl reference electrode, Pt wire counter electrode, scan rate 0.01 V/sec).

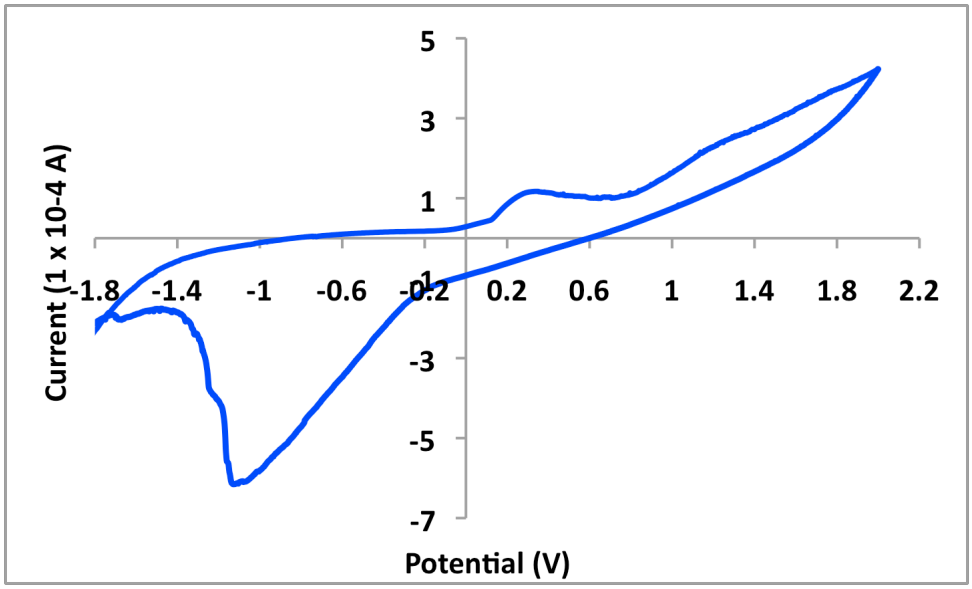

Figure A6: CV obtained for ionogel based on 50 wt.% [emIm][FAP] and 50 wt.% SZ4 on a screen-printed working electrode (Ag/AgCl reference electrode, Pt wire counter electrode, scan rate 0.01 V/sec).

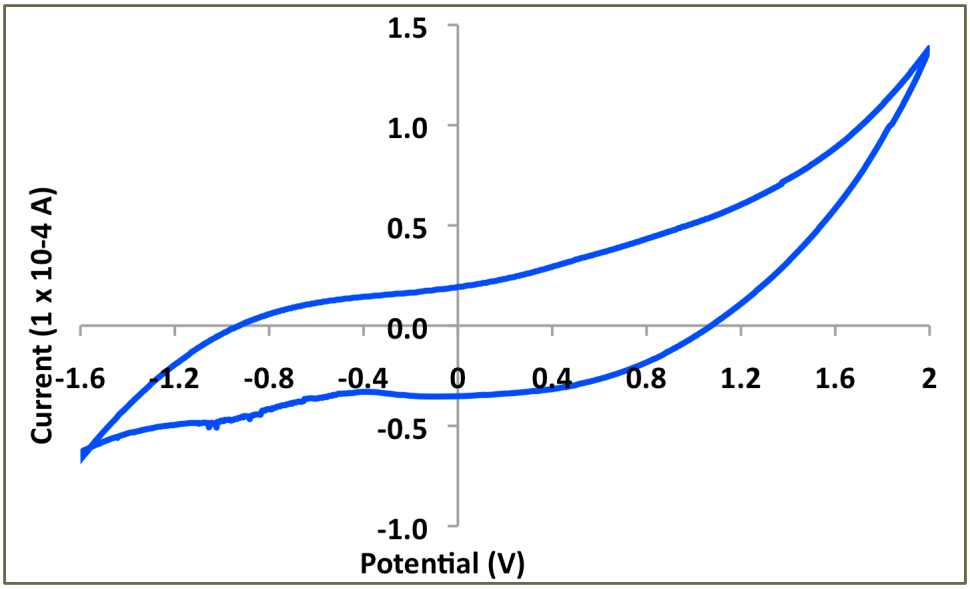

Figure A7: CV obtained for ionogel based on 40 wt.% $[P_{6,6,6,14}][NTf_2]$ and 60 wt.% SZ4 on a screen-printed working electrode (Ag/AgCl reference electrode, Pt wire counter electrode, scan rate 0.01 V/sec).

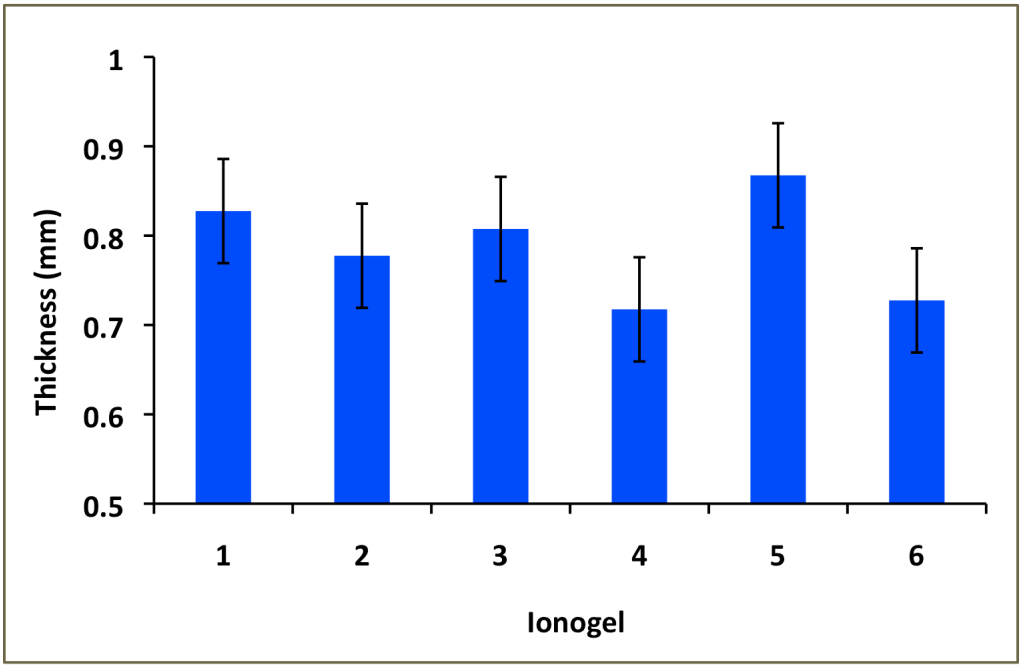

40 wt.% Ionogels	*electrode thickness*		*ionogel thickness*
	mm		mm
1	0.24	**1**	0.8275
2	0.23	**2**	0.7775
3	0.23	**3**	0.8075
4	0.23	**4**	0.7175
5	0.24	**5**	0.8675
6	0.225	**6**	0.7275
average	0.233		0.788
stdev	0.006		0.058

Figure A8: Ionogel thickness reproducibility analysis used to calculate the conductivity of 40 wt.% SZ4 ionogels (Table 6.1).

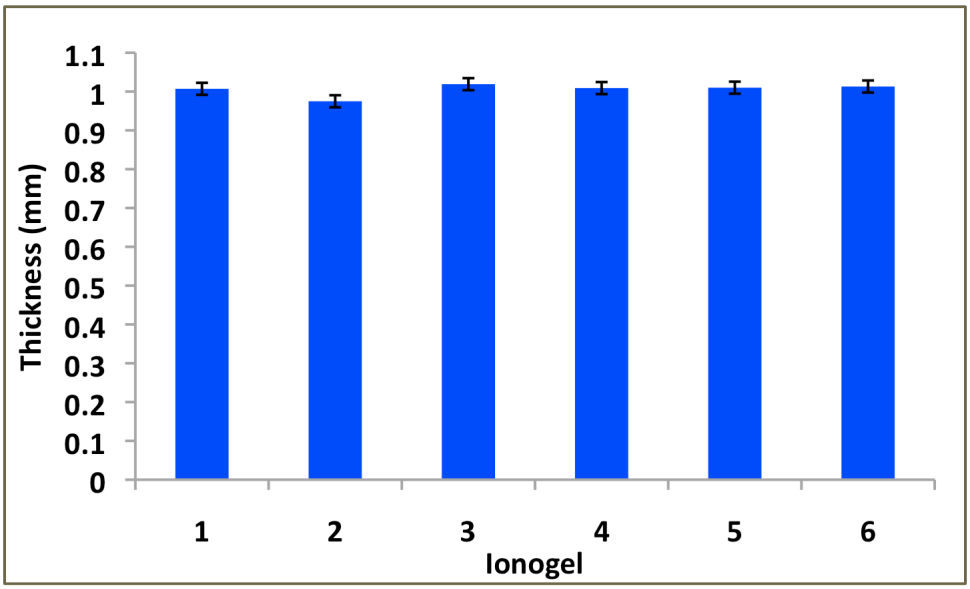

		ionogel thickness
		mm
	1	1.007
	2	0.975
	3	1.019
	4	1.009
	5	1.01
	6	1.013
average		1.006
stdev		0.016

Figure A9: Ionogel thickness reproducibility analysis used to calculate the conductivity of 60 wt.% SZ4 ionogels (Table 6.1).

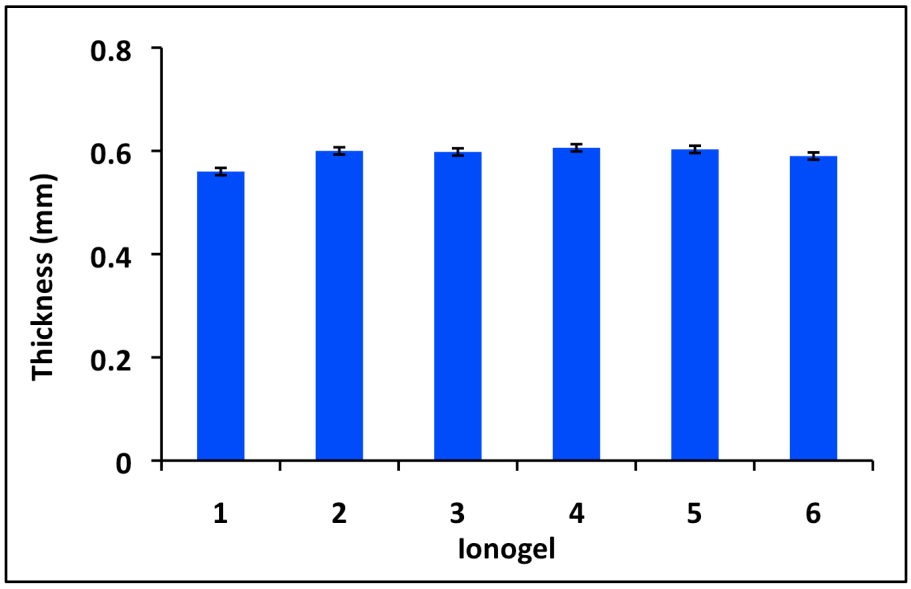

		ionogel thickness
		mm
	1	0.56
	2	0.6
	3	0.598
	4	0.606
	5	0.603
	6	0.59
average		0.599
stdev		0.007

Figure A10: Ionogel thickness reproducibility analysis used to calculate the conductivity of 50 wt.% [emIm][FAP] SZ4 ionogels (Table 6.1).

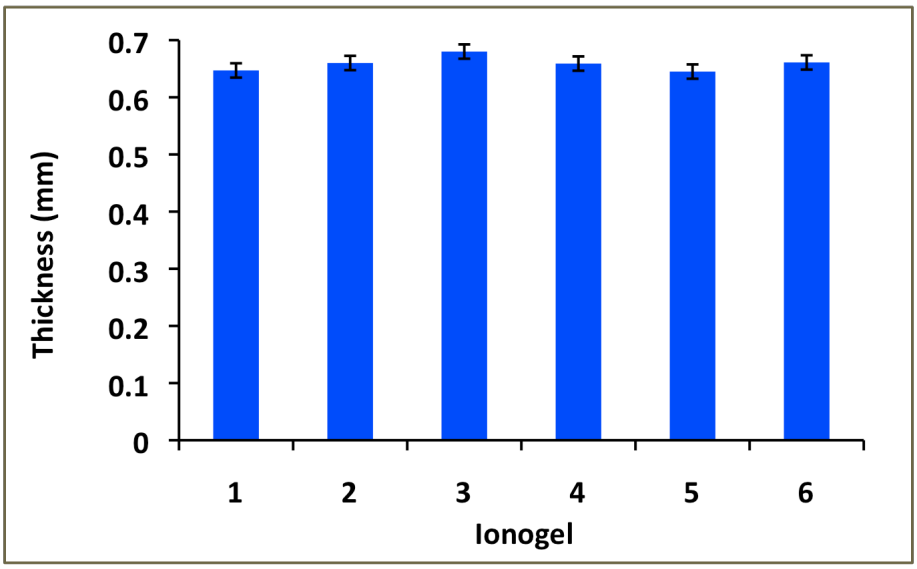

		ionogel thickness
		mm
	1	0.647
	2	0.66
	3	0.68
	4	0.659
	5	0.645
	6	0.661
average		0.659
stdev		0.013

Figure A11: Ionogel thickness reproducibility analysis used to calculate the conductivity of 80 wt.% [emIm][FAP] SZ4 ionogels (Table 6.1).